

See discussions, stats, and author profiles for this publication at: <https://www.researchgate.net/publication/317829234>

GLOBAL PREDICTIVE WILDFIRE MODEL – A Temporal–Spatial GIS Based Risk Analysis Using Data Driven Fuzzy Logic...

Thesis · June 2017

DOI: 10.13140/RG.2.2.13689.47206

CITATIONS

0

READS

75

1 author:



[Gijs van den Dool](#)

CoreLogic

3 PUBLICATIONS 0 CITATIONS

[SEE PROFILE](#)

Some of the authors of this publication are also working on these related projects:



Master Project [View project](#)

GLOBAL PREDICTIVE WILDFIRE MODEL

A Temporal–Spatial GIS Based Risk
Analysis Using Data Driven Fuzzy Logic
Functions

GIJS VAN DEN DOOL

APRIL 2017

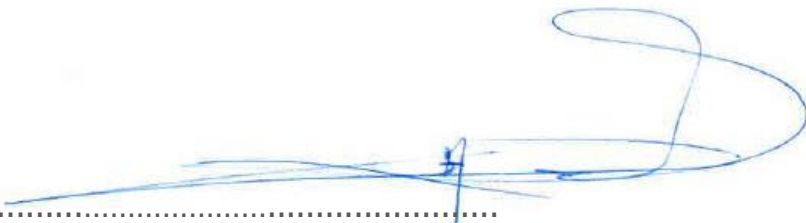
A DISSERTATION SUBMITTED IN PARTIAL FULFILMENT OF THE REQUIREMENTS

SUPERVISOR: JIM WRIGHT

Statement of originality

Except for those parts in which it is explicitly stated to the contrary, this thesis is my own work. It has not been submitted for any degree at this or any other academic or professional institution. The copyright of this thesis rests with the author. Information derived from it should be acknowledged. I agree that the thesis may be made available for reading and photocopying at the discretion of the Head of Geography and Environment. Permission for anyone other than the author to reproduce or photocopy any part of the thesis must be obtained from the Head of Geography and Environment who will give his/her permission for such reproduction only to an extent which he/she considers to be fair and reasonable.

Signed.....

A handwritten signature in blue ink, appearing to be the name "Gijs van den Dool".

Candidate's name: Gijs van den Dool

Abstract

This study is a proof of concept for a global predictive wildfire model, where temporal–spatial characteristics of forest- of wildfires are placed in a Geographical Information System (GIS), and the risk analysis is based on data-driven fuzzy logic functions. The GIS is constructed around three themes: topography, fuel availability and drought. The data sources used in this model are available global, but subsetted for three pilot areas, and are downscaled to the highest resolution (3-arc second). The topographical data is split into six sub-themes, with their basin specific fuzzy membership functions based on the catchment area statistics. The fuel availability score is a composite of land cover, wood loads, biomass, biovolumes. The climatological data is available in daily averages, but the temporal component of the model is aggregated to a weekly time-window (to account for the uncertainty within the climatological model). Therefore the final product is a risk score (from 0 to 1) by week. The sub-models are combined using a multi-criteria approach, and the model results are validated against the Area under the Receiver Operating Characteristic (ROC) curve.

Keywords: Wildfire, GIS, Fuzzy Logic, Data Driven

Table of Contents

GLOBAL PREDICTIVE WILDFIRE MODEL	i
Statement of originality	i
Abstract	ii
Table of Contents.....	iii
List of Tables.....	v
List of Figures	vi
1 Introduction.....	1
2 Background	3
2.1 Key Concepts.....	4
2.1.1 Anthropocentric conditions	4
2.1.2 Topographical conditions	5
2.1.3 Meteorological conditions	7
2.1.4 Igniting conditions	8
2.1.5 Fuel	9
2.2 Literature Review: Wildfire Models	11
2.2.1 Wildfire following models.....	11
2.2.2 Wildfire Risk Models	12
2.2.3 Wildfire Predictive Models.....	12
2.3 Relevancy	13
3 Model Architecture.....	14
3.1 High-Level Design	14
3.2 Model Description	16

GLOBAL PREDICTIVE WILDFIRE MODEL

Table of Contents

3.2.1	Data Components	16
3.2.2	Fuzzy Functions	17
3.2.3	Defuzzification and Scoring	20
3.3	Implementation	24
3.3.1	Study Areas	24
3.3.2	Topographical Risk Database	28
3.3.3	Fuel Risk Database.....	29
3.3.4	Risk Product(s)	32
4	Methodology, Results, and Analysis	34
4.1	Data-Analytics.....	35
4.1.1	Hypothesis: The correlation between "Burnt Area" & "Active Fires is robust enough to be used as data filter	35
4.1.2	Hypothesis: Trapezoid functions for topographical risk scoring are sufficient detailed to construct a topographical risk layers.....	38
4.1.3	Hypothesis: The combination of land use, fuel loads, biomasses and bio-volumes can provide a meaningful fuel risk score	45
4.1.4	Hypothesis: The BKDI is a useful indicator to assess the time-dependency of wildfire risk	51
4.1.5	Topographical Risk Layer Construction	56
4.1.6	Component Integration	58
4.2	Model Results	59
4.3	Model Validation and (Re)Analysis.....	62
4.3.1	Reanalysis of the Spanish study area.....	66
4.3.2	Overall Model robustness.....	67
5	Conclusions	69
6	References	71
	Appendices.....	80

GLOBAL PREDICTIVE WILDFIRE MODEL

List of Figures

Figure 1: Fire Environment Triangle	8
Figure 2: Schematic overview of the model components, and information flow	14
Figure 3: Geo-Database design	17
Figure 4: Fuzzification of Elevation for a sample Basin	18
Figure 5: Risk Scoring of a sample Cell	20
Figure 6: Fuel Sub-model information use and workflow.....	21
Figure 7: Right shoulder sigmoidal function to transform the drought index to a scoring.	22
Figure 8: Study Areas.....	25
Figure 9: Saxaul forest in the Gobi	27
Figure 10: Schematic overview of the Topographical Sub-Model components	29
Figure 11: Schematic overview of the Fuel Sub-Model components	30
Figure 12: Schematic overview of the Drought Sub-Model components, Risk Products,	33
Figure 13: Correlation between Burned Areas and Active Fires in Spain and North America	36
Figure 14: Fuzzy Membership - Elevation.....	39
Figure 15: Fuzzy Membership - Aspect	40
Figure 16: Fuzzy Membership - Slope	41
Figure 17: Fuzzy Membership - TWI.....	42
Figure 18: Fuzzy Membership - Urban	43
Figure 19: Fuzzy Membership - Open Water	44
Figure 20: Transition from land cover to the fuzzy membership	50
Figure 21: Meteorological indicators	52
Figure 22: Keetche-Byram drought index.....	53
Figure 23: Weekly Drought Index and corresponding Drought Factor	54
Figure 24: Downscaled Drought Index.....	55
Figure 25: Constructing the Topographical MCA layer.....	57

Figure 26: Fire Risk Corrected for Drought.....	58
Figure 27: N. America (CA/NV) Wild Fire Risk Scores by cell count	60
Figure 28: Spain (Valencia Wild Fire Risk Scores by cell count.....	61
Figure 29: Mongolia (Gobi Alta) Wild Fire Risk Scores by cell count	62
Figure 30: Fire Risk/Hazard comparison.....	64
Figure 31: Pasture Biomass map of Mongolia	65
Figure 32: Spain (Valencia) Wild Fire Risk Scores Adjusted by cell count	66
Figure 33: Confusion matrix and common performance metrics calculated from it	67
Figure 34: ROC curves for N. America (CA/NV), Spain (Valencia), and Mongolia (Gobi Altai)	68

List of Tables

Table 1: Examples of wildfire restricting variables	3
Table 2: Translation table to go from KBDI values to membership values	23
Table 3: Translation table to go from membership values to drought conditions	23
Table 4: Reclassification tables for fuel loads	30
Table 5: Relation between Fuel Codes (Dry/Wet) and their Classes	31
Table 6: ROC curve classification	32
Table 7: Land Cover under (or near) Active Fires and Burned Areas	37
Table 8: relationship between Land Cover Classification (ESA), Fuelbeds, and Fuel Score	46
Table 9: Fuelbed descriptions and calculated fuel class.....	47
Table 10: Fuelbed description and associated wood loads and ranking	47
Table 11: Land cover classes and percentage Burned Area cover	48
Table 13: Normalised Score by Land Cover Class	49
Table 14: Risk band clasification	56
Table 15: Large wildfires in Lassen, CA	63

GLOBAL PREDICTIVE WILDFIRE MODEL

1 Introduction

Forest or wildfires are one of the most unpredictable, devastating, natural catastrophes, with severe environmental consequences, causing damage to properties, infrastructure, and costing lives. Giglio et al. (2013) estimate that every year on average of 3.5m square kilometres of land is affected by wildfires using the Global Fire Emissions Database GFED4 in combination with the 500 m MODIS burned area maps with active fire data from the Tropical Rainfall Measuring Mission.

The objective of this study is to provide a framework in which globally available datasets can be analysed, and combined, to create a realistic hazard score without the use (or dependency) of local datasets or high-resolution information layers.

The proposed framework consists of three components:

- 1) The topographical database: the Shuttle Radar Topography Mission (SRTM) data in 3 arc-seconds, which is 1/1200th of a degree of latitude and longitude, or about 90 meters (295 feet), has been used to find the topographical indicators.
- 2) The fuel database: to estimate the fuel availability a composite score of land cover, fuel loads, biomass, and biovolume is constructed
- 3) The climatological database: one of the most used indices to find the fire potential in an area is the Keetch-Byram Drought Index (KBDI). The KBDI is calculated by using modelled surface air temperature and precipitation amounts from Department of Civil and Environmental Engineering/Princeton University (Sheffield et al., 2006).

Within the three components, fuzzy logic operators are used to determine the membership values; these values are translated to scoring factors. In the final step, the topographical and fuel availability scores are combined, and the weekly KBDI is used to rescale the score to give a fire risk by week.

In Chapter 2 the focus is on the background of the thesis, including key concepts, like fuel availability and the anthropocentric, topographical, meteorological, and igniting conditions to start a wildfire. Part of the background study is a literature review, which is concentrating on general wildfire models, wildfire following models,

different wildfire risk models, and predictive wildfire models. This chapter concludes with a short section on the relevance of this study.

In chapter three the model architecture is explained, starting with a high-level design plan and general model description, followed by the information sources used in this study and how fuzzy logic is used to convert the used data sources into a realistic hazard score.

The research methodology, model results, and data analysis are described in Chapter four; this includes a detailed description of the four components of the model, and feasibility of using coarse datasets in environmental studies. The methodology section also includes the construction of the Topographical Risk Layer and the Model Component Integration. The model results and validation of the model, with the possible reanalysis of study areas, are handled in the later part of this chapter, as well as a measure of overall model robustness.

2 Background

Wild- or forest fires are a natural phenomenon, but only in recent years considered as a catastrophe (or natural hazard) because of the increasing damages to structures and infrastructure. The fires can start by natural (e.g. by extreme drought, lightning, or volcanic activity) or by anthropocentric causes (e.g. as an agricultural practice, by accident, or with intent (non-agricultural)). Regardless of how the fires start these fires are highly unpredictable, and can quickly spin out of control, but the behaviour is predictable because of biotic and abiotic factors controlling the evolution of the fire (Fischer et al., 2015; Chuvieco et al., 2003). One of the tools available to predict the path of a wildfire is by creating a model, and assess the possible damage such fire could cause. However, modelling fires is not an easy task, because there are many variables/parameters to be taken into consideration, and most models will either be describing the risk on a large scale (Kaene et al, 2001), or at very detailed level (Rochoux et al, 2013). Neither models are wrong, both types of models serve a purpose, and are useful in the domain they were designed for, but there are only a few models developed which can operate in a scalable environment (Papadopoulos and Pavlidou, 2011).

Most of the fire prediction/following models will take some, or all, of the components listed in Table 1 into consideration.

Table 1: Examples of wildfire restricting variables

Topographical	Meteorological	Fuel	Other
elevation	temperature	land use/cover	literature
slope	precipitation	biomass	historical fire
aspect	humidity	biovolume	reports
wetness	wind direction	vegetation	
distance to water (either natural or artificial source),			
distance to infrastructure (roads, railways)			

Most of the data in Table 1 is available in several resolutions or scales (e.g. global, national, and local scales), but some data sources, handling this kind of information, are only stored (in a consistent format) in global databases, or are collected for specific purposes in local studies.

2.1 Key Concepts

Wildfires are a natural catastrophe, which can occur when the starting conditions are met, and set-off by either a natural phenomenon (e.g. lighting) or human-caused. The relationship between meteorological and physical conditions in combination with fire occurrences is studied in depth, and there is a consensus that the forest fires are occurring most often during periods when the temperature is high, and fuel moisture and air humidity are low. (Chandler et al, 1983; Crimmins, 2006; Feltman, et al, 2012; Kaene et al, 2001; Piñol et al, 1998; Turner & Romme, 1994).

In this study four key concepts are considered to model the forest fires on a global scale:

- Anthropocentric conditions
- Topographical conditions
- Meteorological conditions
- Igniting conditions

2.1.1 Anthropocentric conditions

The use of fires, to improve soil conditions, have been general agricultural practice in Europe and the United States for many centuries (Pyne, 1995). In the early 1800s it was found that burning areas will add nutrients to the soil, reduce the undergrowth in forested areas (creating of clearings), and allow the return of otherwise suppressed species), but even before that, some native American tribes were following the same practice. (Bliege Bird et al., 2008; Pausas and Keeley, 2009).

In most cases, fires started with an agricultural purpose are lit under controlled conditions and pose little risk to the environment when managed/monitored; therefore they cannot be seen as a wildfire(s). They can become a risk when started under the wrong conditions or not monitored properly (Keeley, 2009). Hardy (2005) concludes that a risk management strategy cannot be formulated without first defining the temporal and spatial scales for which the fire controlling strategy will be applied. The risk assessment and fire managing strategy will largely depend on the range of time or space, and the wider these ranges, the higher level of uncertainty of controlling the fire(s) (Gitas et al. 2014).

Because of these uncertainties fires started under anthropocentric conditions are not taken into consideration in this study, and the research will be mainly focussed on the natural “fire hazard” and associated starting conditions. However, proximity to urban areas will be taken into consideration, because most of the “uncontrolled” wildfires are caused by human actions, either deliberate or by accident.

2.1.2 Topographical conditions

From Digital Elevation Models (DEM) data three topographical indexes can be obtained: slope, aspect, and elevation. The topographical state of an area is not driving the process to start a forest fire, but are important factors while calculating the fire risk for a region. Several topographical aspects will have to be combined to calculate the risk. In this study slope, aspect, elevation are taken into consideration, because the fire is spreading faster on steep slopes, the ground temperatures on south-facing slopes are higher (and are considered dryer), and some elevation ranges are having more favourable conditions for combustion. (Adab et al., 2011; Lecina-Diaz, 2014; Zhao et al., 2010).

Zhang (1999) finds that the spatial resolution of the DEM is crucial when calculating topographic parameters (e.g. aspect, slope) because too coarse resolutions could lead to an underestimation of the local conditions. Still, using a coarse DEM is appropriate when aggregating the DEM to the same resolution as the satellite data

(approximately ~1 km) when analysing the topographic effects on meteorological parameters. (Dobos et al., 2000; Jovanovic et al., 2013; Wang et al., 2005).

Slope: When trying to model forest fires the slope is the most important topographical parameter because on steeper slopes (larger than 25° from horizontal) the fires will accelerate quicker because the heart of the fire is angled closer to the unburnt area/fuel deposits (Dupuy, 2011). Also, the local wind conditions (generally speaking blowing uphill) could aid the fires by supplying oxygen, creating more intense fires (Butler, 2007; Gerdzheva, 2014).

Aspect: In general the south and west facing slopes are collecting more sunlight than the other aspects. Which result in drier soil conditions, while at the north facing slopes the humidity is higher and cooler microclimates (Ghimire, 2014).

Elevation: Elevation is a difficult indicator (but an important) parameter to use because the climatological parameters are closely related to the elevation. On lower elevations the relative humidity is high, and in general, temperatures are higher as well, while slopes at moderate altitudes will see more rainfall and thus have lower temperatures and higher fuel moisture ratios; this will restrict fires to ignite and propagate (Burgers, 2011). At high altitudes, the air temperature is lower, reducing the drought factor and affect the fire intensities, but at these levels, the available biomass will also be also limiting factor. Forest fires will be most severe at mid-altitude ranges, because in these regions the biomass production in forests is optimal and will consist mainly out of coniferous trees, or mixed forests (Gauchere, 2008).

Derived Elevation Parameters:

It is possible to derive several useful parameters from the DEM data; flow accumulation, Plan/Profile curvature, watershed area, and the Compound Topographic Index are most used (Wilson and Gallant, 2000). When combining the slope and aspect the flow direction and the upslope contributing areas can be

determined, which will represent drainage capacity for each cell. When the flow accumulation is calculated also the flow length is known, and this length can be used as an indication of the proximity to the river(network) instead of the Euclidean distance.

One other common derived parameter is the Compound Topographic Index (CTI) or the Topographical Wetness Index (TWI), which is a function of upstream contributing area and the slope (Vadrevu et al., 2009; Moore et al., 1991). This index can be used to determine the soil moisture (high values) and zones that are derived of runoff (low values). The low CTI values are a good indicator of higher fire probability, in combination with steep slopes, elevation and heat load (Holden et al., 2009). Plan/Profile curvature are used to describe the terrain regarding change because these indicators will highlight the local topographical conditions; the plan curvature controls the flow acceleration or deceleration, the profile curvature is a measure of topographic convergence and divergence (Blaga, 2012).

2.1.3 Meteorological conditions

Cramer (1999) found that temperature and precipitation are the two most important climatic variables used in nearly all physical model simulations for net primary productivity (NPP) for the land biosphere, which is a good indicator for the available biomass (Krawchuk and Moritz, 2011). Also, predominate wind direction and speed are meteorological parameters which should be considered (Tymstra et al., 2007).

To incorporate meteorological parameters into a model, the time-dependency of these parameters should be carefully considered (Veraverbeke et al, 2010); daily averages are useful for dynamic fire following models, while monthly or annual averages are very suitable for static prediction models.

2.1.4 Igniting conditions

The most complex factor in a fire prediction model is the igniting condition, which may be the reason that this component is often ignored, or overly simplified, in most of the models (Laris, 2013). For fires to start three conditions must be fulfilled: fuel, oxygen, and a heat source, also referred to as the “Fire Triangle”. From the three parameters, only for the fuel component is it possible to use remote sensing techniques to predict/identify the fire-starting condition. Recognising a “heat source” through modelling is not feasible because there are too many possible types of sources (both human-caused and natural, see 2.1.1). Oxygen can only be seen as a stable/constant factor at the start of a fire, after ignition the oxygen levels will change rapidly, decreasing in the centre of the fire and increasing at the edges (creating micro-climates).

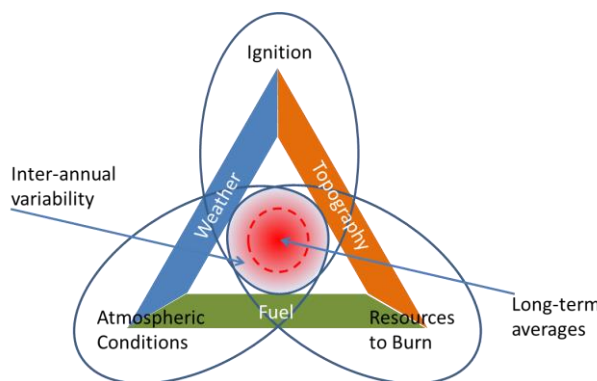


Figure 1: Fire Environment Triangle (adapted from Mortiz (2012) and Laris (2013))

Following Mortiz (2012) findings, the proposed method in this study also acknowledges the interactions between weather, topography, and fuel, which is controlling the ignition point and behaviour of a particular fire event.

Ignition (Figure 1) is now a function of weather and topography, presuming that there is enough fuel to start a fire. There is little (to none) literature on accidental fires, but can be placed into three groups:

- Fires initiated by a non-environmentally related activity (sparks from a high voltage power line, for example),
- activities related to environmental uses (like a campsite cooking fire) or,
- poorly managed controlled fires.

Distinguishing between accidental and planned fires is complicated because this requires local knowledge about practices and policies.

The Fire Environment Triangle is, therefore, a more suitable tool to model wildfire, and has the following components: weather (see 2.1.3), topography (see 2.1.2), and fuel (see 2.1.5) which are all three obtainable by either remote sensing or global predictive models (like in models as FARSITE and BEHAVE).

2.1.5 Fuel

Keane (2001) lists four possible techniques to obtain fuel maps; field reconnaissance, direct remote sensing, indirect remote sensing, and biophysical modelling. The first option is not feasible for large-scale models because this is a costly and time-consuming process. In local/small scale projects this is the most preferred method because it is the most accurate and has the least analytical error. Biophysical modelling is scale-depended and could be integrated into a Monte Carlo simulation to estimate the changes over time, but this is a complex technique and the least accurate because the obtained fuel map will be based on model results and not on observations.

The advantage of the remote sensing approach (either direct or indirect) over the other two is the data availability and the possibility to reuse the obtained products for other application; the largest disadvantage is the classification of the images.

One of the most common remote sensing products for a fuel map is the Normalised Difference Vegetation Index (NDVI), first used by Rouse (1973) and latter by Loveland et al. (2000) for the Development of a global land cover characteristics database, which is a numerical indicator that uses the visible and near-infrared bands (Yebra et al., 2013, p 461; Peterson et al., 2008).

NDVI is not the only index for biomass estimates derived from satellite data, other indicators obtained from remote sensing are for example:

Fuel Moisture Content (FMC): typically split into two components: dead and live, which normally is calculated from field measurements. Chuvieco (2004) used NDVI, Surface Temperature and a time component to derive the FMC for grass and scrublands.

Enhanced Vegetation Index (EVI): the advantage of using EVI over NDVI is the full use of the satellite sensors, where the NDVI only uses the Near Infra-Red and Red, EVI also incorporates blue (Huete et al., 2002). Biomass estimations models are often using both indices, because the NDVI performs better in grasslands, while the EVI will not saturate in forest areas.

Global Vegetation Moisture Index (GVMI): this index is used as a measurement of leaf water content, developed by Ceccato (2002), and is using the Leaf Area Index (LAI) and the equivalent water thickness (EWT). The EWT is the theoretical thickness of a single layer of water averaged over the whole leaf area and obtained by using both the short-wave infrared (SWIR) and the near-infrared (NIR) bands. The LAI is an estimate of canopies density, obtained through empirical fitting functions, using field observations and a (Normalised Difference) Vegetation Index.

Two other useful derived remote sensor products, from Moderate-resolution Imaging Spectroradiometer (MODIS), are the Burn Area (BA) and Active Fires (AF). They are not describing the amount of fuel in an area, but are an indicator of the fuel availability before the event (Chu and Guo, 2014). The BA product (MCD45A1) is monthly gridded 500m dataset which describes the approximate day of burning, the duration of the unchanged state, the pixel information includes land and atmospheric properties, using a predictive bidirectional reflectance modelling approach (Tsela et al., 2014; Roy et al., 2005; Justice et al. 2011; Veraverbeke et al, 2014). Tsela argues that the combining the BA product with the MODIS direct broadcast (DB) burned area product (MCD64A1), which is using detected active fires as a training set, could potentially improve the detection of small burned area (Hoelzemann et al., 2004).

The MODIS Active Fire product (MOD14A1) has an aggregated resolution of 1 km, and reports the daily present of active fires by comparing the surface temperatures

obtained from the Near-Infrared and red bands between overpasses (Roy et al., 2008; Giglio et al., 2003). The BA product has a higher resolution, and will report smaller fires (e.g. burnt areas), while the AF product is only able to detect intense burning fires at the time of the overpass (Hawbaker et al. 2008). Relying on only one fireproduct is discouraged by Freeborn et al. (2014), therefor combining the AF and BA products could provide a search window to find the most characteristic parameters for wildfire ignition.

2.2 Literature Review: Wildfire Models

Modelling forest or wildfires started roughly 40 years ago, with the first fire following model developed by Rothermel in 1973 (Wells, 2007). Rothermel (1973) used a mathematical approach to predict the fire spreading. The Rothermel model consists of 13 fuel models (to describe the fuel conditions in the field) and is using the spread rate, intensity, and flame length under any combination of slope steepness, wind speed, and moisture content, to predict the fire behaviour (Scott and Burgan, 2005) .

2.2.1 Wildfire following models

Finney (1998) saw the potential of Rothermel's model and developed FARSITE, which is using Rothermels equations in combination with weather forecasts (for an improvement of the wind speed assessment) and geographical information (e.g. fuel maps and topography). Examples of other (more sophisticated) fire following models are:

- BehavePlus; uses Rothermel's equations, among ~30 other equations, to forecast and predict wildfire behaviour, and the effects of the fire environment (Andrews et al., 2003).
- Rare Event Risk Assessment Process (RERAP); is a program which calculates the probability that a fire will reach a particular point, before a fire-ending event occurs, by combining weather, fuels, topography, and Rothermel's surface spread and crown fire models on a straight-line transect (Papadopoulos and Pavlidou, 2011).

- FlamMap; is using the same input parameters as FARSITE, and calculates the fire potential over a landscape by keeping constant weather and fuel moisture conditions (Finney, 2006).

Wildfire following models are useful tools for assessing the local fire risks, and environmental conditions, for decision makers and providing detailed information about the fire characteristics. The drawback is that these models require in-depth knowledge (e.g. weather, topography, fuel conditions) of the regions where the model is deployed, and are therefore not useful for risk assessments in data poor environments.

2.2.2 Wildfire Risk Models

Wildfire Risk Models are primarily based on structural or long-term indices (e.g. topography, vegetation), because the risk assessments are attempting to quantify the worst-case scenario, and the use of the temporal variation of the short-term indices (e.g. weather) are better suited for pre- and post-event decision making. (Chuvieco et al., 1997). Most forest departments in countries with a history of wild/forest fires have deployed a model for risk assessment, and in general, all reviewed models are using the same basic parameters to estimate the worst-case scenario. The increasing availability of digital data and Geographic Information Systems (GIS) has made it possible to create regional risk models, such as multi-criteria risk evaluation or expert risk systems (Sirca, 2017).

2.2.3 Wildfire Predictive Models

This third type of model is trying to address the uncertainty in the data by applying a probabilistic approach to the problem. The previously discussed models are using single value input layers, and generating a single output layer, not allowing the introduction of uncertainty in the processes. Probabilistic Predictive models are allowing for random fluctuations in the input variables and predicting a range of fire risk scenarios (Quill, 2016).

Probabilistic Predictive modelling is closely linked to Tobler's (1970) first law of geography, in which he states that "All things are related, but nearby things are more related than distant things". Following this law, the predictive models will look not only in spatial dimensions for relationships but also through time, where fire occurrences in the past are examined to find patterns in the future (Alexander and Cruz, 2013).

2.3 Relevancy

All models in the literature review are either using very detailed local data sources or complex fuel models, in combination with sophisticated software to compute the wildfire risk in a region. The difference between the methodologies described in the literature review and applied in this thesis is the use (and combining) of globally available datasets to determine the local wildfire risk. Particularly, in areas where for example high-resolution data, or mereological measurement stations, are not available the use of a more generic approach for calculating the fire hazard could help decision and policy makers to identify areas with a high-risk factor.

3 Model Architecture

There are several designs to model wildfire; in this study wildfire risk is identified by using two sub-models: Topographical Risk and Vegetation Risk. The result of the two models is combined to form the final risk score. A third sub-model (climate) is the time-dependency model and is used to propagate the wildfire risk by week by setting a drought scoring for the three study areas.

3.1 High-Level Design

The proposed model is modular, and the study area is the central part of the model (Figure 2). The model is divided into three submodules, using globally available data (see Appendix I for an overview of the used materials). The purpose of this model is to provide a method which could be applicable worldwide, and would not depend on local information; the rules found in the literature are only describing the default relationship of the parameter, the final form of the curves used is data-driven. The advantage of using a modular structure is that this setup is applicable for detailed studies as well because both the data and the literature sources can be adapted to reflect the local conditions.

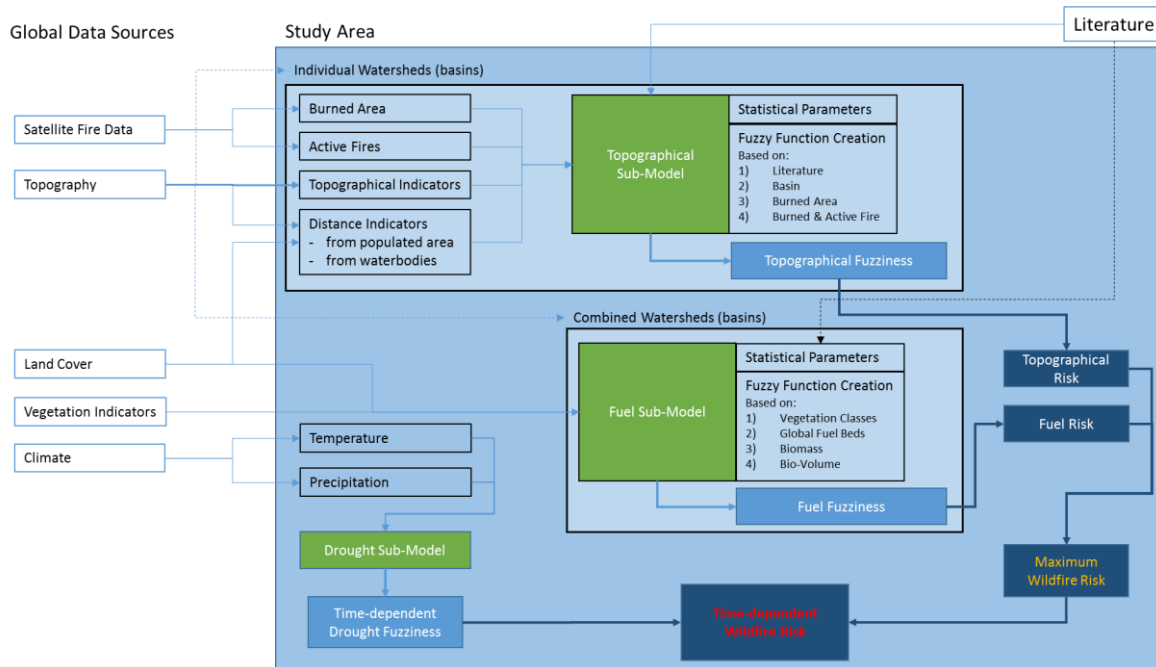


Figure 2: Schematic overview of the model components, and information flow

Most of the functions used in the topographical Sub-Model are data-driven and based on statistical parameters (min, max, mean) for the basin, burned area, and areas affected by fire within a burned area, but supplemented with a curve for which the shape is based on literature reviews.

In the topographical Sub-Model, the study area is divided into smaller statistical units (basins) because the topographical indicators are derived from topographical and hydrological functions (f.e. slope, aspect, flow accumulation). Applying those functions on the whole study area as global parameters would create a biased scoring. For example, in a study area, one basin could have an east-west orientation, with steep slopes on the south side of the hill, while the others basins have a north-south orientation. In this scenario, the most fire-prone hillside would get a low scoring if the score were not calculated for each basin and later combined to one topographical risk score for the whole study area (see 3.3.2 for more details on the calculations).

In the Fuel Risk Sub-Model the risk score is calculated for the whole study area, and not basin by basin. The used information to calculate the score did not allow a subdivision to basins because the spatial resolution is too coarse to calculate the basin score and aggregating this score up in the second phase.

Within the two submodels, the data is transformed to a grid based fuzzy membership function (a score from 0 to 1) with a spatial resolution of ~100m and translated to a risk scoring. The Topographical and Fuel Risk scores are then combined by averaging the two scores on a cell by cell basis; this is the Maximum Wild Fire Risk. The Time-Dependent Wildfire Risk Score is obtained by multiplying the weekly (or daily) drought risk (a score from 0 to 1) by the maximum risk score, at the period with the highest drought score the local wildfire risk has reached its maximum, and will not exceed a score of 1.

The Drought Index (KBDI) developed by Keetch and Byram (1968) is used to calculate the Time-dependent Drought fuzziness for a study area. At the moment this is one curve for all the cells in a study area.

However, it would be possible to create a cell based drought fuzziness, see the discussion in section 4.1.4 for a more detailed view of the possibilities to introduce a cell-based KBDI, and therefore cell-based Time-dependent Drought fuzziness function.

3.2 Model Description

3.2.1 Data Components

The information structure in this study is adapted from a study Vadrevu did in 2009, while he was exploring the use of Analytical Hierarchical Processes (AHP) and fuzzy systems in wildfire research (Figure 3).

To summarise, the *Basins* are obtained from the HydroShed (*Hydrological data and maps based on SHuttle Elevation Derivatives*) dataset, the DEM, as pure elevation, and second level derivatives capture the *Topography*: aspect and slope. The topographical Wetness Index is a third level derivative and calculated by dividing the flow accumulation by the slope (Wilson and Gallant, 2000)

Both the land cover and fuel bed data is used in the vegetation layer and will be fuzzified by using either the same trapezoid methodology as mentioned before or by simple step functions. Climatological indicators are not used in the first phase of the risk classifications, but brought in later to highlight the most critical time period, combining temperature and precipitation to calculate the overall drought index for the three study areas (Alexander (1990).

Fire products, in the model subsets from the MODIS active fires and burned area product are used.

All used data sources are brought together in a Geo-Database, which will have two levels:

- Raster data layer, where the resolution of the raster data is set to be the minimum resolution, which is ~100m
- Time series data layer, the original data is stored in NetCDF format, organised by year, in variable spatial resolutions with a daily temporal resolution, but brought into

the Geo-Database as tables (in the form of extracts from the original NetCDF files for the three study areas).

- Then there is a small portion of the database reserved for shapefile data; this section will store the basins (as polygons) and the burned area pixels as points (for visualisation purposes).

A summary overview of the used layers is presented in Appendix I.

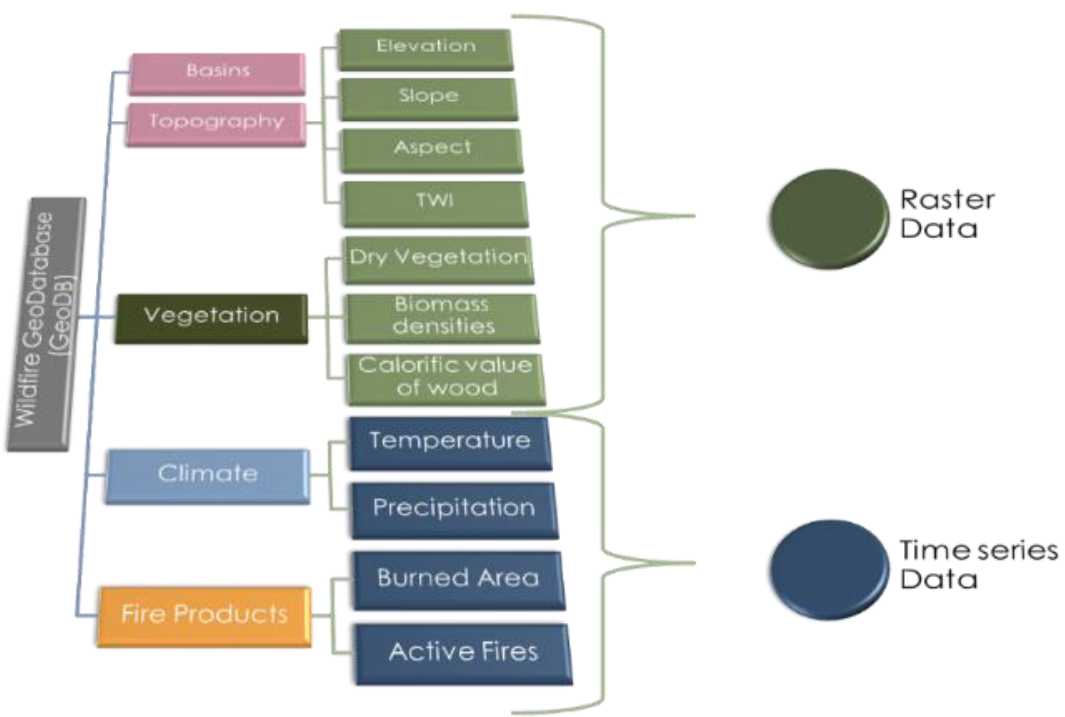


Figure 3: Geo-Database design, adapted from Vadrevu (2009)

3.2.2 Fuzzy Functions

The risk scores (as shown in Figure 2) are computed by using a Fuzzy Logic approach, introduced by Zadeh (1965) and are ranging from 0 (weak) to 1 (strong), based on statistical properties within the study area or a subsection (basin) of the study area. Fuzzy Logic relational functions can have many shapes, most often a linear function is used, but as more information or data is available to describe the relationships more complex forms can be used.

Robinson (2003) found that Gaussian relationships are most commonly used in GIS applications and that, despite the simplicity of the function, the trapezium form for creating a membership function is not applied often. In this study, the relationships are described by using a trapezoid form because creating a Gaussian curve would presume a high confidence in the statistical constraints of the used parameters. In this study, coarse datasets are used, with a high level of uncertainty around the found values, using a Gaussian curve to describe the membership would, therefore, implying high confidence in the used information.

A closed trapezoid function is used with three linear functions; a minimum function (membership from 0 to 1), a constant function (membership is 1) and a maximum function (membership from 1 to 0). The start, and end, of the constant function is set to be one standard deviation away from the average. In the topographical submodel, the final function is a composite of the theoretical function, global basin function (B), the parameters within burned areas (BA), and the areas where active fires (AF) are detected. This process is illustrated in Figure 4 for elevation in a sample basin.

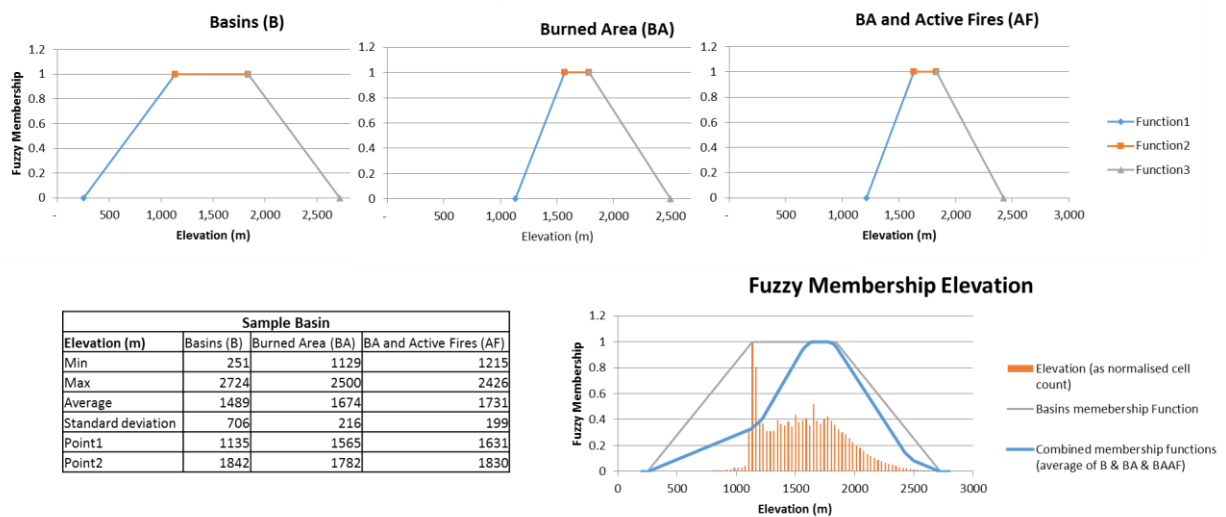


Figure 4: Fuzzification of Elevation for a sample Basin

To transform the data into a suitable form to analyse the fire occurrences a fuzzy logic approach is taken, for which in this example the **elevation (m)** is expressed in **membership functions** of 0 (weak) to 1 (strong), again following the logic described by Zadeh (1983) to combine probability theory with fuzzy logic.

For the other parameters (derived elevation indexes, climate, vegetation) similar functions will be used. To transform the elevation from DEM to a fuzzy membership five points are used:

- A minimum elevation of 251 meter,
- a maximum elevation of 2724 meter,
- an average of 1489 meter,
- and $\frac{1}{2}$ the standard deviation around the average, brings the maximum of the first function to 1136 meter, and the start of the third function at 1842 meter.

The trapezium is constructed with three functions:

- $Y = 0.0011x - 0.2836$ for which x is larger than 251 and smaller than 1136m,
- $Y = 1$ for which x is larger than 1136 and smaller than 1842m, and
- $Y = -0.0011x + 3.0889$, following the general equation: $y = mx + c$

The compact form of this function is: $\mu(x) = \max(\min\left(1, \frac{x-\alpha}{\delta-\beta}, \frac{\delta-x}{\delta-y}\right), 0)$

The membership function of the basin will be combined with the elevation under the Burned Area (BA) and the Active Fires (AF) in the burned area, following the same logic, but using different points to construct the trapezium (table in Figure 4).

The final curve is an average of the three functions because the intent is to find the most elevation which for which the fire risk is the highest and using only the elevation will overestimate the risk, while only looking at the elevation under the burned areas will underestimate the risks. In this example, the right sided linear function is almost not altered by the averaging (all sources are in agreement) while the left-hand side is now much slower reaching the maximum membership (1).

When this averaging was not applied most of the elevation in the basin would be under an elevation risk, while now the most vulnerable elevations are between ~1800 and 2200 meter.

3.2.3 Defuzzification and Scoring

As shown in Figure 1 there are many (spatial) relationships and dependencies while modelling wildfires; some are obvious, like temperature and elevation, others are only manageable through an indirect index, like wetness and seasonality. In the proposed model those dependencies are captured in this Fire Environment Triangle (Fuel, Weather, Topography). The Drought Index indirectly addresses seasonality and Atmospheric Conditions (see Figure 1), the resources needed to keep a fire burning are part of the Fuel submodel, and igniting conditions are conditioned in the topographical submodel and enforced by the time dependency in the model.

In the topographical sub-module six themes are combined to one risk scoring layer (Figure 5), the fuzzification process ensures that the relationships within a theme are preserved, the weighting of the themes are governing the relationships between the layers (the higher the weight, the more confidence a theme has in the model). The Topographical wetness index (as a combination of flow accumulation and slope) and aspect are the two most important layers in the sub model, elevation and the distance layers are valued less important.

The theme risk score is calculated by taking the average fuzzification plus $\frac{1}{4}$ standard deviation value as the average rating (3: medium risk), the other classes have half a standard deviation spacing (1: very low to 5: very high risk).

Fuzzification Results		Defuzzification Process			Min. Risk Score = 11 Max. Risk Score = 53 Range = 42	
Fuzz. Result By Cell	Risk Score	Theme Weight	Weighted Risk Score			
0.7	5 (max)	1	5			
0.2	1	3	3			
0.6	3	2	6			
0.4	2	3	6			
0.6	4 (max)	1	4			
0.8	4 (max)	1	4			
					28 (summed risks)	
						Cell Risk (28-11)/42 = 0.40

Figure 5: Risk Scoring of a sample Cell

The fuel model follows the same logic, but could not be constructed in the same way because the used data layers are not a contiguous raster layers; there are too many areas with "No Data", and the resolutions are not the same. The information for the fuel model is based on much coarser grids (respectively $\sim 300\text{m}$ and $\sim 1\text{km}$). Therefore another approach has been designed to assign fuel membership values to different land cover classes (Figure 6).

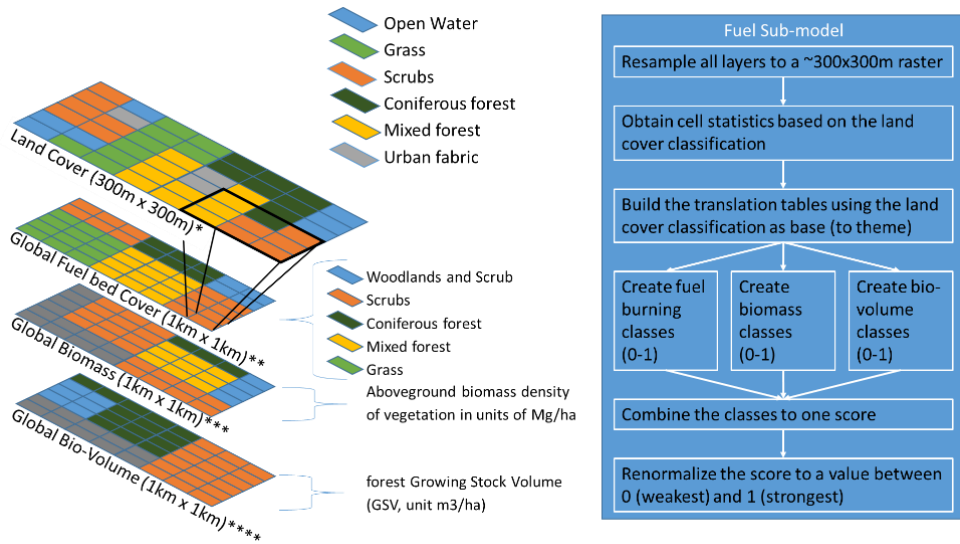


Figure 6: Fuel Sub-model information use and workflow

The Fuel sub-model is based on the land cover, using 44 land cover classes, from ESA (20014) because from all globally available datasets, this dataset is focussed on vegetation and has a spatial resolution nearest to the final resolution of the model ($\sim 100\text{m}$). The other three data layers are resampled (and aligned) to match the land cover dataset. The land cover classes are used as a mask to obtain the underlying spatial data, e.g. fuel bed codes, biomasses (Mg/ha), and biovolume (m³/ha). The global fuel bed cover (Pettinari, 2016) is using the GlobCover landcover and Olson Biome classification to map fuel bed characteristics; a translation table is constructed giving the probability of the presence of a fuel bed class inside the land cover class, these used as one-to-many relationships. The global fuel bed cover consists of 360 unique land cover classes, describe by 70 different parameters.

In this study, only the burn loads are used (sound wood, 1/10/100/1000hr loads in Mg/ha) to calculate the fuel burning score. For each of the 360 vegetation classes, the loads are regrouped in a dry (1 & 10hr) and a wet (100 & 1000hr) load. Within each class, the fuel score is a unique combination of the loads inside each class, and the ranking of all the scores inside the group; a more detailed explanation will be given in section 4.1.3, in which Table 8 shows a calculation example, comparing scrublands between the study areas.

For the global biomass (Thurner et al., 2014), and volume (Santoro et al., 2015), the ratio of the sum of the values inside a land cover class divided by the total value (in the study areas) is used as a membership function.

The final fuel score is the average of the biomass and biovolume ratios, for which the ratios are corrected by multiplying the ratio with the fuel class ((bio-volume ratios * fuel class)+(bio-volume ratios * fuel class) / 2). This score is then normalised to values between 0 and 1 to preserve the relationship between the most, and least, burnable land cover class.

In the next step of the program, the Topographical and Fuel Risk scores are combined to one risk score (Maximum Wildfire Risk: Figure 2). In the validation section, the maximum wildfire score is compared with the active fires in burned areas and adjusted (calibrated) by using a ROC curve identifying the most suitable regional factor to maximise the score or match to the active fire count in burned areas. Finally, the drought index is used as a time-dependent function, where the maximum wildfire score is increasing following the equation in Figure 7.

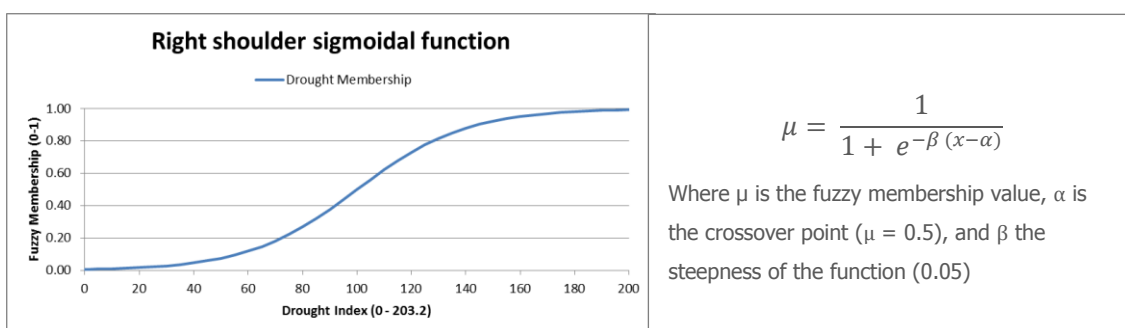


Figure 7: Right shoulder sigmoidal function to transform the drought index to a scoring. Adapted from Robinson (2003).

The found membership value is used to decrease the maximum wildfire score for each week, based on modelled historical climatology information. Using the sigmoidal function instead of the linear scale developed by Keetch/Byram Drought Index (KBDI), as shown in Figure 7, more emphasis will be placed on the mid ranges of the drought index (Table 2: KBDI ~73-130 or ~300-500). The function is designed to create a gradient around the mid range of the values, while the low and high ends of the curve are less important (low DI = low risk, high DI = high risk). In Table 3 the membership values are translated in a drought condition and climatological correction factor, the maximum risk score is multiplied by this factor to get the time-dependent risk indicator.

Table 2: Translation table to go from KBDI values to membership values

KBDI (English units)	KBDI (S.I units)	Membership values
700 - 800	177.8 - 203.2	0.98 - 0.99
600 - 700	152.4 - 177.8	0.93 - 0.98
500 - 600	127 - 152.4	0.78 - 0.93
400 - 500	101.6 - 127	0.5 - 0.78
300 - 400	76.2 - 101.6	0.22 - 0.5
200 - 300	50.8 - 76.2	0.07 - 0.22
100 - 200	25.4 - 50.8	0.02 - 0.07
0 - 100	0 - 25.4	0.01 - 0.02

Table 3: Translation table to go from membership values to drought conditions

Membership values	Drought conditions & factor	KBDI (S.I units)
0.8 - 1.0	Very dry (1)	129.33 - 203.2
0.6 - 0.8	Dry (0.8)	109.71 - 129.33
0.6 - 0.4	Normal (0.6)	93.49 - 109.71
0.2 - 0.4	Wet (0.4)	73.87 - 93.49
0.0 - 0.2	Very wet (0.2)	0 - 73.87

3.3 Implementation

3.3.1 Study Areas

For the proof of concept three areas of interest are chosen:

- North America: California/ Nevada
- South Europe: Spain (Valencia)
- North Asia: Mongolia (Gobi Altai)

The main reason for selecting these areas is that they are on the same hemisphere, at approximately at the same longitude (thus having roughly the same angle towards the sun, receiving the similar amounts of sun hours and intensity), and on three different continents far from each other, and identified by the MODIS Burned Area product as being burnt (more than 2000 pixels classified as burned within the selected area). The areas were not selected because of their history of forest/wildfires, neither because there would be enough fuel to start fires. The areas were chosen to test the hypothesis that a wildfire model can be constructed with coarse globally available datasets anywhere, and yield sensible results.

The selected study areas are approximately the same size, although the one in North America is slightly larger than the other two, and with the same number of basins, hence the slightly larger North America area (Figure 8, and for a more detailed view of the study areas Appendix II). The study areas are only used as an envelope for data extraction, the topographical analyses are done at basin level, while the fuel availability study is performed on the combined basins within a study area.

The reason basins/watersheds/catchments are used to delimitate the limit for the topographical analyses this threefold:

- a) The global climatological conditions within a basin are likely to be uniform
- b) The water balance within a basin is closed; this is important for the flow accumulation calculations, within a basin there are no sharp edges where water can disappear water will accumulate to the lowest points within a basin

- c) The model domain (catchments) remains manageable; modelling an area of 150 by 100km is more complex (time-consuming) than doing the same analyses in an area of 15km by 10km while working with a ~100m raster resolution.

For the fuel availability study more coarse datasets are used (~1km raster resolution), therefore working on basin level there would be not enough variation to draw conclusions on the fuel availability.

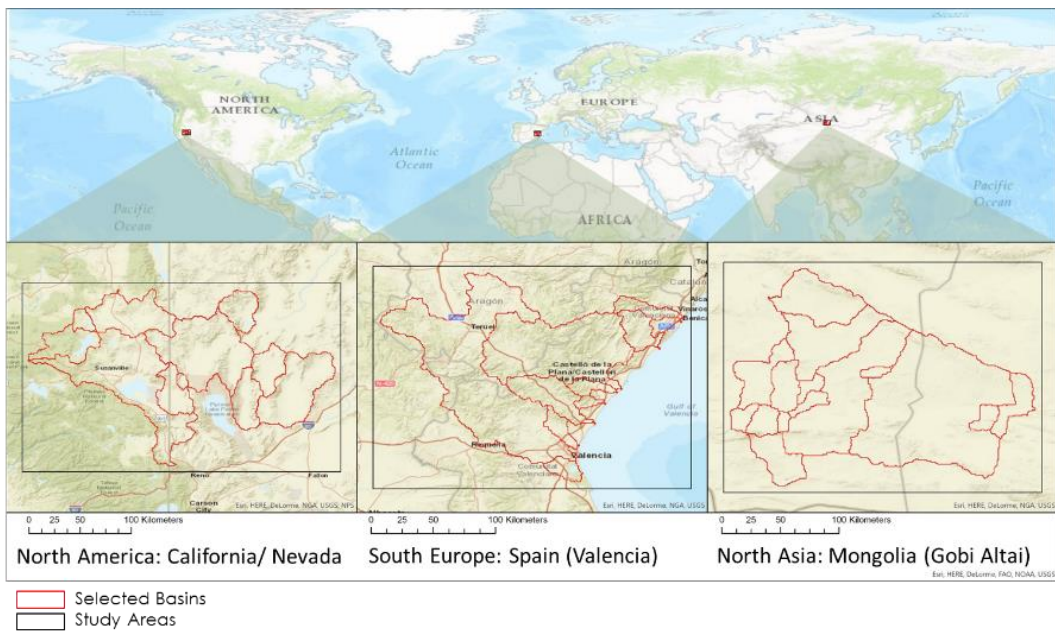


Figure 8: Study Areas

North America: California/ Nevada

The study area in North America is situated on the border of California and Nevada in the counties Lassen (CA), Washoe (NV) with the largest populated area the city of Reno (just south of the selected area), and Pershing (NV). The north-east of California and west Nevada is a remote area, with no large settlements, Susanville (CA) is the largest town in the study area. The terrain is mountainous and volcanic active with hot mud pits and springs (e.g. the last eruption of Mt Lassen was in 1915 (Clyme et al., 1999) which is located west of the study area), with a overall elevation range of 2750m; the highest peak in the study area is Hat Mountain in the north part of the study area.

There are three large lakes (Pyramid Lake, Honey Lake, and Eagle Lake) within the study area, surrounded by four national (forest) parks, while the centre of the study area is primarily desert and sparsely vegetated. The rivers and stream coming down from the mountains are feeding the lakes with the snowmelt during spring; the rest of the year most of the streams are dry, and the lakes are slowly losing their water.

The climate of the study area is defined as Cold Desert (*BWk*), using the Koppel classification (Peel, 2007; Trewartha, 1943), with a small section in the west as "hot-summer Mediterranean" (*Csa*). The landscape is arid, because the evaporation exceeds precipitation (B) and the mountain ridge between the study area and the ocean blocking the rain-bearing winds (W instead of S(tepe)), and even that the maximum temperatures can reach +40°C, the Mean Annual Temperature is below 18°C (k).

South Europe: Spain (Valencia)

The second study area is in Spain, on the east coast, roughly between Valencia (in the south), Castelló de la Plana (in the middle), and Benicarló (in the north), covering most of the province of Castellón, and the southern part of the Teruel Province (with Teruel as the largest city). The terrain is hilly, at the coast, to mountainous, with the Sistema Ibérico mountain range on the border Castelló and Teruel. The Sistema Ibérico mountain range runs northwest-southeast between the Ebro plain and the Meseta Central with the highest peaks in the Teruel province. The elevation in the study area ranges from 0 (at sea level) to 2000m (with the Javalambre (2020 m) as highest point). The vegetation on the mountain slopes is primarily Pine and Oak, with an undergrowth of Juniper (Garcia and Montero, 2000). Aragó (2016) concludes that the topography and geology of Castellón, in combination with the agricultural land use, is allowing for the existence of a wide variety of vegetation types. The most dominant vegetation type is coniferous forests, followed by oak and mixed forests, and a patchwork of shrubs, grasslands and agricultural land covers (e.g. wine yards).

The climate of Castellón is comparable to the climate in California/Nevada, with the exception that proximity to the Mediterranean sea is affecting the annual rainfall, and is therefore classified as BSk according to the Köppen-Geiger climate classification. The average temperature in Castellón below 18°C, and the evaporation exceeds precipitation during the dry summer months, but the annual precipitation is high enough to be classified as Steppe (S) instead of Desert (W). The coastal zone is less arid, and has a Mediterranean climate (C), with dry (s) and hot (a) summers.

North Asia: Mongolia (Gobi Altai)

The third study area is in the Gobi-Altai province, Mongolia, near the border of the People's Republic of China, and Bayankhongor to the east. It is the most remote study area, with no large settlements or infrastructure. The terrain is mountainous and consists of steppe grasslands, rocky landscapes with low hills, the high mountains of the Altai Mountain range and sandy desert of the Gobi. The vegetation in the study area is sparse and identified by IFADAsia as lowland, desert-steppe bunchgrass with brushy plants of the steppe, and Saxaul forest (Figure 9). The Ministry of Nature, Environment and Tourism (2011) has acknowledged Saxaul forests as the primary source of firewood, and the steppe vegetation as most vulnerable to wildfire.



Figure 9: Saxaul forest in the Gobi (Suvdantsetseg et al., 2008, p. 1084)

The mapping of this vegetation type is almost impossible due to the remote locations and extreme conditions; Suvdantsetseg et al. (2008) concludes that remote sensing (RS) techniques alone are not enough to locate, and assess, this type of vegetation, and to estimate the biomass ground surveys are necessary to complement the RS analysis, which is also the position of the Chinese Forest Fire Management (CFFM).

The Gobi-Altai has a typical cold desert climate (BW k), with extreme day/night temperature variation. During the winter, the Gobi Desert experiences extremely low temperatures, which contribute the cold (k) classification; the annual mean temperature in the study area is <10°C.

During the rainy season (June-August) most of the annual precipitation (<48mm) will fall, this is also the warmest period, with the highest temperature over +30°C in July.

3.3.2 Topographical Risk Database

The topographical risk database (Figure 10) is constructed as a relational hierachal database; the top level is the study area, which is broken down into smaller areas (basins). The global data sources are brought into the database based on the study area, and linked to the basins by a unique basin ID. The basin characteristics (topographical parameters) are stored by basin ID, as well as the land cover, so that there is a consistent set of parameters. The Burned Areas, and the intersection of Burned Area and Active Fires, are converted from point locations to raster files by first converting the points to a grid (in the same resolution as the original resolution) and then rescaled to the target resolution (~100m). A simple binary operation calculates the intersection: Burned Area (BA) = 1 and Active Fires (AF) = 1, BA * AF = BAAF (1), which is the intersection of the two raster files. Both datasets (BA & BAAF) are converted to polygons and linked back to the Basins, so that the Basin ID can be placed on the points (in order not to lose the time element of the fire occurrences).

Within the topographical sub-model the (four) fuzzy membership functions are constructed for each of the indicators, and the result of each fuzzification is stored in the database as one raster layer (six components). The individual components are weighted, and the average of the weighted layers is saved as the final Topographical Risk Layer (by study area), following the logic in Figure 5).

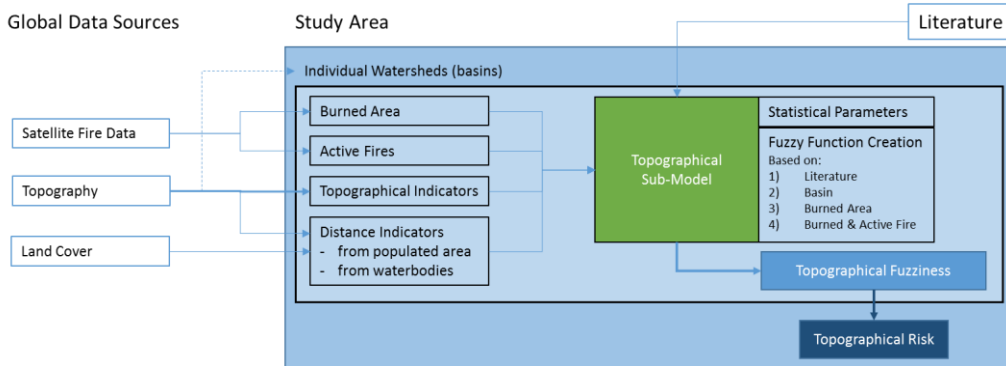


Figure 10: Schematic overview of the Topographical Sub-Model components, and information flow

The parameters for the “Literature Function” has been extracted from various sources, see paragraph 2.1.2 for details, and used as a first filter. The Basin characteristics, e.g. the minimum, maximum, average, and standard deviation, are the second filter. To compute the characteristics each layer the zones (Basins) are analysed using a GIS function: zonal statistics (in ERSI ArcGIS Pro); the functions for BA and BAAF are constructed using the same technique.

3.3.3 Fuel Risk Database

The structure of Fuel Risk Database (Figure 11) is a relational hierachal database, but instead of breaking the study area down by basins the study area is divided into land cover classes. The Land Cover product from ESA is listing 36 distinct land cover classes, of these classes 29 can be used as the basis for a fuel model, the others covers are either classified as bare, urban, water, or “no data” cover.

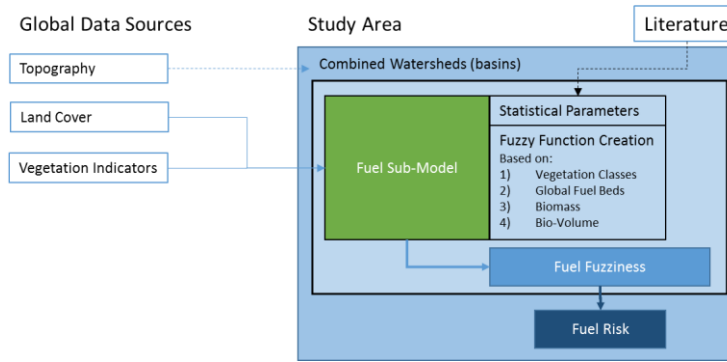


Figure 11: Schematic overview of the Fuel Sub-Model components, and information flow

The second layer in the database is the “Global Fuel Bed” product, which is combined with the land cover data to get a mapping between most probable fuel-bed to land cover. Both, the land cover and “Global Fuel Beds”, are converted to a raster (with a ~100m resolution). There are 359 unique fuel beds, which are overlayed with the land cover data, so it is possible to construct a unique combination of fuel beds per land cover class. This unique combination is used to retrieve the fuel load and assign a fuel score. The fuel score is a composite of the four fuel load values and their distribution within the land cover class (based on total area of the fuel class within the land cover area). In the “Global Fuel Beds” dataset the fuel loads are discrete e.g., 0.1, 0.2, 0.3, for each vegetation class, these discrete numbers are rewritten to a unique number for the four load types, e.g. 20 for 0.1 in 1h/ha, or 1900 for 0.9 in 100/ha (Table 4).

Table 4: Reclassification tables for fuel loads

1 hour		10 hours		100 hours		1000 hours	
Fuel Load	Code	Fuel Load	Code	Fuel Load	Code	Fuel Load	Code
-3	0	-3	0	-3	0	-3	0
-1	0	-1	0	-1	0	-1	0
0	10	0	0	0	1000	0	0
0.1	20	0.1	1	0.1	1100	0.1	1
0.2	30	0.2	2	0.2	1200	0.2	2
0.3	40
...
...	...	0.7	7	0.9	1900	2.6	20
0.9	8	0.9	8	1	2000	2.9	21
				1.1	2100	3	22
				1.2	2200	5.8	23

In the next step the codes are combined into two sub-classes; wet and dry and linked back to the vegetation class table. For example, Fuel bed code 924040, 4 - Temp. Broadleaf and Mixed Forests has the following fuel loads: 0.1, 0.2, 0.3, and 0.4, which is now translated to a dry (1-10hr) code 22, and a wet (100-1000hr) code 1304. The codes for the two classes are assessed over the whole dataset, and a scoring is assigned to each vegetation class based on the presence of this class in the whole dataset.

The Dry/Wet fuel class (0-4) is based on the overall ranking of the fuel codes, in Table 5 the ranking, and score most of the codes is given.

Table 5: Relation between Fuel Codes (Dry/Wet) and their Classes

Dry Codes	Count of Dry	Cum. Sum of Dry	%Cum Dry	Dry Fuel Class	Wet Codes	Count of Wet	Cum. Sum of Wet	%Cum Wet	Wet Fuel Class
0	68	-	-	0	0	68	-	-	0
10	49	49	17%	1	1000	29	29	10%	1
11	81	130	45%	2	1001	5	34	12%	1
12	4	134	46%	2	1100	13	47	16%	1
13	1	135	46%	2	1101	42	89	31%	2
14	1	136	47%	2	1102	21	110	38%	2
21	37	173	59%	3	1103	6	116	40%	2
22	39	212	73%	3	1104	6	122	42%	2
23	18	230	79%	4	1105	5	127	44%	2
24	7	237	81%	4	1123	1	128	44%	2
31	17	254	87%	4	1200	1	129	44%	2
32	1	255	88%	4	1201	1	130	45%	2
33	4	259	89%	4	1202	24	154	53%	3
34	5	264	91%	4
35	2	266	91%	4
36	2	268	92%	4	1921	1	288	99%	4
37	1	269	92%	4	2022	1	289	99%	4
38	1	270	93%	4	2101	1	290	100%	4
42	21	291	100%	4	2211	1	291	100%	4
Total					Total				
Sum					Sum	359			
Fuel					Fuel				
Bed					Bed	291			

The final fuel class is based on both the dry and the wet class: $(\text{Dry Fuel Class}_i + \text{Wet Fuel Class}_i) / (\text{Max. Dry Fuel Class} + \text{Max. Wet Fuel Class})$ [8]. Fuel bed code 924040 has a Dry class of 4 (code 22) and a Wet class of 3 (code 1303), therefore a final score of $7/8 = 0.875$. This is the global scoring, and is in the sub-model adjusted for the presence (total area) of this class in the study area within the land cover class.

Also, the scoring of the biomass and bio-volumes is based on the distribution of volume, or mass, between land cover classes within the study areas.

3.3.4 Risk Product(s)

The final step is the combining the results of the topographical and fuel sub-models with the drought sub-model to create a time-dependent wildfire risk score (Figure 12). The Drought sub-model is the BKDI for the whole study area. Downscaling to a raster is possible (see 4.1.4), but falls outside of the scope of this study, in this study the BKDI is calculated for the whole study area as an average index. The index is transformed to a time-dependent drought fuzzy membership function, using the equation in Figure 7, and used with a week time step to determine the drought score over the whole year.

The initial maximum wildfire risk is the cell-by-cell product of the topographical, fuel risk layers and drought factor. This is the first guess of the maximum risk and is corrected with the intersecting area between gridded Burned Area points (~100m resolution) and Active Fires so that the most optimal score is preserved as maximum wildfire risk using receiver operating characteristic curve, or ROC curve, to adjust the wildfire risk.

The ROC curve is constructed using the full study area data for the initial wildfire risk score to find the fit of the model. A traditional academic point system (Table 6) is used for classifying the accuracy of the diagnostic test:

Table 6: ROC curve classification

Score	Description
>0.90 – 1.00	excellent (A)
>0.80 – 0.90	good (B)
>0.70 – 0.80	fair (C)
>0.60 – 0.70	poor (D)
>0.50 – 0.60	fail (F)
>0.00 – 0.50	Unable to classify

The data is broken down to 0.1 interval steps, and false positive/negatives are assigned based on the standard deviation (finding the “true” false positives/negatives in this type of data (with a generic method) is not possible/feasible)

By scaling the maximum wild fire risk up (or down), within the calibration area (BAAF), with 0.05 points the best fitted scenario (with at least a B classification) is passed as most representative wildfire risk for the whole study area.

Currently the model’s time-dependency is based on the BKDI curve for the study area, and to calculate the wildfire risk by week the maximum wildfire risk is multiplied by the BKDI factor for that week.

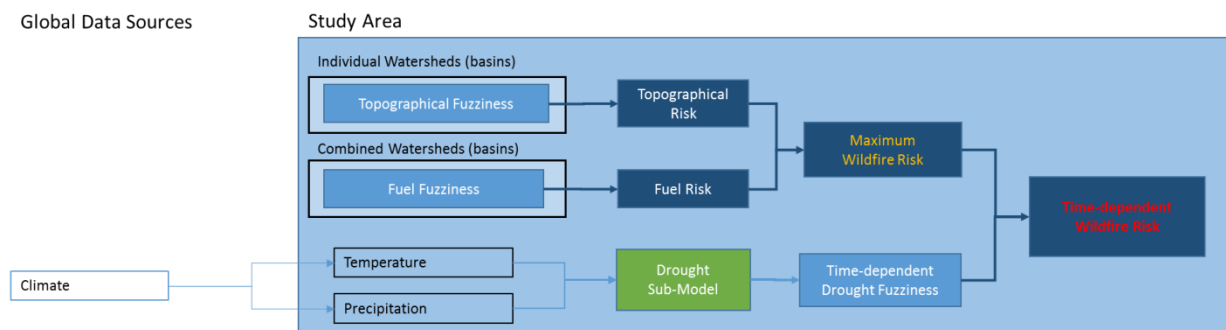


Figure 12: Schematic overview of the Drought Sub-Model components, Risk Products, and information flow

4 Methodology, Results, and Analysis

To test the usefulness of global datasets in the way described in the previous chapter the three study areas are following the same procedures, and the assessment includes the following hypotheses:

- There is a correlation between “burned areas” and “active fires”, e.g. both fire products will detect wildfire in the same location within the same time window (aggregated to a weekly time step). This correlation is crucial, for the following steps, because when there is no relationship between the two fire products the narrowing of the data search, to construct four trapezoid functions, is not possible.
- The trapezoid functions are, even when a simplification, capturing the basin characteristics sufficiently to construct topographical risk layers, and the merging the individual layers will form the topographical risk scoring layer.
- It is possible to combine land use, fuel loads, biomasses and biovolumes to one fuel score, which provide enough detail to distinguish between land use classes, and can be used to refine the risk scoring.
- The BKDI is, even when not downscaled, a useful indicator to determine the fire hazard over time.

In the next paragraphs the four hypotheses, forming the test case, are presented in the order as shown above and is identical to the information flow in the model (Figure 2)

4.1 Data-Analytics

The MODIS fire products are first analysed using the whole study area before breaking them down to basins (for the topographical risk scoring). The trapezoid functions for topographical risk scoring are based on the watersheds (basins) because applying one function to the whole area is not granular enough to capture the important topographical features e.g. dominant slope or aspect in a region. Furthermore, this will give an average score which will not be useful to determine the risk(s) on a local level. To investigate the usefulness of a fuel risk and the integration of the BKDI the whole study areas are taken into consideration, splitting the study area into smaller regions is not supported by the data, e.g. scale and resolution.

4.1.1 Hypothesis: The correlation between “Burnt Area” & “Active Fires is robust enough to be used as data filter

One of the inputs for the wildfire model is the Fire Product from the MODIS dataset; this study is using all available data in this series (2000/01 – 2016/01) for both the Burn Areas and Active Fires. In the MODIS algorithm, pixels are classified as Burned Areas (BA) when there is a rapid change in InfraRed and Near IR between the pixel and neighbouring pixels, and to detect Active Fires (AF) areas the algorithm is using estimated surface temperatures above a threshold based on IR measurements.

The resolution of the BA product is four times smaller than the Active Fire (AF) product. Therefore, the count of burned area cells is higher for the BA product (500m vs. 1000m). In Figure 13 the pixel count is normalised for both products to plot the relation between burned areas and active fires; the spatial selection is the intersection of BA & AF (the black and red dots on the maps in Appendix XXX), the filtered selection is a subset of this selection.

While there are areas classified as being burnt in Mongolia the algorithm detected no Active Fires. The burned area detection happened primarily in winter (in week 9 under subzero conditions), and this abnormally is most likely caused by the

reflectivity change of the bare rocks on south facing slopes (small patches, with the same behaviour, are spotted in the other two study areas).

For North America, the burned area and active fires are detected in the same time periods, with one exception in week 34. The relatively high amount of burned cells in comparison to the low count of active fires is due to a fast-spreading event, but this has a limited effect on the correlation between the active fires and burned areas.

When comparing the occurrence of active fire in burned areas there is a strong correlation ($R^2 \approx 0.871$), removing the outlying event makes the correlation slightly stronger ($R^2 \approx 0.895$).

The correlation between BA & AF in Spain is weaker overall, but very strong when one event is removed from the dataset. Smoke and cloud cover during the fire in 2012, week 26, made the burned area detection difficult, the time-lapse is approximately 4-9 days.



Figure 13: Correlation between Burned Areas and Active Fires in Spain (left) and North America (left)

The spatial distribution of the burned areas and active fires is very different for the between the study area, see Appendix II for detailed maps.

For North America, there is a good spatial relation between burned areas and active fires. In Spain, primarily in the coastal regions, there are more active fires detected without underlying burned areas; these fires occur in areas with an urban or agricultural land use (Table 7). The Corine dataset is used in combination with the ESA land cover classification because the classification in the Corine dataset is more suitable to identify agricultural land cover, where the ESA dataset is useful for the classification of natural land covers.

Table 7: Land Cover under (or near) Active Fires and Burned Areas

Aggregated classes*	Active Fires	Burned Areas
<i>Urban areas</i>	26.1%	-
<i>Agricultural Cover</i>	31.4%	12.2%
<i>Natural Vegetation</i>	31.2%	70.6%
<i>Other**</i>	11.3%	17.2%

* Combination of ESA CCI and the Corine Land Cover Classification
 ** Not agricultural or natural cover in either classifications schemes

Most of the burned areas in Mongolia are found on south – south-east facing slopes, further investigation is needed to determine why the reflectivity on these slopes are changing so much that the algorithm is flagging those areas up as burned area.

There are no active fires detected in the study area in Mongolia.

Conclusion: it is possible to use the Fire Product from the MODIS dataset as input for the wildfire model, but they can not be used as single data source to identify areas with a high fire risk. Neither will it be advisable to use a single product (either BA or AF), combining the BA data with the AF product will give a more precise assessment of the risk. In this study the BA and the intersection of BA with AF (BAAF) are inputs for the trapezoid functions, BAAF is afterwards used to validate the model using a ROC curve.

4.1.2 Hypothesis: Trapezoid functions for topographical risk scoring are sufficient detailed to construct a topographical risk layers

The Topographical Risk Database holds the topographical characteristics of the study areas organised by basins for seven themes (Elevation, Aspect, Slope, TWI, Distance to Population, and Distance to Water, similar to the indices Chuvieco and Congalton used in their study (1989)). The general function, to calculate the risk membership, is a trapezoid, based on the standard deviation around the mean (membership = 1), minimum, and maximum (membership = 0). It is possible to calculate the risk memberships with functions, but the aim is to create a generic model which can be applied everywhere.

In the paragraphs below all six themes are addressed and explained with the use of an example basin (Spain – 119758). The same method is used for all other basins in this study; the result maps by theme are presented in Appendix IV for the three study areas.

Elevation

The elevation in the basin has an elevation range of 0 to 1250m (Figure 14), with the most dominant elevation range of 300 to 475m (Basin Function (B)) based on $\frac{1}{4}$ standard deviation around the average elevation. The Burned Area (BA) and Active Fire region (BAAF) are within this range as well; this explains the bell-shaped curve around the average elevation. Because of this narrow band, the maximum elevation membership (1) is found at mid elevation on the slopes and most profound on the south facing slopes of the Sistema Ibérico mountain range in the North of the basin.

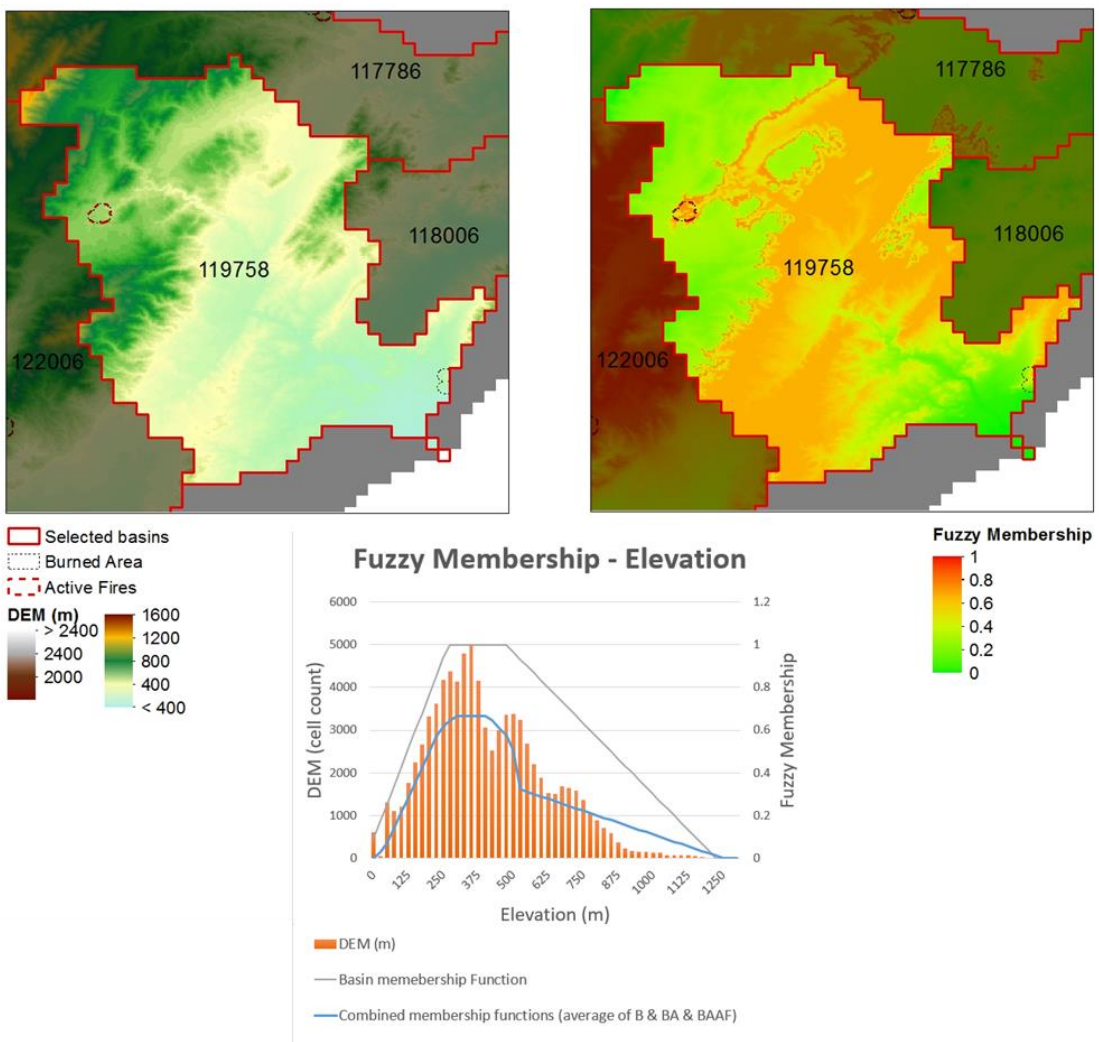


Figure 14: Fuzzy Membership - Elevation

Aspect

From literature (Adab et al, 2011; Balga, 2012; Burgers, 2011, Banu et al, 2014, Chuvieco and Congalton, 1989) an initial curve is designed, based on the assumption that South facing slopes (in the northern hemisphere) have higher temperatures, collect more sunlight, have a lower humidity, and contain less soil moisture. East facing slopes, compared to west facing slopes, have more favourable conditions since these slopes receive the most ultraviolet light during the day. In the literature, the maximum membership (1) is found between an aspect of 120 to 240 degrees, with the south facing slopes on 180 degrees. The basin functions (B, BA, and BAAF) are following the literature curve closely (Figure 15).

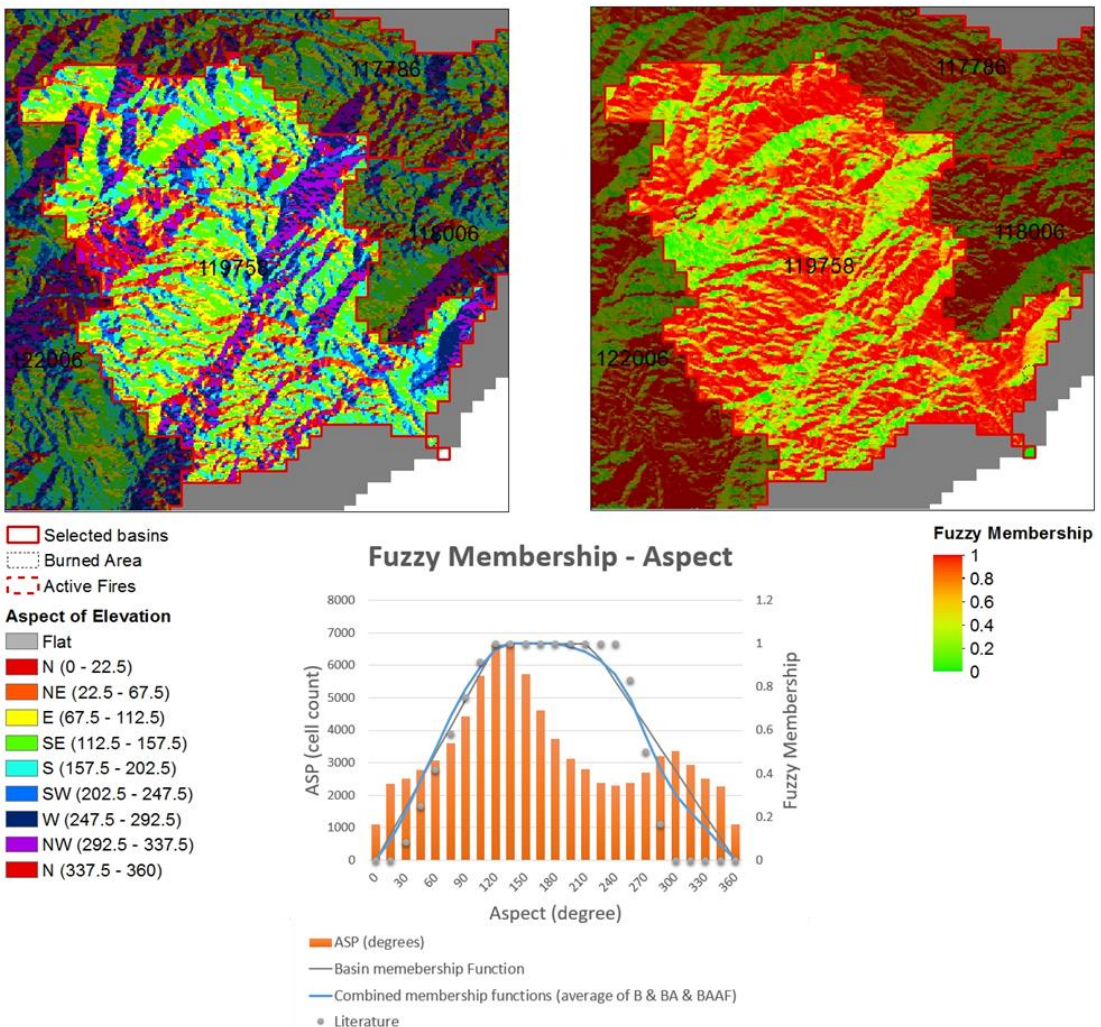


Figure 15: Fuzzy Membership - Aspect

Slope

Rothermel (1991) found that “Slope” is one of the most influential parameters on the behaviour, and spread, of wildfires. The steepness of the slope (and direction) determines the intensity of the fire, steeper slopes are burning faster and more intense, due to the proximity to the fuel. The literature cure starts, therefore, more rapidly and declines more slowly, with a maximum membership (1) between 25 and 65% (100% is a slope of 45 degrees).

Within the example watershed, most cells have a slope smaller than 15%, which means that the maximum slope membership (1) for the basin can not be reached and is around 0.5 (+/- 0.1).

This will have a profound effect on the final risk score because this will mean that the topographical risk will not be higher than 0.8 for this basin (Figure 16).

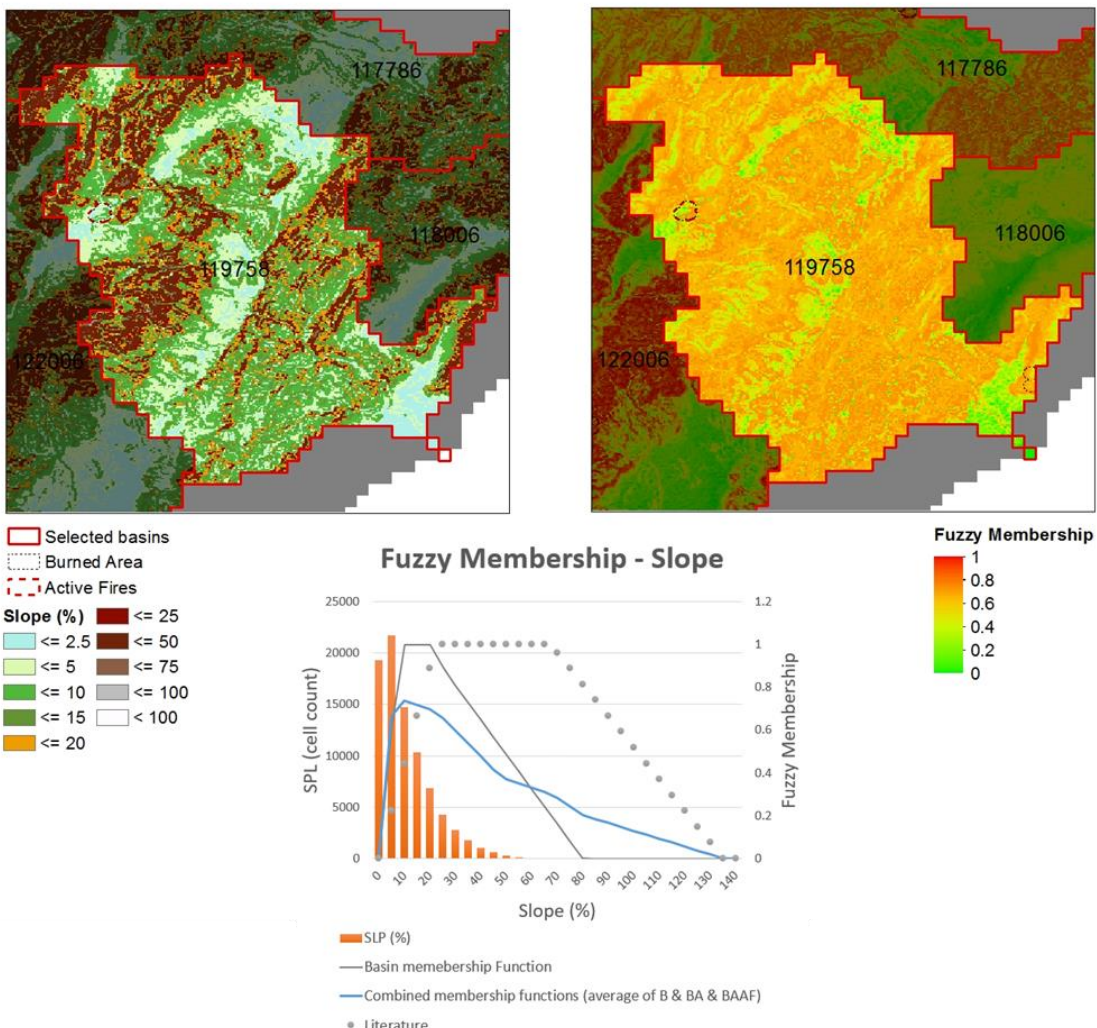


Figure 16: Fuzzy Membership - Slope

Topographical Wetness Index TWI

The Topographical Wetness Index (TWI) is the driving parameter in the topographical risk model (with a weighting score of 3) because this index combines the flow accumulation and slope of the basin (Moore, 1991). The literature curve is a negative linear function with a maximum membership (1) at the lowest index (1) and a minimum membership (0) at the highest index (10) to account for the water availability in the cells.

Within the basin most cells are dry (TWI between 2 – 3.5), and within the BAAF area between 3 and 3.5, which is expected because too dry or too wet areas are unfavourable for high vegetation e.g. scrubs and trees (Figure 17).

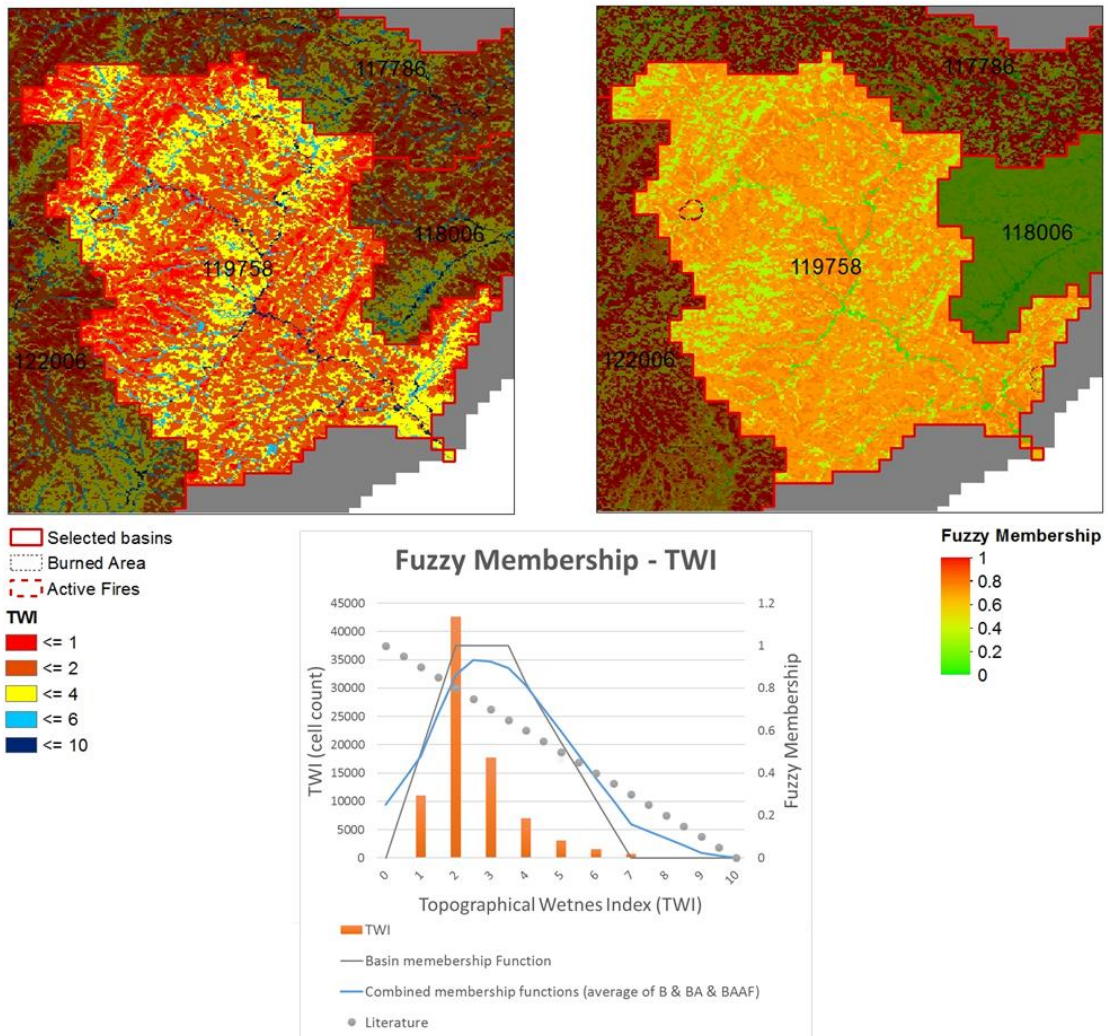


Figure 17: Fuzzy Membership - TWI

Cost Distance from Population

The cost distances function is a derived topographical function because the function combines the Land Cover Classification “Urban” with the DEM to calculate the cost it would take to travel from the nearest urban cell to the next, taking into consideration the slope of the terrain (using the standard functions in ERSI ArcGIS PRO).

This function is included in the analysis because it is an indication of how quickly a forest fire could be detected, and how easily to location could be reached (not taking into consideration the road network). Within the proximity of the basin there are seven populated areas. The fuzzy membership is based on the cost distribution within a 1000m buffer around the populated areas. Most cells (>50%) have a score of 43, with a standard deviation of 70, which set the breakpoint of this membership function at 78 (mean + 1/2 standard deviation). Areas with a cost higher than 78 are set to the maximum membership (1) because they are too far from populated areas to have a significant decrease in fire detection (Figure 18).

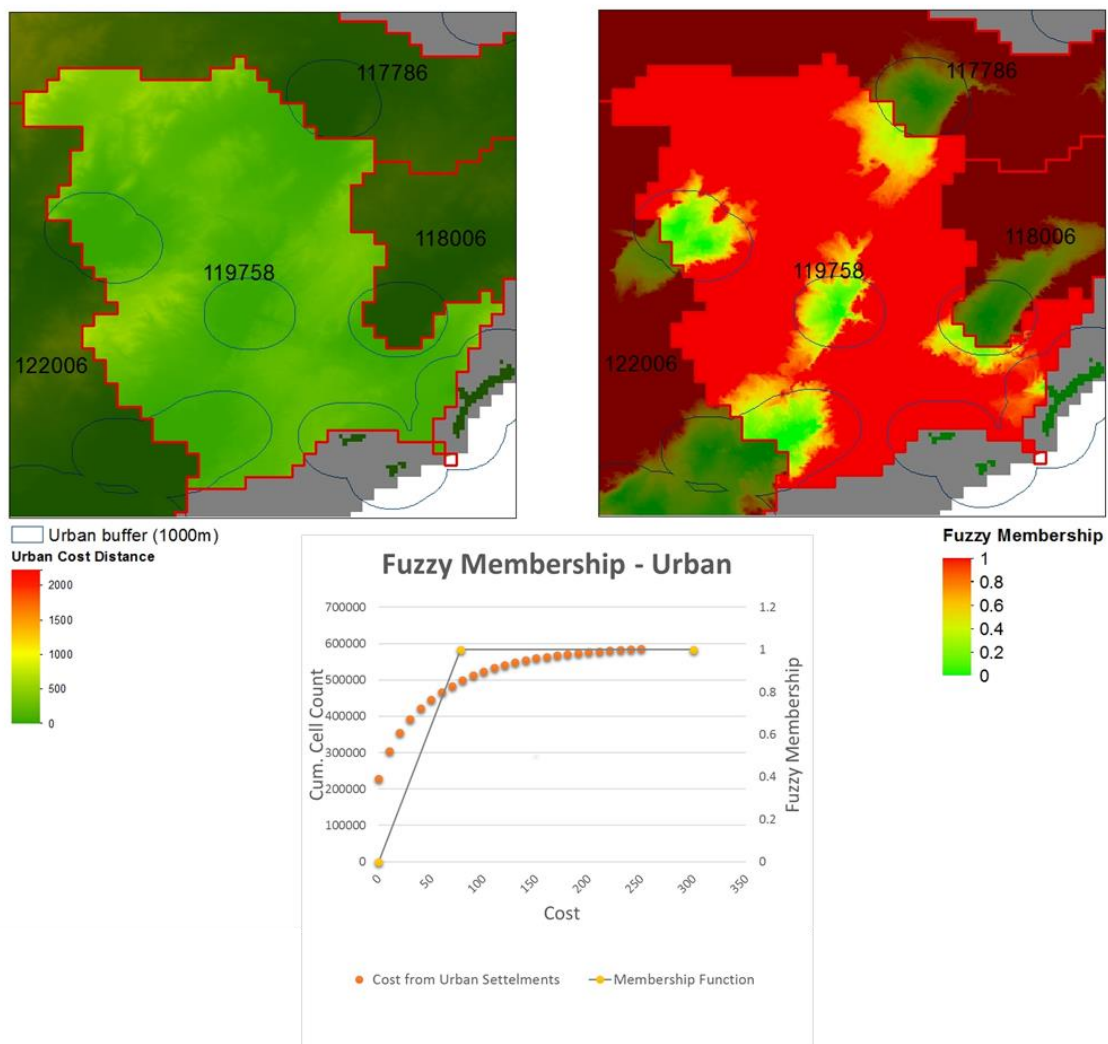


Figure 18: Fuzzy Membership - Urban

Cost Distance from Open Water

The cost distance function from Open Water (Figure 19) is following the same principle; areas close to cells classified as “Open Water” have a lower risk score than the cells further away. In the selected basin there are no cells classified as being “Open Water”. The whole basin is therefore classified as having a high potential for wildfire risk (membership = 1).

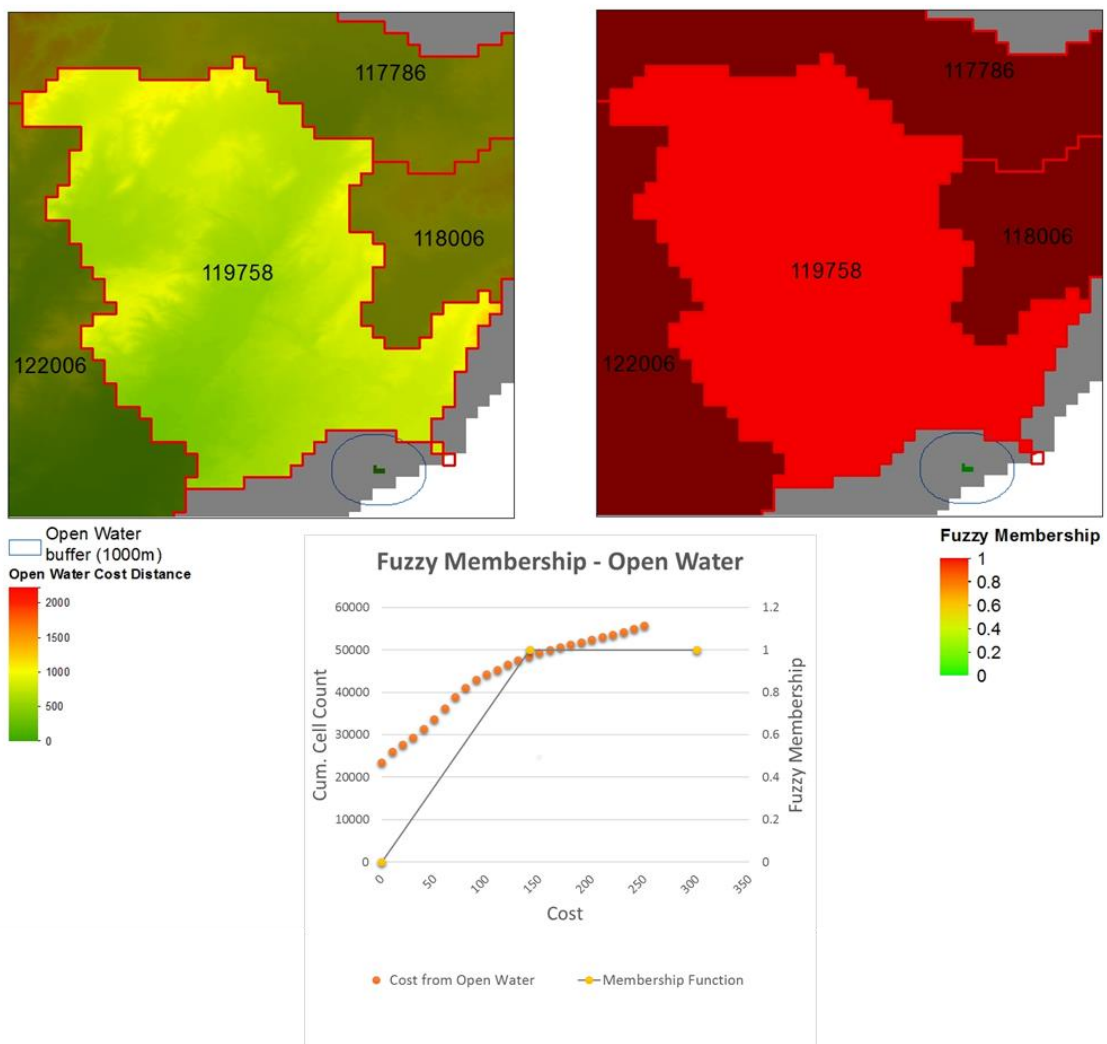


Figure 19: Fuzzy Membership - Open Water

Conclusion

The simplified fuzzy membership functions are providing a robust framework for calculating the theme fuzziness, and has been applied to the three study areas without altering the breakpoint logic. Elevation, Aspect, and TWI are following a normal distribution (within the example basin), which could have been described using a Gaussian curve, the distribution of Slope is more a negative exponential function, while Distance to population is exponential, and Distance from Open Water is linear. However, this might not be true for all the other basins. Therefore, a trapezoid function is capturing the general form of the distribution for all basins in the study areas. It is possible to express the fuzzy membership by more complex functions, but creating more complex functions, while there is much uncertainty around the used data, is not necessarily improving the model (Appendix IV shows the result of the fuzzification).

4.1.3 Hypothesis: The combination of land use, fuel loads, biomasses and bio-volumes can provide a meaningful fuel risk score

The main problem to generate a generic fuel risk score is the vegetation diversity between different locations. Most fire risk studies are done for one area/location while in this study multiple locations are investigated using the same method. The basis (like in most other studies) is the land cover (Hansen et al. 2013) because this will give a breakdown in areas susceptive to fire risk (e.g. shrub- and woodlands) and areas with a lower fire risk (e.g. built-up areas, grasslands). However, not all shrub- or woodlands have the same fuel loads, therefore relying only on a global land cover dataset is not enough. To illustrate this two land cover classes are selected, which are present in the study areas in Spain and North America (the Mongolian study area has no comparable land use class).

In Table 8 the land cover classification (LCC) is combined with the fuel bed layer, and the relation between fuel bed and land cover is expressed as percentage cover (see Appendix V for the fuel indicators).

For LCC 70 in Spain, this means that there are two dominant fuel beds within this land cover class, while in North America the same land cover is shared with three dominant fuel beds. Providing one fuel score for this LCC would either overestimating the risk in North America or underestimating the risk in Spain; the Fuel Score is a combination of fuel bed characteristics (fuel class), biomass, and biovolume, using all fuel beds within a land cover class. In the examples below the focus remains on the most dominant classes, and each step is explained in separation going top down.

Table 8: relationship between Land Cover Classification (ESA), Fuelbeds, and Fuel Score

Land Cover Classification (ESA)		Spain			North America		
LCC	Description	Fuelbed class	Cover	Fuel Score	Fuelbed class	Cover	Fuel Score
70	Tree cover, needleleaved, evergreen, closed to open (>15%)	12130	41%	0.328	915091	46%	0.252
		9112091	42%		925091	30%	
120	Shrubland	Other (9 classes)	17%		13091	11%	
		12130 12150	32% 55%	0.133	13130	85%	0.462
		Other (9 classes)	13%		Other (23 classes)	15%	

The Fuel class by LCC is the combination of a dry and a wet component (Table 9), expressed as ratio score. The maximum score within either the dry or wet class is 4 (based on their relative ranking within the class). For Spain in LCC 70 there are two fuel class scores computed (12130: 0.5 & 9112091: 0.75), in North America the same LCC has three scores. The Dry/Wet classes (1 – 4) are set using the relative ranking of the ordered scoring (see Table 5 for the relation between Fuel Codes (Wet/Dry) and their Classes).

Table 9: Fuelbed descriptions and calculated fuel class

Study Area	LCC	Fuelbed	Description	Dry Class	Wet Class	Fuel Class
Spain	70	12130	Mediterranean Forests, Woodlands and Scrub / Shrubs	3	1	0.5
		9112091	Mediterranean Forests, Woodlands and Scrub / Needleleaf evergreen trees			0.75
	120	12130	Mediterranean Forests, Woodlands and Scrub / Shrubs	3	1	0.5
		12150	Mediterranean Forests, Woodlands and Scrub / Sparse vegetation			0.25
North America	70	915091	Temp. Coniferous Forest / Needleleaf evergreen trees	2	4	0.75
		925091	Temp. Coniferous Forest / Needleleaf evergreen trees			0.625
		13091	Desert and Xeric Shrublands / Needleleaf evergreen trees			0.5
	120	13130	Desert and Xeric Shrublands / Shrubs	4	1	0.625

The Dry/Wet classes (as shown in Table 10) are stored in the database and lookup functions are assigning the score for each fuelbed by land cover class. In Table 10 the LCC 120 is broken down to fuel beds and the sound wood load values are given. As explained in 3.3.3 the loads are translated into a Dry/Wet code and ordered by code. The ranking is the cumulative count of the fuel bed class expressed as a ratio so that in Spain 12130 get a dry ranking of 0.574 and a wet ranking of 0.144, which translate to a dry class of 3 and a wet class of 1. The classes for the Desert and Xeric Scrublands / Shrubs (13130) in North America are set using the same table, and because the dry component (1h – 10h) of this fuel bed is higher also the score is higher (4).

Table 10: Fuelbed description and associated wood loads and ranking

Study Area	LCC	Fuelbed	Description	Sound Wood Load (Mg/ha)				Code		Rank	
				1h	10h	100h	1000h	Dry	Wet	Dry	Wet
Spain	120	12130	Mediterranean Forests, Woodlands and Scrub / Shrubs	0.10	0.10	0.10	-	120	0110	0.574	0.144
		12150	Mediterranean Forests, Woodlands and Scrub / Sparse vegetation	-	-	-	-			0.168	0.100
North America	120	13130	Desert and Xeric Shrublands / Shrubs	0.10	0.20	-	-	220	0100	0.780	0.100

Within the two study areas the two most dominant land cover classes are the needle-leaved evergreens (LCC 70) and the Scrublands (LCC 120). These areas are also the most receptive for forest fire occurrences is confirmed by overlaying the Burned Areas (BA) and areas affected by Active Fire (BAAF). The average percentage of area affected is used in the calculation of the risk score to adjust for local fire conditions (Table 11).

Table 11: Land cover classes and percentage Burned Area cover

LCC	Description	Spain			North America		
		Cover Study Area	BA	BAAF	Cover Study Area	BA	BAAF
70	Tree cover, needleleaved, evergreen, closed to open (>15%)	24%	29%	34%	12%	3%	5%
	BA/BAAF Weight			0.315			0.039
120	Shrubland	30%	36%	38%	75%	90%	89%
	BA/BAAF Weight			0.370			0.895

To summarise, first the fuel classes are calculated for each land cover class, then the BA/BAAF factor is obtained to adjust for local fire conditions. Using zonal statistics (standard function in ESRI ArcGIS PRO) the Bio-Mass / Bio-Volumes are extracted by LCC and used to calculate the two fuels scores. The final fuel score (as shown in Table 11) is the average of the Fuel class corrected with biomass/volume ((Bio Mass*Fuel Class) + (Bio Volume*Fuel Class)/2) and the Fuel class corrected with BA/BAAF weight (BAAF Weight*Fuel class) to make the transition from the global datasets to the local conditions in the study areas. The last step is to normalise the final fuel score (in the range 0 – 1) to be able to combine this score with the topographical risk and preserve the differences between fuel classes in the study areas.

By using this method, the local fuel conditions are taken into consideration, and for Spain, this means that areas with a tree cover of needle-leaved evergreens (LCC 70) are more vulnerable to forest fires than the same LCC in North America.

Table 12: Normalised Score by Land Cover Class

Land Cover Class	Spain		North America		Comment
	70	120	70	120	
Fuel Class	0.605	0.357	0.656	0.583	Composite of all fuel beds in a land cover class
BA/BAAF Weight	0.315	0.370	0.039	0.895	
Bio Mass (t/ha)	45%	28%	33%	62%	Contribution of biomass by land cover class*
Bio Volume (m ³ /ha)	64%	18%	79%	13%	Contribution of biovolume by land cover class**
Fuel Score1	0.465	0.133	0.479	0.401	Fuel class corrected with bio-mass/volume ((Bio Mass*Fuel Class) + (Bio Volume*Fuel Class)/2)
Fuel Score2	0.190	0.132	0.026	0.522	Fuel class corrected with BA/BAAF weight (BAAF Weight*Fuel class)
Final Fuel Score	0.328	0.133	0.252	0.462	Average of Fuel Score1 & Fuel Score2
Normalised Score	1.000	0.405	0.546	1.000	Fuzzy Membership function for all landcover classes in the study areas

Figure 20 illustrates the transition from land cover to the fuzzy membership for two selected basins in Spain and North America. The land cover in the selected area in Spain is more diverse than the example area in North America, but in both areas, scrublands are the dominant land cover class. Due to the diversity, also the variation in fuel classes in Spain is higher (ranging from 0.125 to 0.75), while for example in North America the range is more narrow (0.25 – 0.5). The final fuzzy membership values are showing that the example area in North America is more vulnerable to fire than the example area in Spain. The dominant land cover in Spain is still vulnerable (fuzzy membership value of 0.5) but less vulnerable than the same land cover in North America (fuzzy membership value of 1).

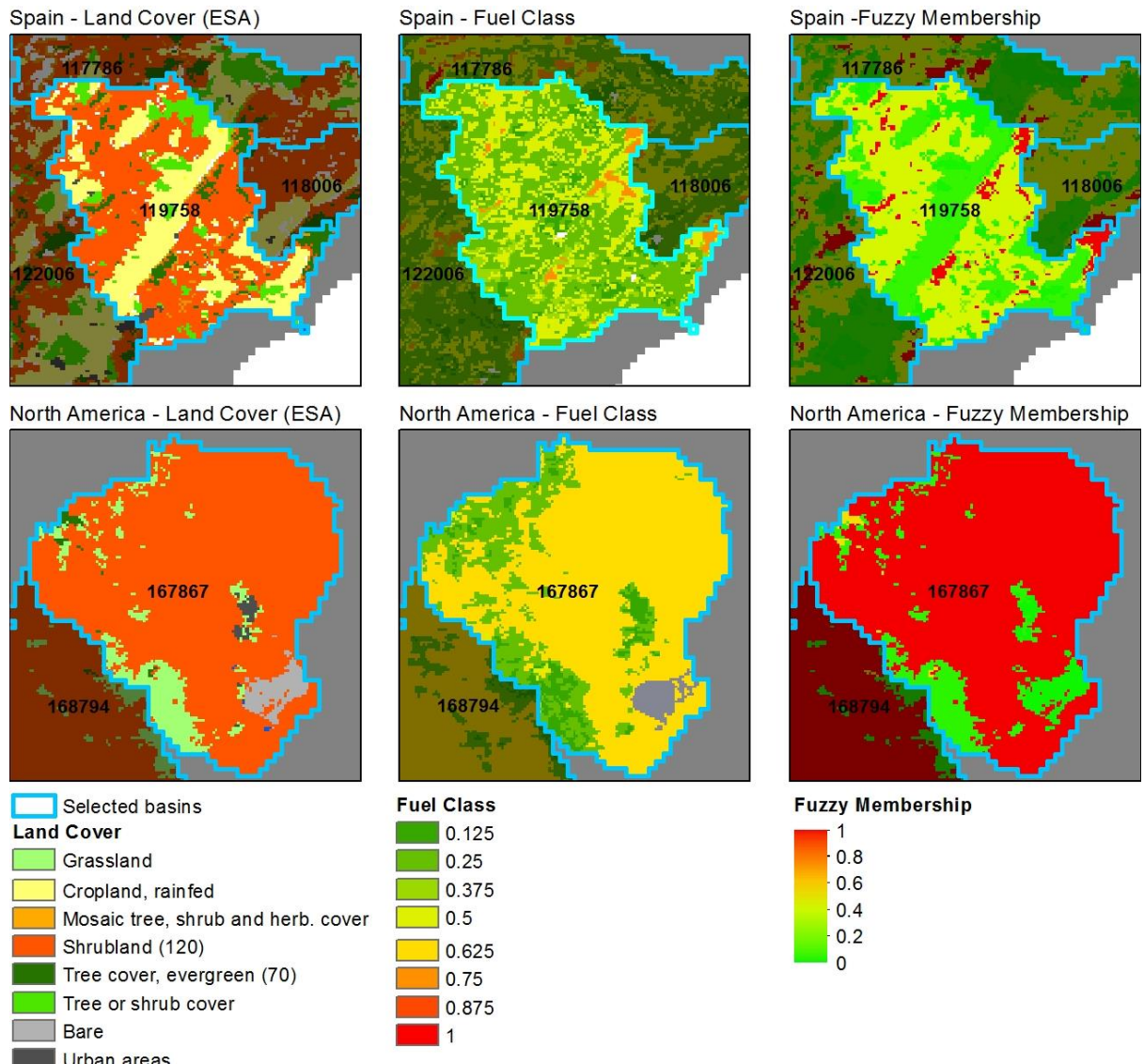


Figure 20: Transition from land cover to the fuzzy membership (Appendix VI presents the results by study area)

Conclusion

Normally fuel risk scores are constructed with the aid of local knowledge, and expert opinions, and for small-scale problems, this is the preferred method to derive a fuel risk score from land covers. In a generic approach, this is not a feasible option because neither the expert knowledge or equivalent detailed datasets are available. The method used in this study is combining fuel risk indicators, like fuel bed loads, available biomass, and volumes, to a scoring scheme which applies to the data domains of the used information. For North America and Spain it was possible to

calculate a fuel risk score, unfortunately, within the Mongolian study area there was no suitable land cover to apply the same technique; more than 99% of the area is bare rock/sand. Cross referencing the Mongolian land cover with the other sources confirmed that within this study area there is not enough fuel available to compute a score. The final fuel score for Mongolia is therefore set to 0.0001, while for the other study areas the fuel risk ranges from 0.00001 (very low risk) to 1 (high risk).

4.1.4 Hypothesis: The BKDI is a useful indicator to assess the time-dependency of wildfire risk

There are several metrological indicators developed (Heim, 2002) to indicate drought risk, but the Keetch-Byram drought index (KBDI; Keetch and Byram, 1968) was specifically designed as a fire weather warning system (Eastaugh and Hasenauer, 2014) and is using the soil water shortage as a measure of the drought risk.

To test if the KBDI is suitable for a generic forest fire model the 50-Year High-Resolution Global Dataset of Meteorological Forcing for Land Surface Modelling from the University of Princeton (2006) is used as input (Sheffield et al., 2006). This dataset contains the two parameters used in the KBDI equation: temperature and precipitation. In Figure 21 the two metrological indicators are plotted in combination with the Burned Areas and Active Fires, with temperature on the left graph, and precipitation on the right graph, for the three study areas.

There is a strong correlation between high temperature and low precipitation in North America; most fires are detected after the warmest and driest period. The trend in the Spanish study area is less obvious, this is mainly due to the wet springs and autumns, and the close vicinity to the coast (Mediterranean versus a land climate in North America (section 3.3.1)). The period with the most active fires is at the same time when the temperatures are the highest (mid-summer), and with low precipitation (< 0.5 mm/day); this is confirmed by the wildland fire analysis Cardil et al. (2016) performed in the Aragón region. The records for Mongolia show that the temperatures and precipitation are low in the winter and that there are high temperatures (>30°C) and moderate rainfall in the summer (< 2 mm/day).

The weekly averages for temperature and precipitation are computed (Figure 21) by using three subsets from the 50-Year High-Resolution Global Dataset, 84 points for North America, 63 points for Spain and 80 points for Mongolia; the same data points are later used to create the input data for the KBDI equation.

Originally the KBDI equation was developed in English units, for this study the metric version, as corrected by Crane (1982, cited by Alexander, 1990), is used since the meteorological data is stored in S.I.

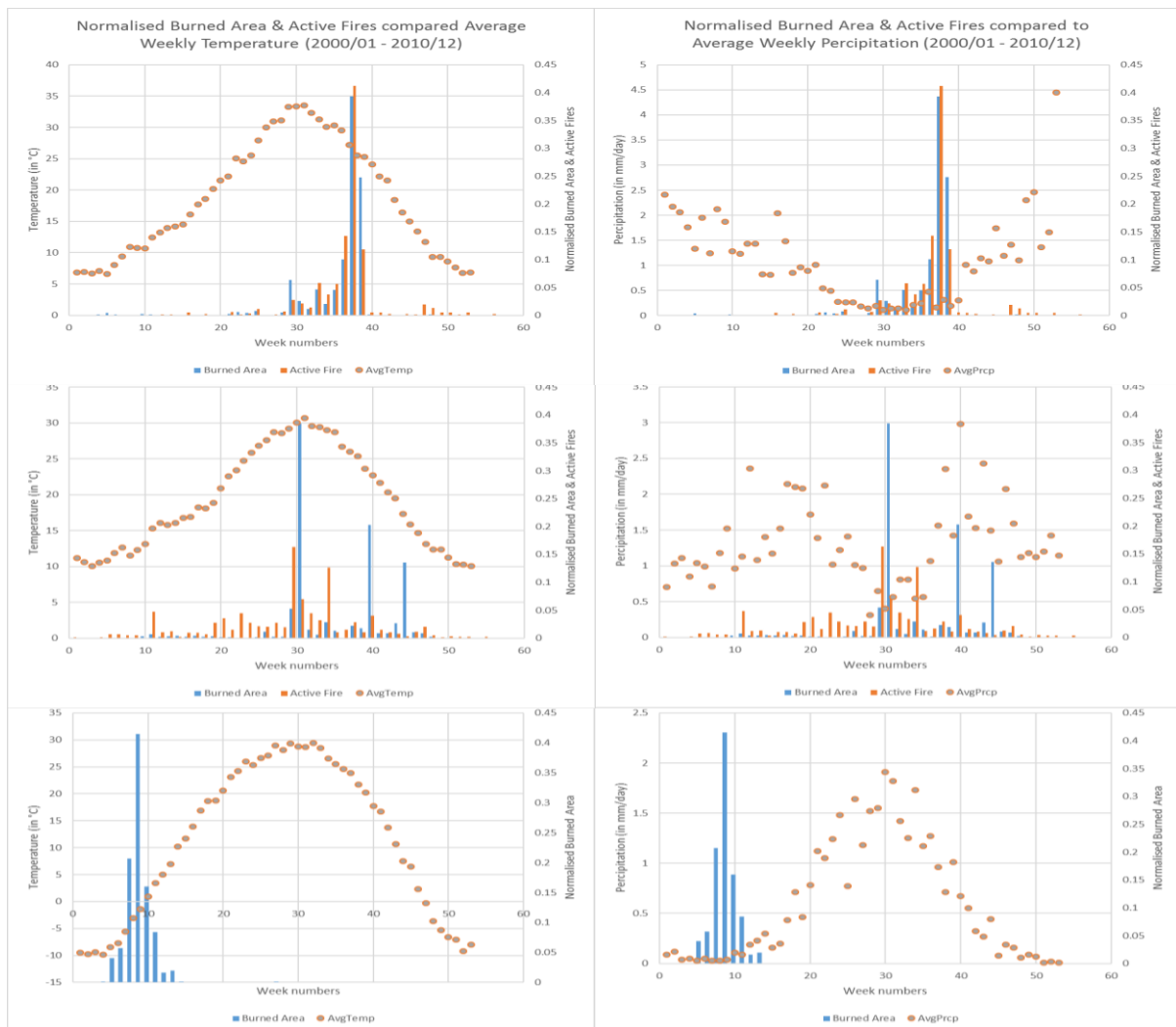


Figure 21: Meteorological indicators; top: North America (California/ Nevada), middle: Spain (Valencia), bottom: Mongolia (Gobi Altai)

In the equation (Figure 22) $KBDI^*_{t-1}$ is the previous day's moisture deficiency less the net rainfall; T_{max} the maximum daily temperature; R_{av} the annual average precipitation in the study area (based on 50-year data); and dK the daily addition to moisture deficiency. The KBDI increases daily according to temperature and humidity and decreases by the net rainfall when the precipitation over consecutive days exceeds 5.1 mm; the buffer of 5.1 mm (0.2 inches) will account for infiltration and evapotranspiration (Keetch and Byram, 1968; Dolling et al, 2005; Goodrick, 2002).

$$dK = 10^{-3} \frac{(203.2 - KBDI^*_{t-1})(0.968e^{(0.0875T_{max} + 1.5552)} - 8.3)}{1 + 10.88e^{-0.001736R_{av}}}$$

Figure 22: Keetche-Byram drought index (Eastaugh and Hasenauer, 2014)

The daily Drought Index (DI) is computed using the formula in Figure 22 and the 50-year modelled data for the three study areas, the Drought Factor DF is the maximum average weekly index, transformed from DI to FD with the formula in Figure 7.

In Figure 23 both the DI and the DF/FM are plotted on a weekly time scale:

- For North America (NA) the most vulnerable period is between week 35 and week 42 and receives a Drought Factor of 1 ($FM > 0.8$)
- In Spain (S) the period of maximum drought is earlier (week 33-37, and a factor of 0.6 ($FM > 0.4$) is assigned to this study area.
- The DI in Mongolia (M) is low (ranging from 45 to 65), and there is no significant period of maximum vulnerability to drought; this area has the lowest drought factor 0.4 ($FM > 0.2$).

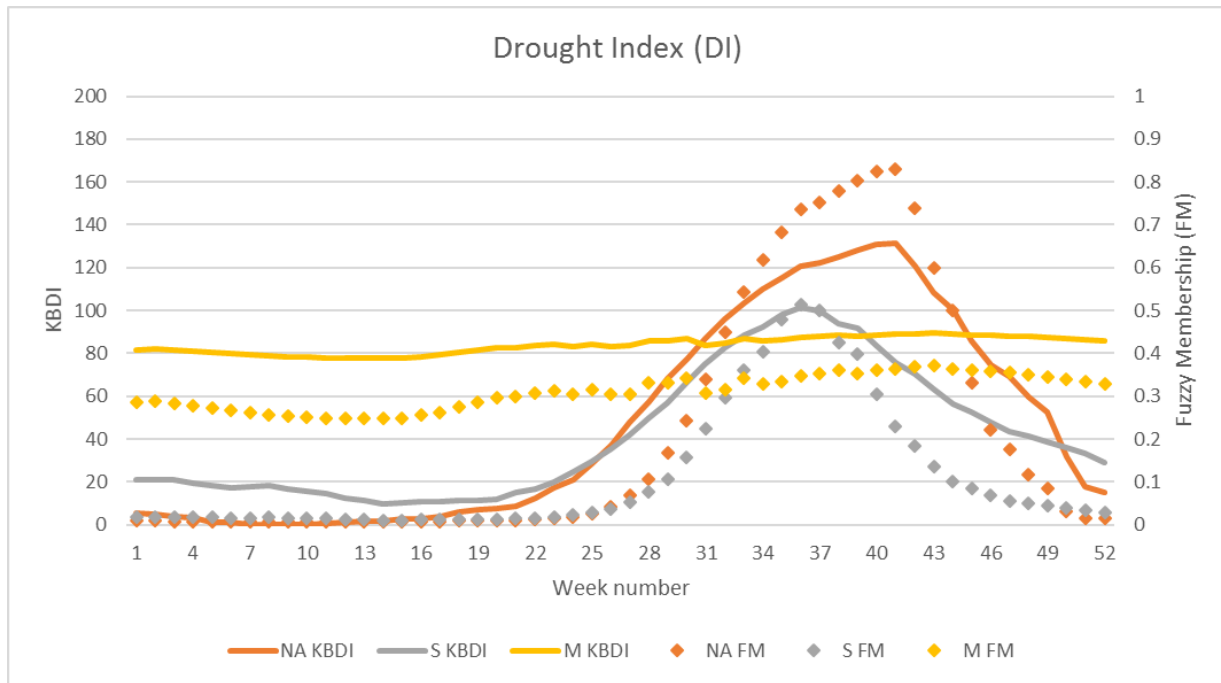


Figure 23: Weekly Drought Index and corresponding Drought Factor

Downscaling

The drought factors, mentioned above, are computed for the study areas, averaging out the temperatures and precipitation records. One possible solution to refine the Drought component of the model is to downscale the temperature and precipitation by using the DEM. In Figure 24 the drought factor is downscaled for two profiles (A-A' & B-B') using an inverse distance weighting interpolation over the data points and a temperature correction based on height difference (temperature decreases 6.5°C of 1000m rise (Environmental Lapse Rate)), the precipitation is kept as an area average. Applying the downscaled drought factor to compute a risk score falls outside the scope of this project, but will be considered in future research to improve the model.

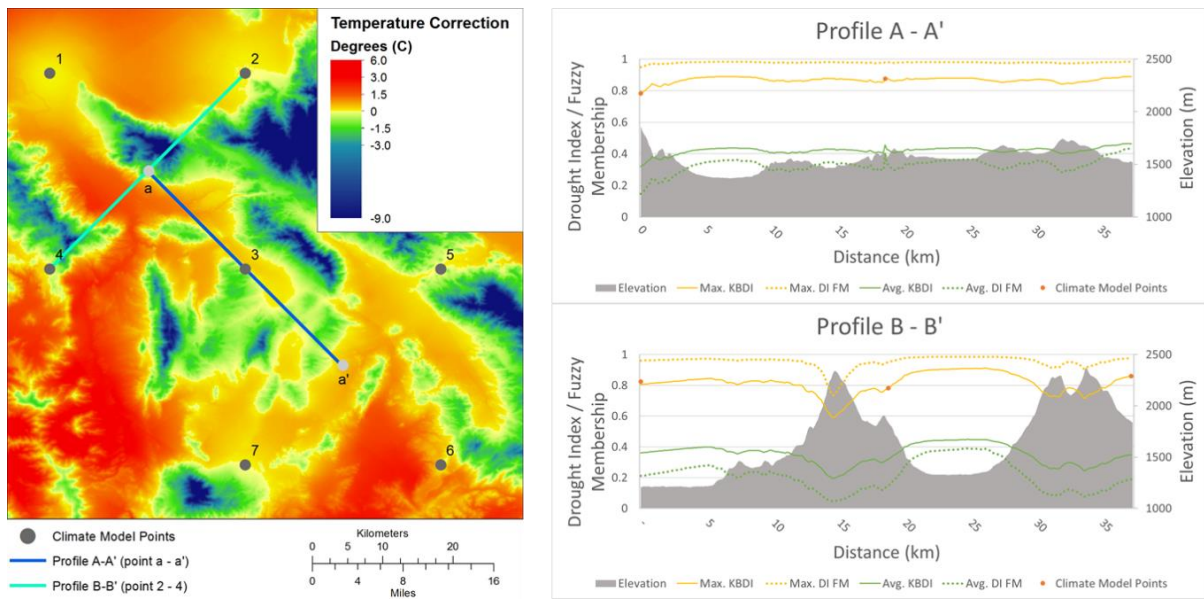


Figure 24: Downscaled Drought Index

Conclusion

Combining the BKDI with the meteorological forced 50-Year high-resolution global dataset provides a robust framework to model drought indexes. The BKDI has been implemented in various programs and is valued as one of the most suitable methods for drought monitoring and wildfire prevention (Takeuchi et al., 2015). The meteorologically forced dataset is developed with the aim to provide a dataset in the highest resolution possible while being consistent in time and space when integrating variables from contributing datasets (Sheffield et al., 2006). The classes designed by Keetch and Byram are a good indication of drought but are less useful when trying to assess the fire risk. The transformation function in Figure 7 is emphasising the low and the high end of the curve, and providing an almost linear transition from medium low to medium high risk (similar to the Keetch and Byram scale). The drought factors by study area will adjust the fire hazard for each study area, but the implementation of a downscaled index could give a more realistic view of the local drought risk.

4.1.5 Topographical Risk Layer Construction

The topographical risk layer is the result of a Multi-Criteria Analysis (MCA) combining the individual topographical components (from section 3.3.2) to one risk score.

Before performing a MCA, the topographical layers will have to be prepared to allow such operation. In this case, this required reclassification of the fuzzy membership values of individual layers to a discrete scale (1 – 5).

In Table 13 the statistics are presented for the six topographical layers with their resulting risk bands. The base risk band (Risk3) is between the mean value $+/- \frac{1}{4}$ standard deviation (std), the other bands are $+/- \frac{1}{2}$ standard deviation away from this band, with a maximum of 1.

Table 13: Risk band clasification

Study Area	Layer	Study Area Statistics						Risk bands				
		MIN	MAX	MEAN	STD	1/4 std	1/2 std	Risk1	Risk2	Risk3	Risk4	Risk5
NA	SLP	-	1.0000	0.5771	0.3201	0.0800	0.1601	< 0.33	< 0.49	< 0.65	< 0.81	≤ 1.00
	ASP	-	1.0000	0.6306	0.3345	0.0836	0.1673	< 0.37	< 0.54	< 0.71	< 0.88	≤ 1.00
	TWI	0.0250	0.9422	0.8137	0.1529	0.0382	0.0765	< 0.69	< 0.77	< 0.85	< 0.92	≤ 1.00
	DEM	-	1.0000	0.5968	0.3490	0.0873	0.1745	< 0.33	< 0.50	< 0.68	< 0.85	≤ 1.00
	210	-	1.0000	0.8265	0.3281	0.0820	0.1641	< 0.58	< 0.74	< 0.90	≤ 1.00	X
	190	-	1.0000	0.9038	0.2542	0.0636	0.1271	< 0.71	< 0.84	< 0.96	≤ 1.00	X
S	SLP	-	1.0000	0.6704	0.2843	0.0711	0.1422	< 0.45	< 0.59	< 0.74	< 0.88	≤ 1.00
	ASP	-	1.0000	0.6668	0.3417	0.0854	0.1709	< 0.41	< 0.58	< 0.75	< 0.92	≤ 1.00
	TWI	0.0250	0.9500	0.8455	0.1466	0.0367	0.0733	< 0.73	< 0.80	< 0.88	< 0.95	≤ 1.00
	DEM	-	1.0000	0.4626	0.2081	0.0520	0.1041	< 0.30	< 0.41	< 0.51	< 0.61	≤ 1.00
	210	-	1.0000	0.9553	0.1684	0.0421	0.0842	< 0.82	< 0.91	< 0.99	≤ 1.00	X
	190	-	1.0000	0.8047	0.3502	0.0876	0.1751	< 0.54	< 0.71	< 0.89	≤ 1.00	X
M	SLP	-	0.9059	0.6229	0.1652	0.0413	0.0826	< 0.49	< 0.58	< 0.66	< 0.74	≤ 1.00
	ASP	-	1.0000	0.6456	0.3733	0.0933	0.1867	< 0.36	< 0.55	< 0.73	< 0.92	≤ 1.00
	TWI	0.0333	0.9000	0.8038	0.1250	0.0313	0.0625	< 0.71	< 0.77	< 0.83	< 0.89	≤ 1.00
	DEM	-	1.0000	0.7102	0.2810	0.0703	0.1405	< 0.49	< 0.63	< 0.78	< 0.92	≤ 1.00
	210*	-	1.0000	0.9571	0.1533	0.0383	0.0767	< 0.84	< 0.91	≤ 1.00	X	X
	190*	-	1.0000	0.9799	0.1020	0.0255	0.0510	< 0.90	< 0.95	≤ 1.00	X	X

After reclassification, all the cells in the layer have a value associated with the risk band (1 – 5), and are combined to one risk score using the weighting scheme in Figure 5.

The distance layers (190 & 210 in Table 13) are not reaching the highest classification because of the design of the decisions made in the fuzzification process; restriction condition is the 1000m buffer, would a different buffer been used the spread of FM values would also be different with a lower or higher mean values. In Figure 25 the individual layers are combined to the topographical risk score layer using a cell-by-cell operation:

```
Float(((Float("ASP" * 3) + Float("TWI" * 3) + Float("SLP" * 2) + Float("DEM") +
Float("lc190") + Float("lc210")) - 11) / 42)
```

The result is a MCA layer ranging from 0 to 1 and will be used in the next step to calculate the wildfire risk uncorrected for drought (See Appendix VII for the MCA results by study area).

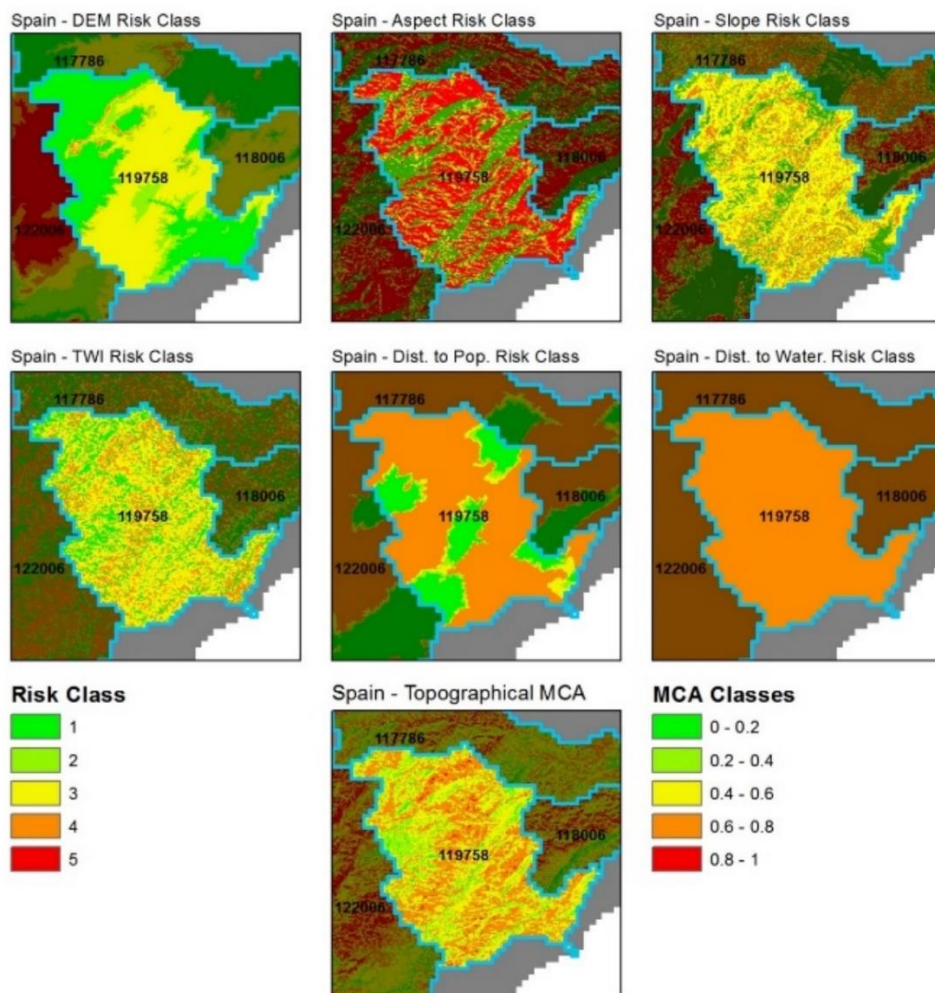


Figure 25: Constructing the Topographical MCA layer

4.1.6 Component Integration

The final step in the process is the integration of the three sub-models: Topography, Fuel, and Drought. The maximum wildfire risk is the average, on a cell-to-cell basis, of the topographical risk scores from the previous step, and the fuels scores from section 3.3.3. Figure 26 is showing the effect of the averaging; within the selected basin (119758) the topographical fire risk is profound in the agricultural area (located in the centre of the basin), but the fuel risk is relatively low in this area, therefore the average risk in this area is between 0.2 and 0.4.

The final hazard score layer is the maximum fire risk product adjusted with the Drought Factor for this study area (Table 3). In the selected basin there are pockets of medium risk (<0.6), but most of the basin has a low-risk score.

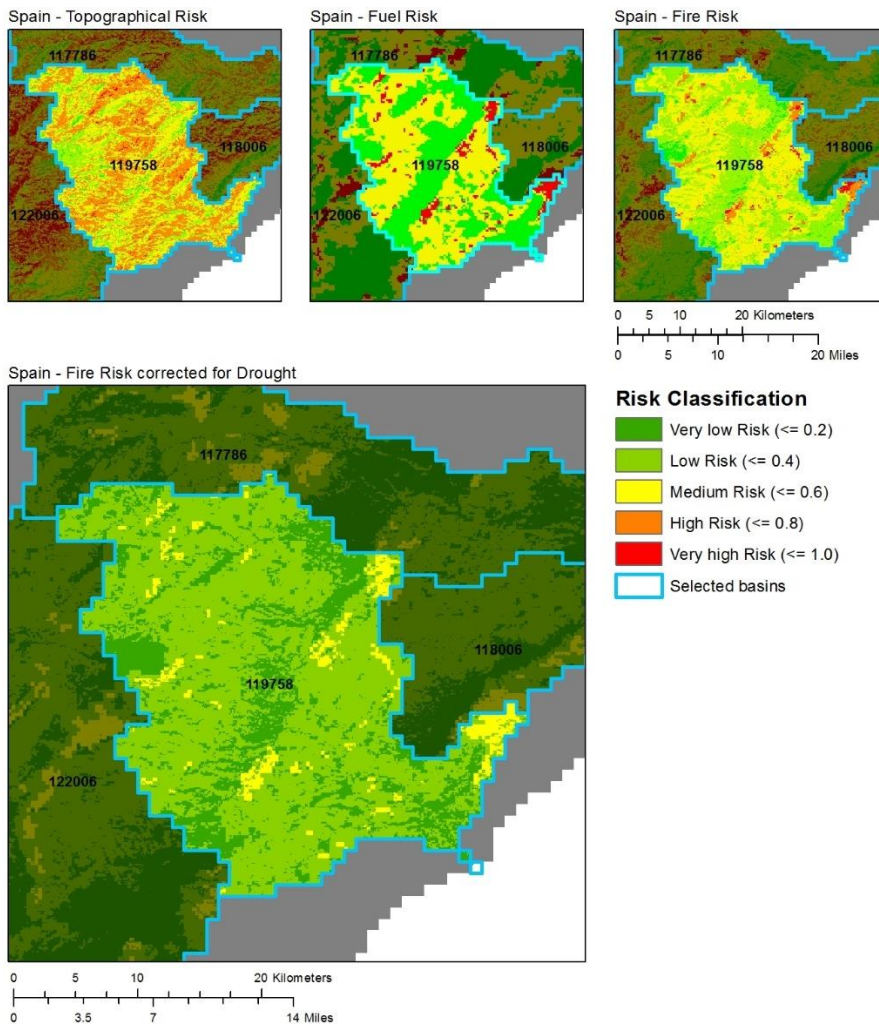


Figure 26: Fire Risk Corrected for Drought

4.2 Model Results

In the next paragraphs, the results of the Wild Fire Risk Scoring Model are presented by study area. The fire risks are classified by 10% intervals, excluding areas with no risk (0), and the contribution of each class to the total number of cells is expressed as a percentage. The Risk Scoring Maps are placed in Appendix XXXX, showing the spatial distribution of the hazard over the three study areas.

The Burned Area and Active Fires (BAAF) areas are included in the results because this gives an indication of the model performance. The resolution of the input data for the BAAF polygons is different to the model resolution, so it is not likely that 100% of the cells within these areas will have a high risk (>75%). However, the model performance is good when more than 50% of the cells have a hazard index of more than 0.5.

North America (California/Nevada)

The model is performing well in the North America study area, most cells in this model have a risk above average (>50%), and within the BAAF areas, 90% of all cells have a fire hazard larger than 50% (Figure 27).

The most vulnerable part of the study area is the stretch in the middle (catchments 169114, 168794, and 167867), and this is the same area where The Rush Fire went through. This fire event started on 12th of August 2012, by lightning, and was finally contained on the 30th of August 2012, after burning 1280 square kilometres in California and Nevada (Top 20 Largest California Wildfires, 2015).

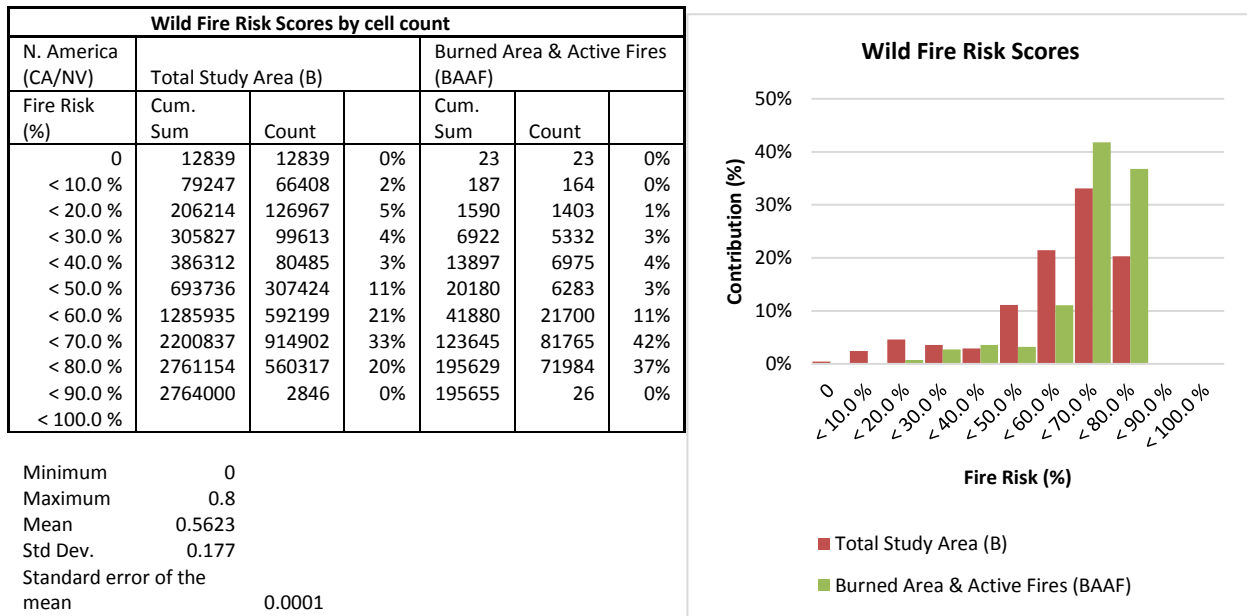


Figure 27: N. America (CA/NV) Wild Fire Risk Scores by cell count

Spain (Valencia)

In the study area for Spain, the model is behaving as expected but produces a moderate hazard due to the correction for Drought (maximum risk of 0.57), only 10% of all the cells in the study area have a core higher than 50% (Figure 28).

Within the BAAF area, 84% of the cells have a score lower than 0.50 Fire Risk, which is not acceptable because for the model to be realistic more than half of the cells should have a classification of medium risk or higher. Nevertheless, the BAAF areas are still more vulnerable to wildfire than the overall fire danger in the study area.

The areas with medium fire risk are mainly in catchments 125567 and 122006; these are also the catchments with the highest percentage needle-leaved evergreens (LCC: 070) and shrub lands (LCC: 120) and received the highest fuel score.

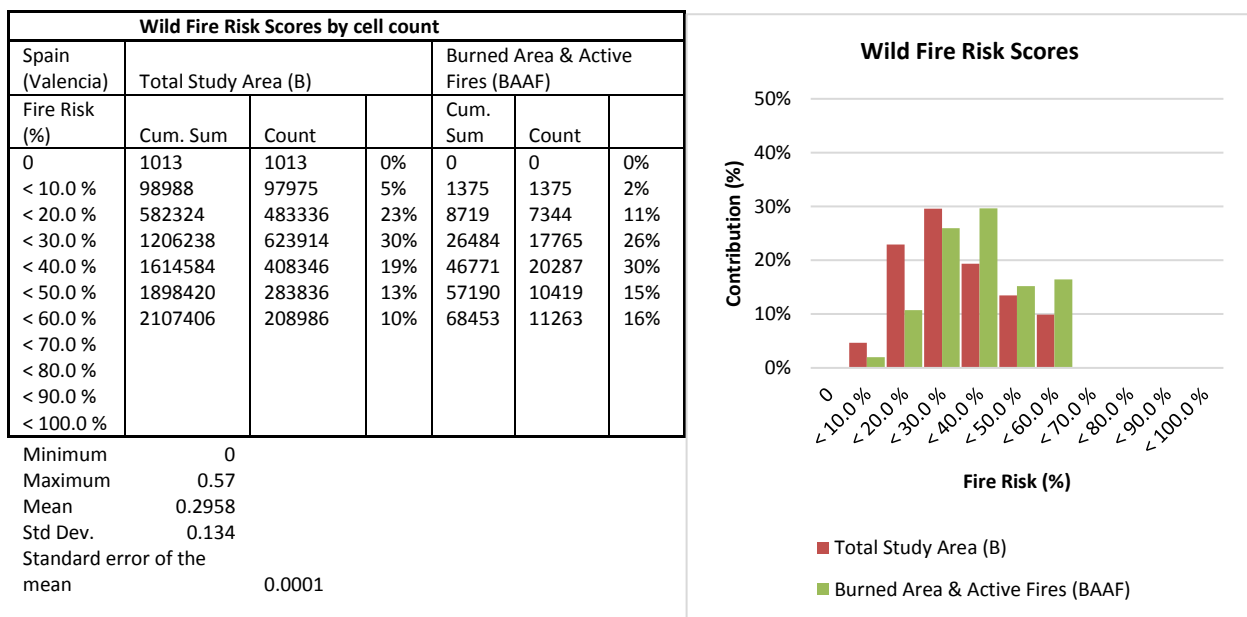


Figure 28: Spain (Valencia Wild Fire Risk Scores by cell count)

Mongolia (Gobi Altai)

The model results for Mongolia (Figure 29) are poor but considering the available input data, and the results from the sub-models, this was to be expected. In Mongolia, most cells were classified as bare ground (without vegetation), the drought index is low, and there are no active fires detected (so cross-validating the results is not possible).

Overall the model places the Mongolian study area at a low risk (<20%) because of lack of fuel and relatively low drought index. Nevertheless, a higher score would have indicated that the model is not behaving as foreseen.

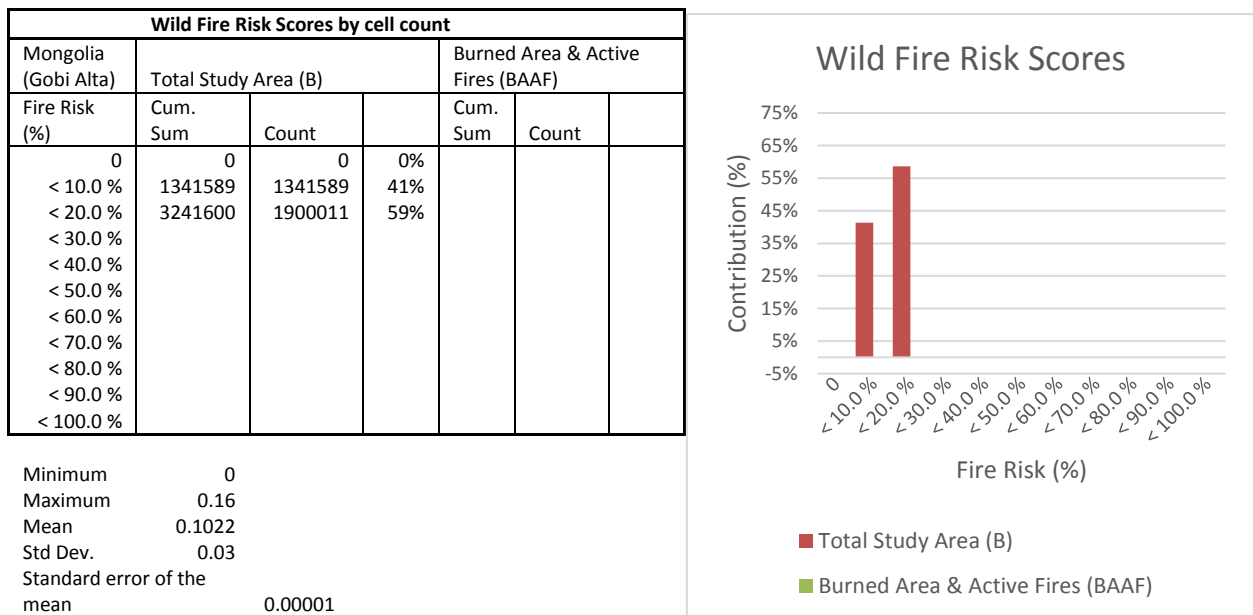


Figure 29: Mongolia (Gobi Alta) Wild Fire Risk Scores by cell count

4.3 Model Validation and (Re)Analysis

Model validation of a complex model like the proposed wildfire risk model in this study is difficult because the model consists of many data sources and processes. To get a measure of the performance of the model the fire-risk scores in the three study areas are validated against:

- Literature and (newspaper) reports
- Percentage burnt area within the BAAF regions
- The area under the Receiver Operating Characteristic (ROC) curve

North America (California/Nevada)

One of the organisations monitoring wildfires in North America is the California Department of Forestry and Fire Protection (CAL FIRE), which also is covering partial reporting for Nevada. The most severe event, captured by CAL Fire, in the study area is the Rush Fire.

Table 14 lists all events in the Lassen county, which covers 90% of the study area in California, from 2006 to 2015 exceeding 1,000 acres (4.0 km²); the fires are in the time-period identified as being most receptive to wildfire and are located in areas with high fuel loads.

Table 14: Large wildfires in Lassen, CA (Cdfdata.fire.ca.gov, 2016)

Name	County	Acres	Km2	Start Date	Contained Date
Observation Complex	Lassen	4300	17.4	25 June 2006	30 June 2006
Creek	Lassen	1234	5	18 July 2006	21 July 2006
Cub Complex	Lassen	19718	79.8	21 June 2008	20 July 2008
Peterson Complex	Lassen	7842	31.7	21 June 2008	02 July 2008
Popcorn	Lassen	3000	12.1	22 June 2008	08 July 2008
Corral	Lassen	12500	50.6	23 June 2008	07 July 2008
Dodge Complex	Lassen	1600	6.5	01 August 2009	03 August 2009
W-4	Lassen	1500	6.1	01 August 2009	07 August 2009
McDonald	Lassen	9408	38.1	27 July 2010	10 August 2010
Spanish	Lassen	1169	4.7	18 July 2012	21 July 2012
Rush	Lassen	271911	1100.4	12 August 2012	31 August 2012
Likely	Lassen	9838	39.8	05 Sept. 2012	14 Sept. 2012
Frog	Lassen	4863	19.7	30 July 2015	20 August 2015
Dodge	Lassen	10570	42.8	03 August 2015	17 August 2015

In the Nevada region, the model could be validated against a Landscape-Scale Wildland Fire Risk/Hazard/Value Assessment for the Pershing County (Figure 30). Two catchments (169085 & 169119) are both in the report and in the model. The risk classification in Catchment 169119 is matching the report well, the dominant features in this catchment are present in both maps, although the model results are higher than the rating in the report. The hazard in the Selenite Range (Catchment 169085) is underestimated in the model, while the plains are receiving a higher classification, this effect is due to the small BAAF region which is emphasising the local conditions under the BAAF area more than the landscape-scale model.

The high-risk features in the hazard assessment are not captured in the risk classification because they are buffered transmission lines and other right-of-way corridors determined to be of high-value; these are elements unique to this study and can not be taken into consideration in a generic model.

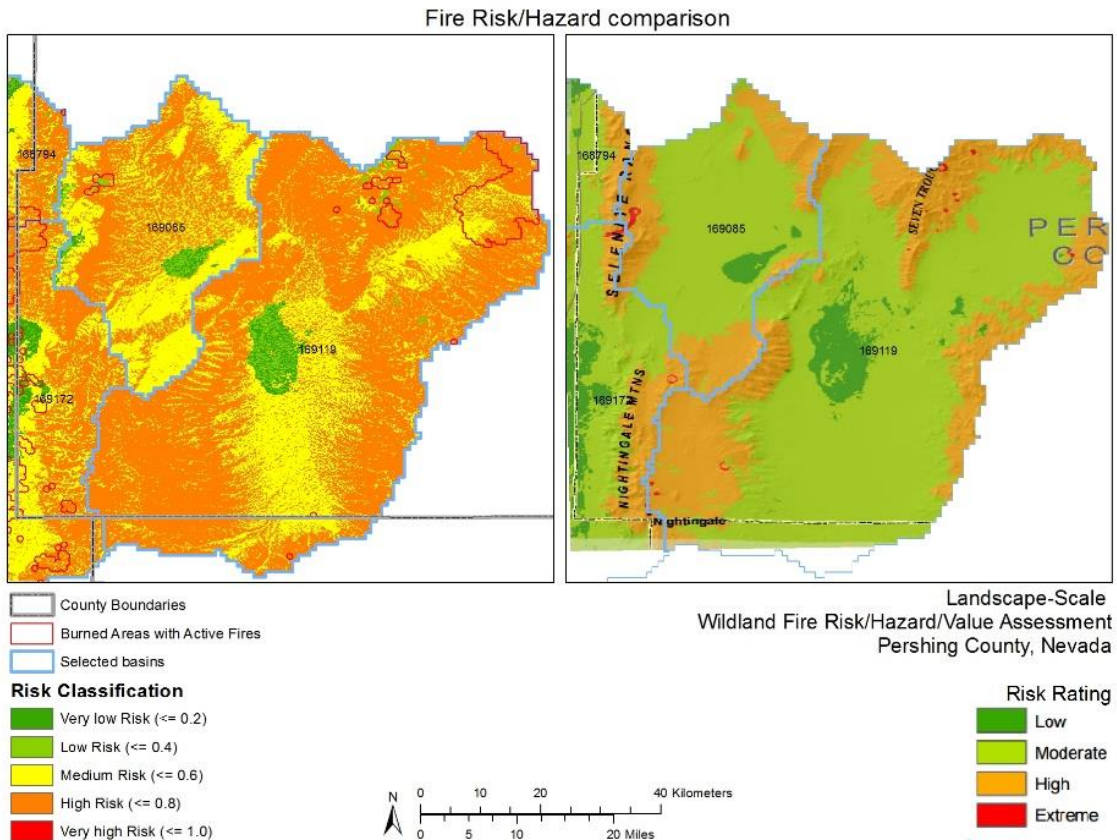


Figure 30: Fire Risk/Hazard comparison. Left: Wildfire Risk Classification for selected catchments Pershing County, Nevada as a subset from the North America Study Area. Right: Landscape-Scale Wildland Fire Risk/Hazard/Value Assessment Pershing County, Nevada adapted from Wildland Fire Associates (2009)

Spain (Valencia)

Cardil et al. (2013) estimate that there are on average 4-6 large wildfire events are in the Aragon region (in the north-west of the study area), and that there were 193 events in the period from 1978 to 2010. The burned area and active fire records are showing high activity in this part of the study area too (Appendix II), but the corrected Fire Score (Appendix VIII) is indicating a moderate risk. The decrease in the fire hazard is due to the drought correction factor, which is an environmental factor and (very likely) underestimating the drought in the areas further away from the coast.

Also, as shown in the results section, the BAAF areas are underperforming for the study area in Spain. To correct this low scoring of the BAAF areas the total Fire Score layer will be multiplied by 0.05 increments until the scoring in the BAAF areas is matching the validation rule; no further validation is possible until the BAAF areas are behaving as expected.

Mongolia (Gobi Altai)

Validation of the Mongolian study area is difficult because there are no reports of wildfires in the Gobi Altai region. Although, the Ministry of Nature, Environment and Tourism (2011) is mentioning that (steppe) fires are starting in early spring/late autumn and that the area around Bayan-Uul (Adrc.asia, n.d.: Table 4) has a moderate risk for steppe/wildfires. The analysis done by Erdenetuya (2011) confirms the time periods in which fires occurring most, and classifies the biomass in the study area around two tonnes per hectare; the burned areas (Appendix II) are in locations with biomasses higher than one tonne per hectare areas (Figure 31). Due to the lack of Active Fires reanalysis of the Mongolian study area is not possible; the wildfire risk remains unadjusted and classified as Low.

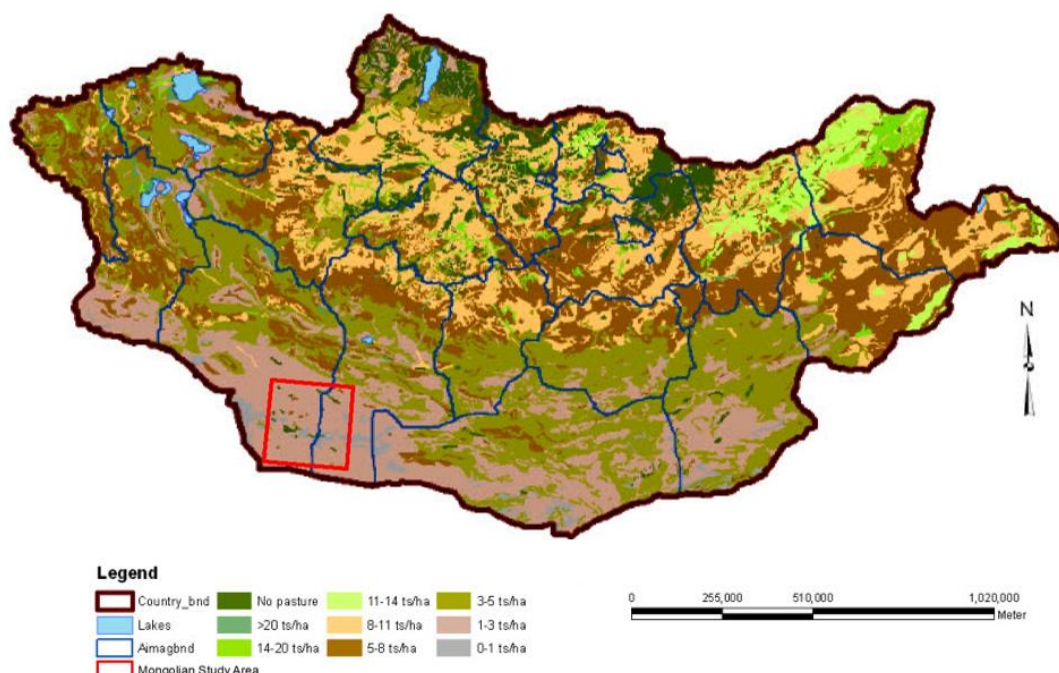


Figure 31: Pasture Biomass map of Mongolia (adapted from Erdenetuya, 2011)

4.3.1 Reanalysis of the Spanish study area

To reach the rule that within a BAAF area more than 50% of the cells must have a risk score of 0.5 or higher the study area has been lifted with a factor of 1.5 (10 iterations of 0.05 increments). The result of the adjustment (Figure 32) is that the overall risk in the study area has been increased, but is not exceeding the risk scoring of the California/Nevada area (which is more vulnerable to wildfire than the Spanish study area). Also, the risk is more equally distributed, were in the post-adjustment most of the risk was around a 0.3 risk score the adjusted scoring ranges from 0.3 to 0.5. The BAAF areas are receiving the highest scores, up to 0.86, and the highest scores are in the regions with the highest density of active fires.

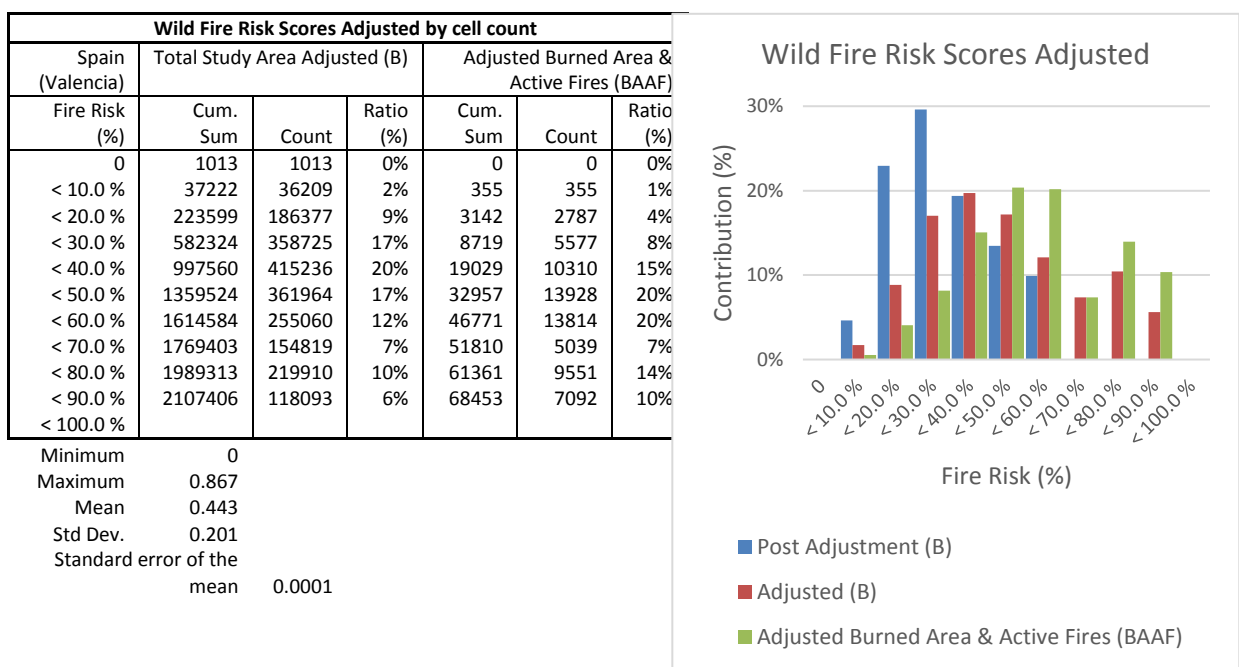


Figure 32: Spain (Valencia) Wild Fire Risk Scores Adjusted by cell count

Unfortunately, there are no local risk assessment studies available (in English) to compare the model results with expert hazard assessments. Although, Aragó (2016), Garcia-Martin (2008), and Sá (2014) all agree that this region is very vulnerable to wildfire.

4.3.2 Overall Model robustness

To test the robustness of the model, and visualisation of the performance, a Receiver Operating Characteristic (ROC) curve is created, in which the three models are tested for sensitivity (true positive rate) and specificity (false positive rate). Normally the true/false positive rates are determined from sample class/population, in this case, it is not possible to clearly identify if a cell in the model is a true/false positive. Therefore, for each breakpoint (fire hazard class) the true/false negative rates are set to be half a standard deviation as the estimated error rate (Winner, 2009). Following Fawcett (2006) example, the fire scores are used as breakpoints, and for each breakpoint the sensitivity and specificity rates are calculated using a fixed factor ($\frac{1}{2}$ standard deviation) to compute the False positives/negatives (Figure 33).

		True class			
		P	N	fp rate = $\frac{FP}{N}$	tp rate = $\frac{TP}{P}$
Hypothesized class	Y	True Positives	False Positives	precision = $\frac{TP}{TP+FP}$	recall = $\frac{TP}{P}$
	N	False Negatives	True Negatives		
Column totals:		P	N	accuracy = $\frac{TP+TN}{P+N}$	F-measure = $\frac{2}{\frac{1}{precision} + \frac{1}{recall}}$

Figure 33: Confusion matrix and common performance metrics calculated from it (Fawcett, 2006)

The sensitivity is also known as the recall, and specificity is $1 - FP$ rate, in Figure 34 the Area under a ROC curve (AUC) is shown for the tree models (see Appendix XXX for the calculations of the AUC).

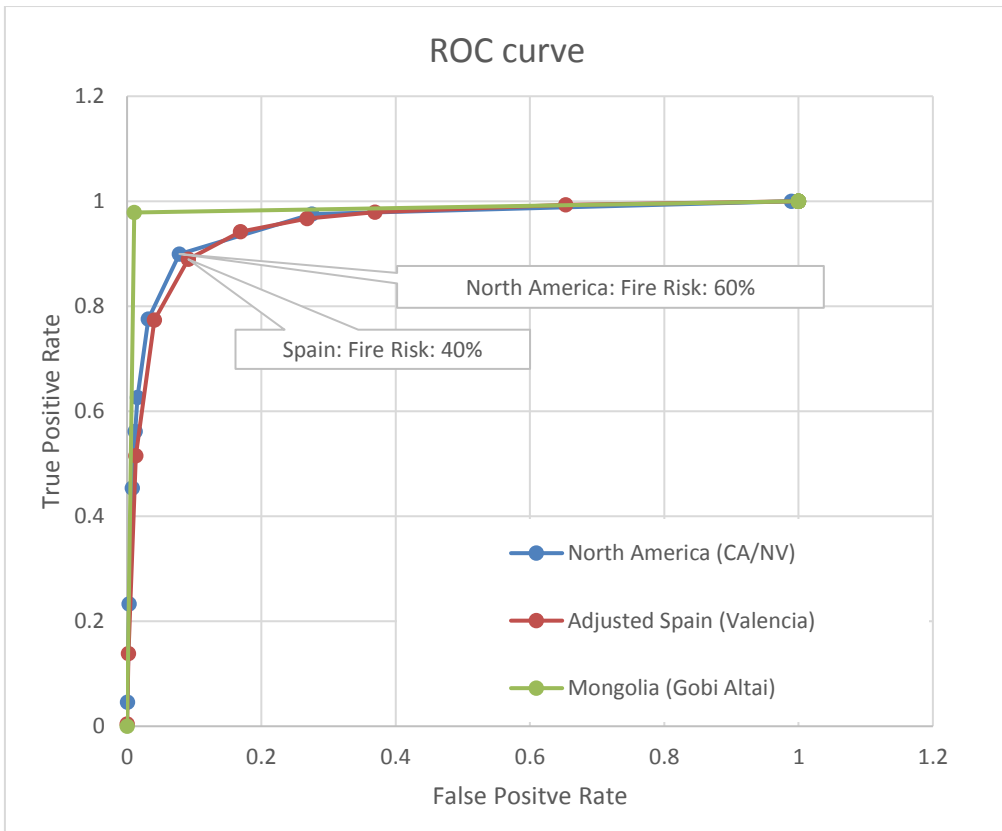


Figure 34: ROC curves for North America (CA/NV), Spain (Valencia), and Mongolia (Gobi Altai)

All three models are behaving well, with an $AUC > 0.95$, but with only two fire rates used to create the Mongolian curve the result for the study area in Mongolia are not very reliable. The models for Spain and North America are behaving well, and the fire classification is sound for both models (AUC classification is Excellent (Table 6)). The North America Model is (with a breakpoint of 60%) more susceptible to wildfire than the study area in Spain (breakpoint set to 40%).

5 Conclusions

The aim of this study was to test the possibility of creating a temporal–spatial predictive wildfire model, based on global datasets and fuzzy logic functions and data-driven operations. The developed methodology has successfully been applied in three study areas, and the results are a realistic representation of the wildfire hazard in those areas. One of the objectives was to creating a risk score with the use of coarse datasets, e.g. fuel and climatological parameters, in combination with a less coarse DEM; in all three study areas it was possible to downscale the coarse datasets to the highest resolution and derive a risk score.

One of the weak areas of the methodology is the identification of false positives in the burnt area product (like in the Mongolia study area). More research is needed to classify the areas of false positives correctly, and develop a rule-set to prevent the model to calculate a score in these regions because false positives are likely to be in areas with a low fuel load.

The individual model components (topographical derivatives, fuel loads, and meteorological indicators) are providing a robust framework for calculating a risk score. The creating of fuzzy membership functions with basic statistics offers a solid foundation for the scoring, but the Multi-Criteria Analysis is setup without the consultation of (local) experts. Including expert opinions, in more detailed studies, might provide a less subjective process and an in the validation phase an independent resource to adjust the hazard scores when the overall processes are not generating the correct score.

The fuel score is a composite of four different information layers, each with product-specific limitations and resolutions, but the used method is creating a fuel score which is a good representation of the fuel availability in the study areas.

By using the BKDI as the temporal aspect for fire occurrences, it is possible to predict the risk of fire for each week. Although, this is an area where the model could be improved.

In this study only one factor for each study area is used, a better solution would be to calculate the BKDI for each grid cell and use the local maximum to scale the score and calculate the weekly hazard.

Finally, it is possible to compute a realistic hazard score by using coarse datasets, remote sensing products and GIS techniques. Using the proposed methodology can help to establish a better understanding of the fire risk, especially in regions where high-quality data is not available, and assist decision makers and environmental agencies with the development of management policies and approaches to mitigate the fire risks in those regions.

Recommendations:

- The dependencies in the model should further investigated in areas where local risk scoring maps are available (like in the Nevada part of the North American study area)
- A more detailed study of the relation between land cover, climate, and MODIS products might provide better insight in the detection of false positives of the burned area
- Including (local) expert knowledge in the MCA process might create more defendable weighting factors and an independent validation resource
- Including seasonality in the fuel-score might be another time-dependent element, which is not taken into consideration in this study. Neither is the effect of historic fire events on the vegetation; land cover, fuel scores, bio-volume and -mass are kept constant between years. Modelling land cover change due to forest/wildfires will give a better estimation of available fuel loads.

6 References

- Adab, H., Kanniah, K.D. and Solaimani, K. (2011) 'GIS-based probability assessment of fire risk in grassland and Forested landscapes of Golestan province, Iran', 2011 International Conference on Environmental and Computer Science, 19, pp. 170–175.
- Adrc.asia. (n.d.). Country Report on Natural Disasters in Mongolia. [online] Available at: http://www.adrc.asia/countryreport/MNG/MNGeng98/#_Toc452879156 [Accessed 15 Apr. 2017].
- Alexander, M.E. (1990) 'Computer calculation of the Keetch-Byram Drought Index-programmers beware', Fire Manage Notes, 51(4), pp. 23–25.
- Alexander, M.E. and Cruz, M.G., 2013. Limitations on the accuracy of model predictions of wildland fire behaviour: a state-of-the-knowledge overview. *The Forestry Chronicle*, 89(3), pp.372-383.
- Amraoui, M., Liberato, M.L.R., Calado, T.J., DaCamara, C.C., Coelho, L.P., Trigo, R.M. and Gouveia, C.M. (2013) 'Fire activity over Mediterranean Europe based on information from Meteosat-8', *Forest Ecology and Management*, 294, pp. 62–75. doi: 10.1016/j.foreco.2012.08.032.
- Andrews, P. L., Bevins, C. D., Seli, R. C. (2003). 'BehavePlus fire modeling system, version 2.0: User's Guide.' Gen. Tech. Rep. RMRS-GTR-106WWW. Ogden, UT: Department of Agriculture, Forest Service, Rocky Mountain Research Station. 132 p.
- Aragó, P., Juan, P., Díaz-Avalos, C. and Salvador, P. (2016) 'Spatial point process modeling applied to the assessment of risk factors associated with forest wildfires incidence in Castellón, Spain', *European Journal of Forest Research*, 135(3), pp. 451–464. doi: 10.1007/s10342-016-0945-z.
- Balga, L. (2012) 'Aspects regarding the significance of the curvature types and values in the studies of geomorphometry assisted by GIS', *Annals of the University of Oradea, Geography Series*, 2/2012(XXII), pp. 327–337.
- Banu, T.P., Banu, C.A. and Banu, C. (2014) 'GIS-based assessment of fire risk in national park Domogled- Cerna valley', *JOURNAL of Horticulture Forestry and Biotechnology*, 18(2), pp. 52–56.
- Bliege Bird, R., Bird, D., Codding, B., Parker, C. and Jones, J. (2008). The "fire stick farming" hypothesis: Australian Aboriginal foraging strategies, biodiversity, and anthropogenic fire mosaics. *Proceedings of the National Academy of Sciences*, 105(39), pp.14796-14801.
- Burgess, R. (2011) Development of a spatial, dynamic, fuzzy fire risk model for Chitwan district, Nepal. MSc thesis. Available at: http://www.itc.nl/library/papers_2011/msc/gem/burgess.pdf (Accessed: 18 June 2016).
- Butler, B. W., Anderson, W. R. and Catchpole E. A. (2007). 'Influence of Slope on Fire Spread Rate', USDA Forest Service Proceedings RMRS-P-46 CD p.75– 83.
- Cardil, A., Merenciano, D. and Molina-Terrén, D. (2016). Wildland fire typologies and extreme temperatures in NE Spain. *iForest - Biogeosciences and Forestry*, 10(1), pp.9-14.

- Cardil, A., Molina, D., Ramirez, J. and Vega-García, C. (2013). Trends in adverse weather patterns and large wildland fires in Aragón (NE Spain) from 1978 to 2010. *Natural Hazards and Earth System Science*, 13(5), pp.1393-1399.
- Ceccato, P., Gobron, N., Flasse, S., Pinty, B., & Tarantola, S. (2002). 'Designing a spectral index to estimate vegetation water content from remote sensing data: Part 1'. *Theoretical approach*. *Remote Sensing of Environment*, 82, 188–197.
- CFFM (no date) Satellite remote-sensing technologies used in forest fire management. Available at: http://219.239.221.19/cffm_office/english/content.asp?id=386 (Accessed: 18 June 2016).
- Chandler, C., Cheney, P., Thomas, P., Trabaud, L., and Williams, D. (1983), *Fire in Forestry, Vol I. Forest Fire Behaviour and Effects*, John Wiley, New York, p. 450.
- Chu, T. and Guo, X. (2013) 'Remote sensing techniques in monitoring post-fire effects and patterns of Forest Recovery in Boreal forest regions: A review', *Remote Sensing*, 6(1), pp. 470–520. doi: 10.3390/rs6010470.
- Chuvieco, E. and Congalton, R.G. (1989) 'Application of remote sensing and geographic information systems to forest fire hazard mapping', *Remote Sensing of Environment*, 29(2), pp. 147–159. doi: 10.1016/0034-4257(89)90023-0.
- Chuvieco, E., Salas, J. and Vega, C., 1997. Remote sensing and GIS for long-term fire risk mapping. A review of remote sensing methods for the study of large wildland fires, pp.91-108.
- Chuvieco, E., Riaño, D., Van Wagtendok, J. and Morsdof, F. (2003). Fuel Loads and Fuel Type Mapping. Series in Remote Sensing, pp.119-142.
- Chuvieco, E., Cocero, D., Riaño, D., Martin, P., Martínez-Vega, J., de la Riva, J. and Pérez, F. (2004) 'Combining NDVI and surface temperature for the estimation of live fuel moisture content in forest fire danger rating', *Remote Sensing of Environment*, 92(3), pp. 322–331. doi: 10.1016/j.rse.2004.01.019.
- Clynne, M.A., Christiansen, R.L., Felger, T., Stauffer, P. and Hendley, J. (1999) 1915: Lassen's most recent eruption. Available at: <https://www.nature.nps.gov/Geology/usgsnps/lassen/lassenfact.html> (Accessed: 4 February 2017).
- Cramer, W., Kicklighter, D.W., Bondeau, A., Moore Iii, B., Churkina, G., Nemry, B., Ruimy, A. and Schloss, A.L. (1999) 'Comparing global models of terrestrial net primary productivity (NPP): Overview and key results', *Global Change Biology*, 5(S1), pp. 1–15. doi: 10.1046/j.1365-2486.1999.00009.x.
- Crimmins, M.A. (2006) 'Synoptic climatology of extreme fire-weather conditions across the southwest United States', *International Journal of Climatology*, 26(8), pp. 1001–1016. doi: 10.1002/joc.1300.
- Dobos, E., Micheli, E., Baumgardner, M.F., Biehl, L. and Helt, T. (2000) 'Use of combined digital elevation model and satellite radiometric data for regional soil mapping', *Geoderma*, 97(3-4), pp. 367–391. doi: 10.1016/s0016-7061(00)00046-x.

- Dolling, K., Chu, P. and Fujioka, F. (2005) 'A climatological study of the Keetch/Byram drought index and fire activity in the Hawaiian Islands', *Agricultural and Forest Meteorology*, 133(1-4), pp. 17–27. doi: 10.1016/j.agrformet.2005.07.016.
- Dupuy 2011 The effects of slope and fuel bed width on laboratory fire behaviour International Journal of Wildland Fire 2011, 20, 272–288
- Eastaugh, C. and Hasenauer, H. (2014). Deriving forest fire ignition risk with biogeochemical process modelling. *Environmental Modelling & Software*, 55, pp.132-142.
- ESA Climate Change Initiative - Land Cover project 2014
- ESRI (2016) ArcGIS Pro: Release 1.3.1. Redlands, CA: Environmental Systems Research Institute.
- Fawcett, T. (2006). An introduction to ROC analysis. *Pattern Recognition Letters*, 27(8), pp.861-874.
- Feltman, J.A., Straka, T.J., Post, C.J. and Sperry, S.L. (2012) 'Geospatial analysis application to forecast Wildfire occurrences in South Carolina', *Forests*, 3(4), pp. 265–282. doi: 10.3390/f3020265.
- Finney M.A., (1998) 'FARSITE: Fire Area Simulator – Model Development and Evaluation.' USDA For. Serv. Res. Pa RMRS-RP-4 revised February 2004, access 2016/07/17 from: http://www.fs.fed.us/rm/pubs/rmrs_rp004.pdf
- Finney, M.A. (2005) 'The challenge of quantitative risk analysis for wildland fire', *Forest Ecology and Management*, 211(1-2), pp. 97–108. doi: 10.1016/j.foreco.2005.02.010.
- Finney, M. A. (2006) 'An overview of FlamMap fire modeling capabilities'. Pages 213-220 in P. L. Andrews and B. W. Butler, editors. *Fuels Management--How to Measure Success*, Portland, OR.
- Fischer, M., Di Bella, C. and Jobbágy, E. (2015). Influence of fuel conditions on the occurrence, propagation and duration of wildland fires: A regional approach. *Journal of Arid Environments*, 120(September 2015), pp.63-71.
- Freeborn, P., Cochrane, M. and Wooster, M. (2014) 'A decade long, multi-scale map comparison of fire regime parameters derived from Three publically available satellite-based fire products: A case study in the Central African Republic', *Remote Sensing*, 6(5), pp. 4061–4089. doi: 10.3390/rs6054061.
- García, F.M. and Montero, G. (2000) 'TYPOLOGY OF Pinus sylvestris L. FORESTS IN SPAIN EVOLUTION OF Pinus sylvestris L. FORESTS IN THE IBERIAN PENINSULA SINCE THE LAST GLACIATION', *Forest Systems*, 9(1), pp. 41–65.
- Garcia-Martin, A., Perez-Cabello, F., de la Riva Fernandez, J. and Montorio Lloveria, R. (2008) 'Estimation of Crown Biomass of Pinus spp. From Landsat TM and Its Effect on Burn Severity in a Spanish Fire Scar', *IEEE Journal of Selected Topics in Applied Earth Observations and Remote Sensing*, 1(4), pp. 254–265. doi: 10.1109/jstars.2008.2011623.

- Gaucherel, C., Guiot, J. and Misson, L. (2008) 'Changes of the potential distribution area of french Mediterranean forests under global warming', *Biogeosciences*, 5(6), pp. 1493–1504. doi: 10.5194/bg-5-1493-2008.
- Gerdzheva, A.A. (2014) 'A comparative analysis of different wildfire risk assessment models (a case study for Smolyan district, Bulgaria)', *European Journal of Geography*, 5(3), pp. 22–36.
- Ghimire, B. (2014) Fire hazard zonation of Bardia National Park, Nepal: a disaster preparedness approach., MSC thesis. Institute of Science and Technology Tribhuvan University Kirtipur, Kathmandu, Nepal.
- Giglio, L., Descloitres, J., Justice, C.O. and Kaufman, Y.J. (2003) 'An enhanced Contextual fire detection algorithm for MODIS', *Remote Sensing of Environment*, 87(2-3), pp. 273–282. doi: 10.1016/s0034-4257(03)00184-6.
- Giglio, L., Randerson, J. and van der Werf, G. (2013). Analysis of daily, monthly, and annual burned area using the fourth-generation global fire emissions database (GFED4). *Journal of Geophysical Research: Biogeosciences*, 118(1), pp.317-328.
- Gitas, I.Z., San-Miguel-Ayanz, J., Chuvieco, E. and Camia, A. (2014) 'Advances in remote sensing and GIS applications in support of forest fire management', *International Journal of Wildland Fire*, 23(5), p. 603. doi: 10.1071/wf14117.
- Goodrick, S.L. (2002) 'Modification of the Fosberg fire weather index to include drought', *International Journal of Wildland Fire*, 11(4), pp. 205–211. doi: 10.1071/wf02005.
- Hansen, M.C., Potapov, P.V., Moore, R., Hancher, M., Turubanova, S.A., Tyukavina, A., Thau, D., Stehman, S.V., Goetz, S.J., Loveland, T.R., Kommareddy, A., Egorov, A., Chini, L., Justice, C.O. and Townshend, J.R.G. (2013) 'High-resolution global maps of 21st-century Forest Cover change', *Science*, 342(6160), pp. 850–853. doi: 10.1126/science.1244693.
- Hardy, C.C. (2005) 'Wildland fire hazard and risk: Problems, definitions, and context', *Forest Ecology and Management*, 211(1-2), pp. 73–82. doi: 10.1016/j.foreco.2005.01.029.
- Hawbaker, T.J., Radeloff, V.C., Syphard, A.D., Zhu, Z. and Stewart, S.I. (2008) 'Detection rates of the MODIS active fire product in the United States', *Remote Sensing of Environment*, 112(5), pp. 2656–2664. doi: 10.1016/j.rse.2007.12.008.
- Heim, R.R. (2002) 'A Review of Twentieth-Century Drought Indices Used in the United States', *Bulletin of the American Meteorological Society*, 83(8), pp. 1149–1165. doi: 10.1175/1520-0477(2002)083<1149:AROTDI>2.3.CO;2.
- Hoelzemann, J.J., Schultz, M.G., Brasseur, G.P. and Granier, G. (2004) 'Global Wildland fire emission model (GWEM): Evaluating the use of global area burnt satellite data', *Journal of Geophysical Research*, 109(D14), pp. 1–18. doi: 10.1029/2003jd003666.
- Holden, Z.A., Morgan, P. and Evans, J.S. (2016) 'A predictive model of burn severity based on 20-year satellite-inferred burn severity data in a large southwestern US wilderness area', *Forest Ecology and Management*, 258(11), pp. 2399–2406. doi: 10.1016/j.foreco.2009.08.017.

- Huete, A., Didan, K., Miura, T., Rodriguez, E.P., Gao, X. and Ferreira, L.G. (2002) 'Overview of the radiometric and biophysical performance of the MODIS vegetation indices', *Remote Sensing of Environment*, 83(1-2), pp. 195–213. doi: 10.1016/s0034-4257(02)00096-2.
- IFADAsia (no date) Mongolia - About - Gobi-Altai. Available at: <https://asia.ifad.org/web/mongolia/gobi-altai> (Accessed: 6 February 2017).
- Jovanovic, R., Bjeljac, Z., Miljkovic, O. and Terzic, A. (2013) 'Spatial analysis and mapping of fire risk zones and vulnerability assessment: Case study mt. Stara planina', *Journal of the Geographical Institute Jovan Cvijic, SASA*, 63(3), pp. 213–226. doi: 10.2298/ijgi1303213j.
- Justice, C.O., Giglio, L., Roy, D., Boschetti, L., Csiszar, I., Davies, D., Korontzi, S., Schroeder, W., O'Neal, K. and Morisette, J. (2011) 'MODIS-Derived Global Fire Products', in Ramachandran, B., Abrams, M.J., and Justice, C.O. (eds.) *Land remote sensing and global environmental change: NASA's earth observing system and the science of Aster and Modis*. United States: Springer Science+Business Media, pp. 665–680.
- Keane, R.E., Burgan, R. and van Wagtendonk, J. (2001) 'Mapping wildland fuels for fire management across multiple scales: Integrating remote sensing, GIS, and biophysical modeling', *International Journal of Wildland Fire*, 10(4), pp. 301–319. doi: 10.1071/wf01028.
- Keeley, J.E. (2009) 'Fire intensity, fire severity and burn severity: A brief review and suggested usage', *International Journal of Wildland Fire*, 18(1), pp. 116–126. doi: 10.1071/wf07049.
- Keetch, J.J. and Byram, G.M. (1968) 'A drought index for Forest Fire control', Res. Pap. SE-38. Asheville, NC: U.S. Department of Agriculture, Forest Service, Southeastern Forest Experiment Station.
- Krawchuk, M.A. and Moritz, M.A. (2011) 'Constraints on global fire activity vary across a resource gradient', *Ecology*, 92(1), pp. 121–132. doi: 10.1890/09-1843.1.
- Laris, P. (2013). Integrating Land Change Science and Savanna Fire Models in West Africa. *Land*, 2(4), pp.609-636.
- Lecina-Diaz, J., Alvarez, A. and Retana, J. (2014) 'Extreme fire severity patterns in topographic, Convective and wind-driven historical Wildfires of Mediterranean pine forests', *PLoS ONE*, 9(1), p. e85127. doi: 10.1371/journal.pone.0085127.
- Loveland, T.R., Reed, B.C., Brown, J.F., Ohlen, D.O., Zhu, Z., Yang, L. and Merchant, J.W. (2000) 'Development of a global land cover characteristics database and IGBP dISCover from 1 km AVHRR data', *International Journal of Remote Sensing*, 21(6-7), pp. 1303–1330. doi: 10.1080/014311600210191.
- Ministry of Nature, Environment and Tourism (2011) REPORT ON STATE OF THE ENVIRONMENT OF MONGOLIA, 2008-2010. Available at: <http://bic.iwlearn.org/en/documents-1/state-of-the-environment-report-mongolia-2008-2010-english> (Accessed: 6 February 2017).
- Moore, I. D., Grayson, R. B., & Ladson, A. R. (1991). Terrain based catchment partitioning and runoff prediction using vector elevation data. *Water Resources Research*, 27, 1177–1191. doi:10.1029/91WR00090.

- Moritz, M., Parisien, M., Batllori, E., Krawchuk, M., Van Dorn, J., Ganz, D. and Hayhoe, K. (2012). Climate change and disruptions to global fire activity. *Ecosphere*, 3(6), p.art49.
- Papadopoulos, G.D. and Pavlidou, F.-N. (2011) 'A comparative review on Wildfire simulators', *IEEE Systems Journal*, 5(2), pp. 233–243. doi: 10.1109/jsyst.2011.2125230.
- Pausas, J.G. (2004) 'Changes in fire and climate in the eastern Iberian peninsula (Mediterranean basin)', *Climatic Change*, 63(3), pp. 337–350. doi: 10.1023/b:clim.0000018508.94901.9c.
- Pausas, J. and Keeley, J. (2009). A Burning Story: The Role of Fire in the History of Life. *BioScience*, 59(7), pp.593-601.
- Peel, M., Finlayson, B. and McMahon, T. (2007). Updated world map of the Köppen-Geiger climate classification. *Hydrology and Earth System Sciences*, 11(5), pp.1633-1644.
- Peterson, S., Roberts, D. and Dennison, P. (2008) 'Mapping live fuel moisture with MODIS data: A multiple regression approach', *Remote Sensing of Environment*, 112(12), pp. 4272–4284. doi: 10.1016/j.rse.2008.07.012.
- Pettinari, M.L. and Chuvieco, E. (2016) 'Generation of a global fuel data set using the fuel characteristic classification system', *Biogeosciences*, 13(7), pp. 2061–2076. doi: 10.5194/bg-13-2061-2016.
- Piñol, J., J. Terradas, and F. Lloret. (1998). 'Climate warming, wildfire hazard, and wildfire occurrence in coastal Eastern Spain.', *Climate Change* 38: 345–357
- Pradhan, B. and Awang, M.A. (2007) 'Application of remote sensing and gis for forest fire susceptibility mapping using likelihood ratio model.', *Proceedings of Map Malaysia*
- Department of Civil and Environmental Engineering/Princeton University (2006): Global Meteorological Forcing Dataset for Land Surface Modeling. Research Data Archive at the National Center for Atmospheric Research, Computational and Information Systems Laboratory. <http://rda.ucar.edu/datasets/ds314.0/>. Accessed 16 Sep 2016.
- Quill, R. (2016) Fire Modeling in an Uncertain World. Available at: <http://wildfiremagazine.org/article/fire-modeling-in-an-uncertain-world/> (Accessed: 18 July 2016).
- Robinson, V.B. (2003) 'A perspective on the fundamentals of fuzzy sets and their use in geographic information systems', *Transactions in GIS*, 7(1), pp. 3–30. doi: 10.1111/1467-9671.00127.
- Rochoux, M., Delmotte, B., Cuenot, B., Ricci, S. and Trouv  , A. (2013). Regional-scale simulations of wildland fire spread informed by real-time flame front observations. *Proceedings of the Combustion Institute*, 34(2), pp.2641-2647.
- Rothermel, R.C. (1972) 'A mathematical model for predicting fire spread in wildland fuels', USDA Forest Service Research Paper, INT-115.
- Rouse, J. W., Jr., Haas, R. H., Schell, J. A., Deering, D. W. (1973), 'Monitoring Vegetation Systems in the Great Plains with ERTS', Third Earth Resources Technology Satellite-1 Symposium- Volume I: Technical Presentations. NASA SP-351 p. 309–317

- Roy, D.P., Jin, Y., Lewis, P.E. and Justice, C.O. (2005) 'Prototyping a global algorithm for systematic fire-affected area mapping using MODIS time series data', *Remote Sensing of Environment*, 97(2), pp. 137–162. doi: 10.1016/j.rse.2005.04.007.
- Roy, D.P., Boschetti, L., Justice, C.O. and Ju, J. (2008) 'The collection 5 MODIS burned area product — global evaluation by comparison with the MODIS active fire product', *Remote Sensing of Environment*, 112(9), pp. 3690–3707. doi: 10.1016/j.rse.2008.05.013.
- Santoro, M., A. Beaudoin, C. Beer, O. Cartus, J.E.S. Fransson, R. Hall, C. Pathe, C. Schmullius, A. Shvidenko, D. Schepaschenko, M. Thurner and U. Wegmüller (2015): Forest growing stock volume of the northern hemisphere: an estimate for 2010 derived from Envisat ASAR data, *Remote Sensing of Environment*, 168, 316-334.
- Schulz, J.J., Cayuela, L., Echeverria, C., Salas, J. and Rey Benayas, J.M. (2010) 'Monitoring land cover change of the dryland forest landscape of central Chile (1975–2008)', *Applied Geography*, 30(3), pp. 436–447. doi: 10.1016/j.apgeog.2009.12.003.
- Sheffield, J., G. Goteti, and E. F. Wood, 2006: Development of a 50-yr high-resolution global dataset of meteorological forcings for land surface modeling, *J. Climate*, 19 (13), 3088–3111
- Scott, J.H. and Burgan, R.E. (2005) Standard Fire Behavior Fuel Models: A Comprehensive Set for Use with Rothermel's Surface Fire Spread Model. General Technical Report RMRS-GTR-153. Fort Collins, CO: United States Department of Agriculture, , Forest Service, Rocky Mountain Research Station. 72 p.
- Sirca, C., Casula, F., Bouillon, C., García, B., Fernández Ramiro, M., Molina, B. and Spano, D. (2017). A wildfire risk oriented GIS tool for mapping Rural-Urban Interfaces. *Environmental Modelling & Software*, 94, pp.36-47.
- Suvdantsetseg, B., Fukui, H. and Tsolmon, R. (2008) 'SAXAUL FOREST AREA DETERMINATION BY REMOTE SENSING IN MONGOLIA'S GOBI REGION', *The International Archives of the Photogrammetry, Remote Sensing and Spatial Information Sciences.*, 37(B8), pp. 1081–1086.
- Svoboda, M. (2000) 'An introduction to the drought monitor', *Drought Network News*, 12(1), pp. 15–20.
- Sá, A., Benali, A., Pinto, R., Fernandes, P., Russo, A., Santos, F., Trigo, R., Pereira, J., Jerez, S. and Camara, C. da (2014) 'Improving wildfire spread simulations using MODIS active fires: the FIRE-MODSAT project', in *Advances in forest fire research*. Coimbra: Imprensa da Universidade de Coimbra
- Takeuchi, W., Darmawan, S., Shofiyati, R., Khiem, M.V., Oo, K.S., Pimple, U. and Heng, S., 2015, October. Near-real time meteorological drought monitoring and early warning system for croplands in Asia. In *Proceedings of the 36th Asian Conference on Remote Sensing*, Manila, Philippines.
- Thurner, M., C. Beer, M. Santoro, N. Carvalhais, T. Wutzler, D. Schepaschenko, A. Shvidenko, E. Kompter, B. Ahrens, S.R. Levick and C. Schmullius (2014): Carbon stock and density of northern boreal and temperate forests, *Global Ecology and Biogeography*, 23, 3, 297-310.

- Tobler, W.R. (1970) 'A computer movie Simulating urban growth in the Detroit region', *Economic Geography*, 46, p. 234. doi: 10.2307/143141.
- Tsela, P., Wessels, K., Botai, J., Archibald, S., Swanepoel, D., Steenkamp, K. and Frost, P. (2014) 'Validation of the Two standard MODIS satellite burned-area products and an empirically-derived merged product in South Africa', *Remote Sensing*, 6(2), pp. 1275–1293. doi: 10.3390/rs6021275.
- Turner M.G, Romme, W.H, (1994) 'Landscape dynamics in crown fire ecosystems', *Landscape Ecology* vol. 9 no. 1 pp 59-77 SPB Academic Publishing bv, The Hague
- Tymstra, C., Flannigan, M.D., Armitage, O.B. and Logan, K. (2007) 'Impact of climate change on area burned in Alberta's boreal forest', *International Journal of Wildland Fire*, 16(2), pp. 153–160. doi: 10.1071/wf06084.
- UN-SPIDER (2015) Data Application of the Month: Forest Fires. Available at: <http://www.un-spider.org/links-and-resources/data-sources/daotm-fire> (Accessed: 18 June 2016).
- Vadrevu, K.P., Eaturu, A. and Badarinath, K.V.S. (2009) 'Fire risk evaluation using multicriteria analysis—a case study', *Environmental Monitoring and Assessment*, 166(1-4), pp. 223–239. doi: 10.1007/s10661-009-0997-3.
- Veraverbeke, S., Lhermitte, S., Verstraeten, W.W. and Goossens, R. (2010) 'The temporal dimension of differenced normalized burn ratio (dNBR) fire/burn severity studies: The case of the large 2007 Peloponnese wildfires in Greece', *Remote Sensing of Environment*, 114(11), pp. 2548–2563. doi: 10.1016/j.rse.2010.05.029.
- Veraverbeke, S., Sedano, F., Hook, S.J., Randerson, J.T., Jin, Y. and Rogers, B.M. (2014) 'Mapping the daily progression of large wildland fires using MODIS active fire data', *International Journal of Wildland Fire*, 23(5), pp. 655–668. doi: 10.1071/wf13015.
- Wang, Q., Ni, J. and Tenhunen, J. (2005) 'Application of a geographically-weighted regression analysis to estimate net primary production of Chinese forest ecosystems', *Global Ecology and Biogeography*, 14(4), pp. 379–393. doi: 10.1111/j.1466-822x.2005.00153.x.
- Wells, G. (2007) 'The Rothermel fire-spread model: Still running like a champ', *JFSP Fire Science Digest* pp. 1–11.
- Wildland Fire Associates, (2009). Landscape-Scale Wildland Fire Risk/Hazard/Value Assessment Pershing County, Nevada. [online] Pershing County, Nevada: Nevada Fire Board, Nevada State Office. Available at: <http://forestry.nv.gov/wp-content/uploads/2013/12/Pershing-County-Assessment-Final.pdf> [Accessed 17 Apr. 2017].
- Winner, L. (2009). Applied Statistical Methods. 1st ed. Department of Statistics, University of Florida.
- Wilson, J.P. and Gallant, J.C. (2000) 'Digital terrain analysis', in Wilson, J.P. and Gallant, J.C. (eds.) *Terrain analysis: Principles and applications*. Wiley, pp. 1–27.

- Xiao-rui, T., Mcrae, D.J., Li-fu, S., Ming-yu, W. and Hong, L. (2005) 'Satellite remote-sensing technologies used in forest fire management', *Journal of Forestry Research*, 16(1), pp. 73–78. doi: 10.1007/bf02856861.
- Yebra, M., Dennison, P.E., Chuvieco, E., Riaño, D., Zylstra, P., Hunt, E.R., Danson, F.M., Qi, Y. and Jurdao, S. (2013) 'A global review of remote sensing of live fuel moisture content for fire danger assessment: Moving towards operational products', *Remote Sensing of Environment*, 136, pp. 455–468. doi: 10.1016/j.rse.2013.05.029.
- Zadeh (1965) 'Fuzzy sets, Information and Control', Volume 8, Issue 3, June 1965, Pages 338–353, ISSN 0019-9958, [http://dx.doi.org/10.1016/S0019-9958\(65\)90241-X](http://dx.doi.org/10.1016/S0019-9958(65)90241-X).
- Zadeh, L.A. (1983) 'The role of fuzzy logic in the management of uncertainty in expert systems', *Fuzzy Sets and Systems*, 11(1-3), pp. 199–227. doi: 10.1016/s0165-0114(83)80081-5.
- Zhao, N., Yang, Y. and Zhou, X. (2010) 'Application of geographically weighted regression in estimating the effect of climate and site conditions on vegetation distribution in Haihe Catchment, china', *Plant Ecology*, 209(2), pp. 349–359. doi: 10.1007/s11258-010-9769-y.
- Zhang X.Y., Drake N.A., Wainwright J., Mulligan M. (1999) Comparison of slope estimates from low resolution DEMs: scaling issues and a fractal method for their solution. *Earth Surf Process Landf* 24:763–779

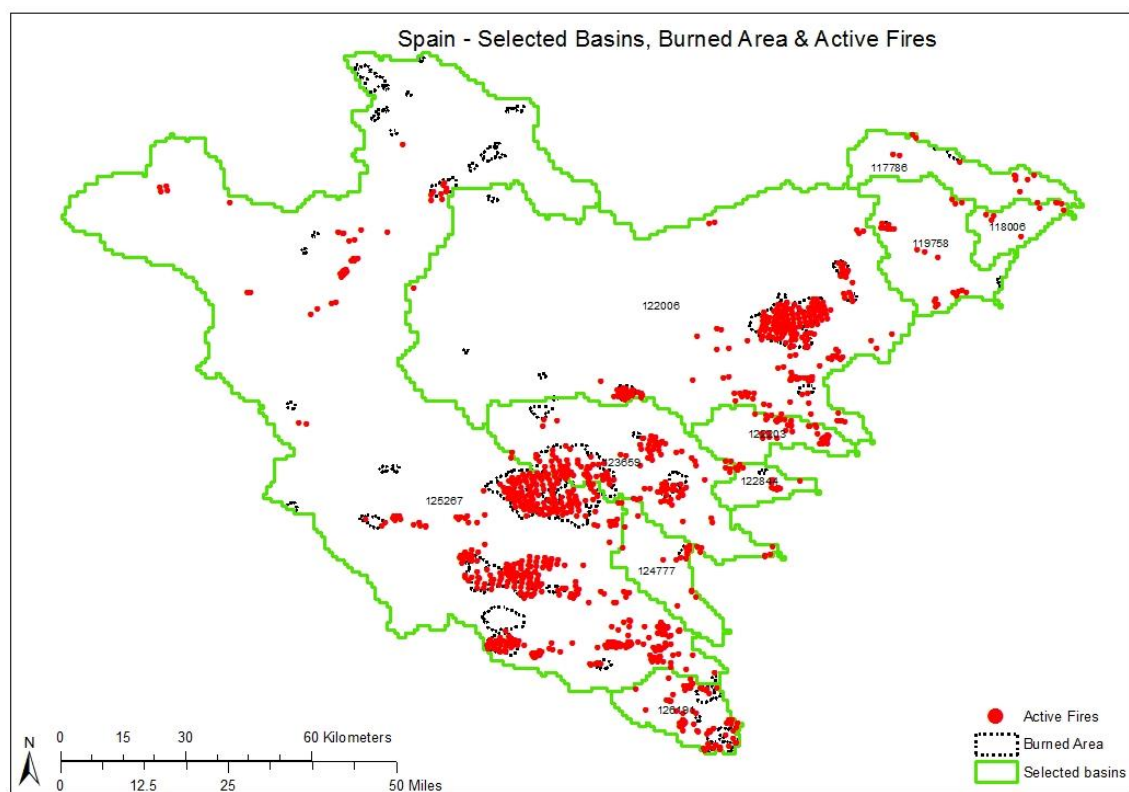
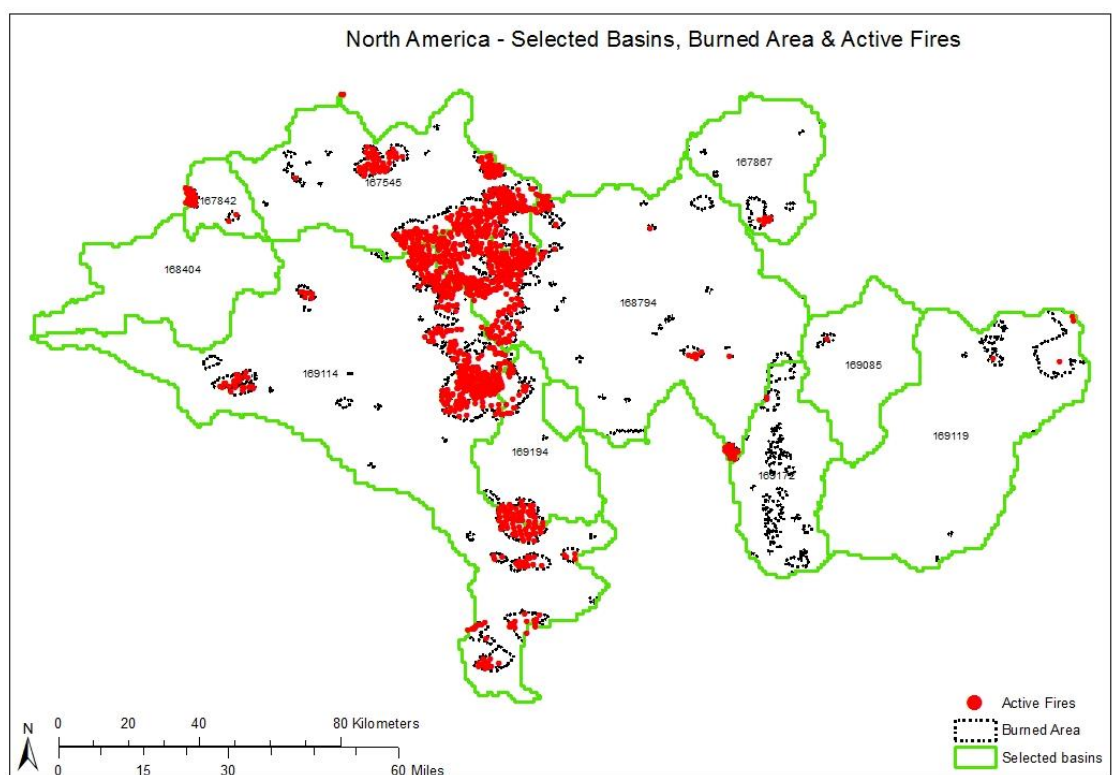
Appendices

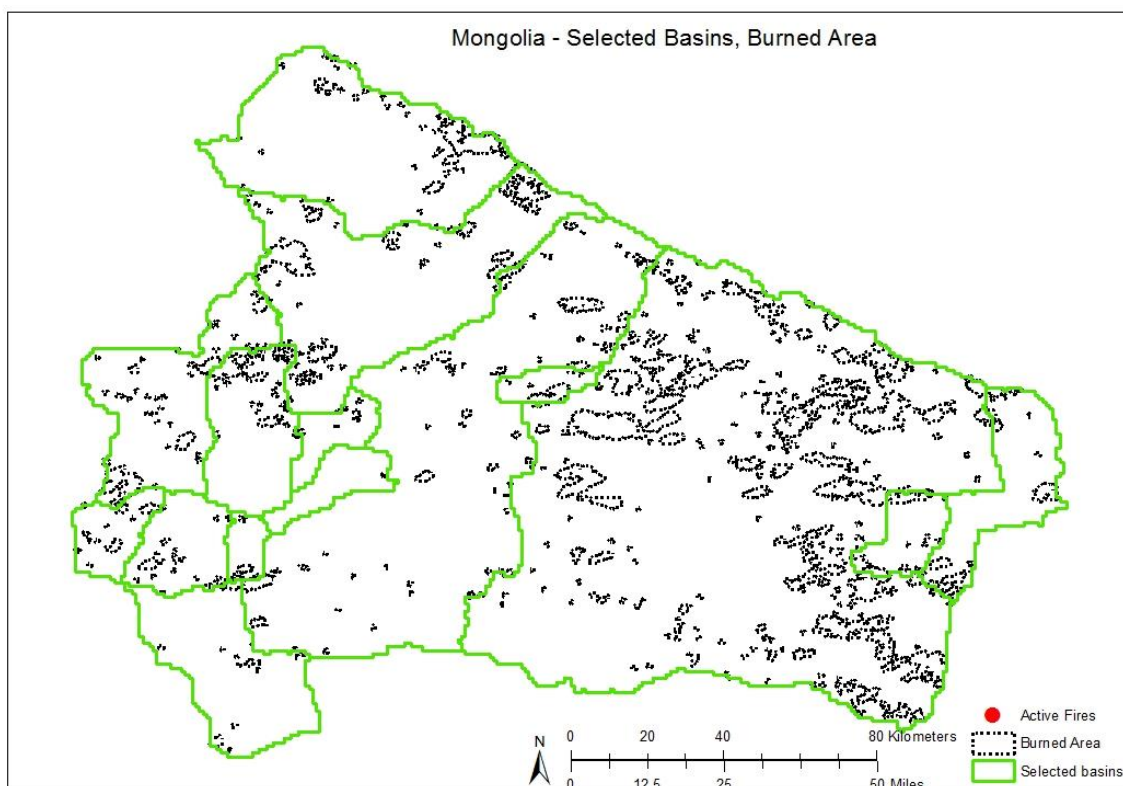
- Appendix I – Data sources
- Appendix II – Study Areas
- Appendix III – Topographical Indicators
- Appendix IV – Topographical Fuzzy Membership
- Appendix V – Fuel indicators
- Appendix VI – Fuel Fuzzy Membership (Score)
- Appendix VII – Topographical MCA Results
- Appendix VIII – Fire Risk corrected for Drought

Appendix I: Data sources

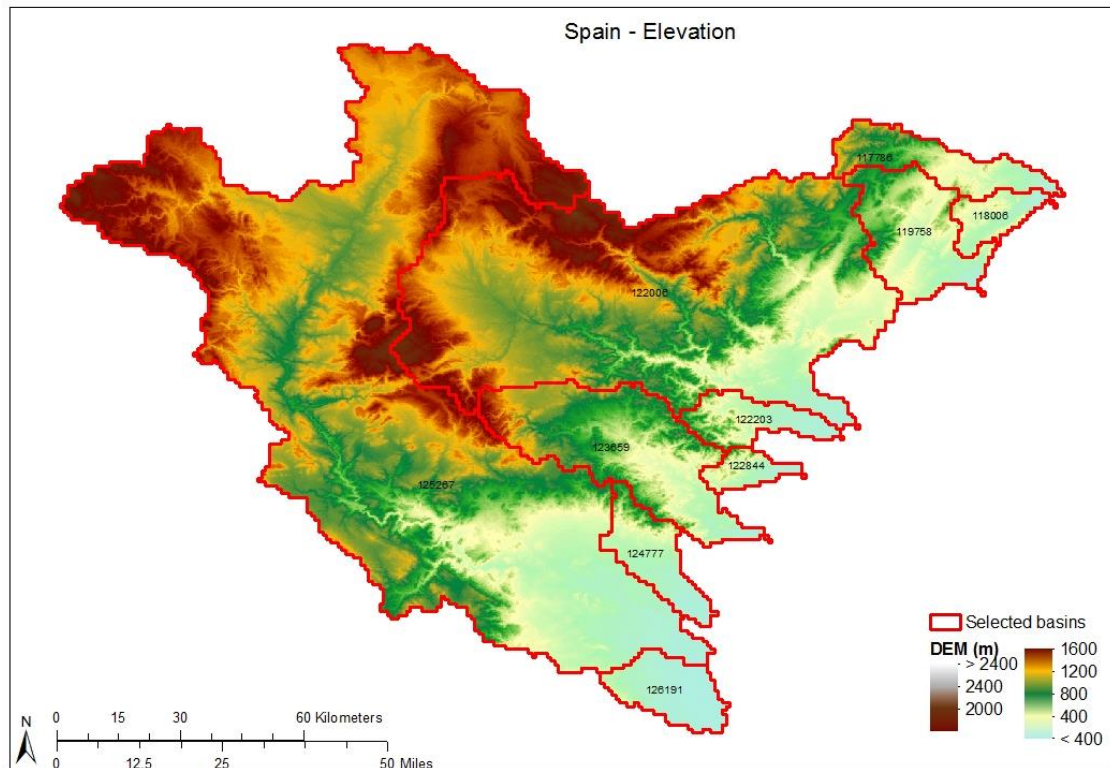
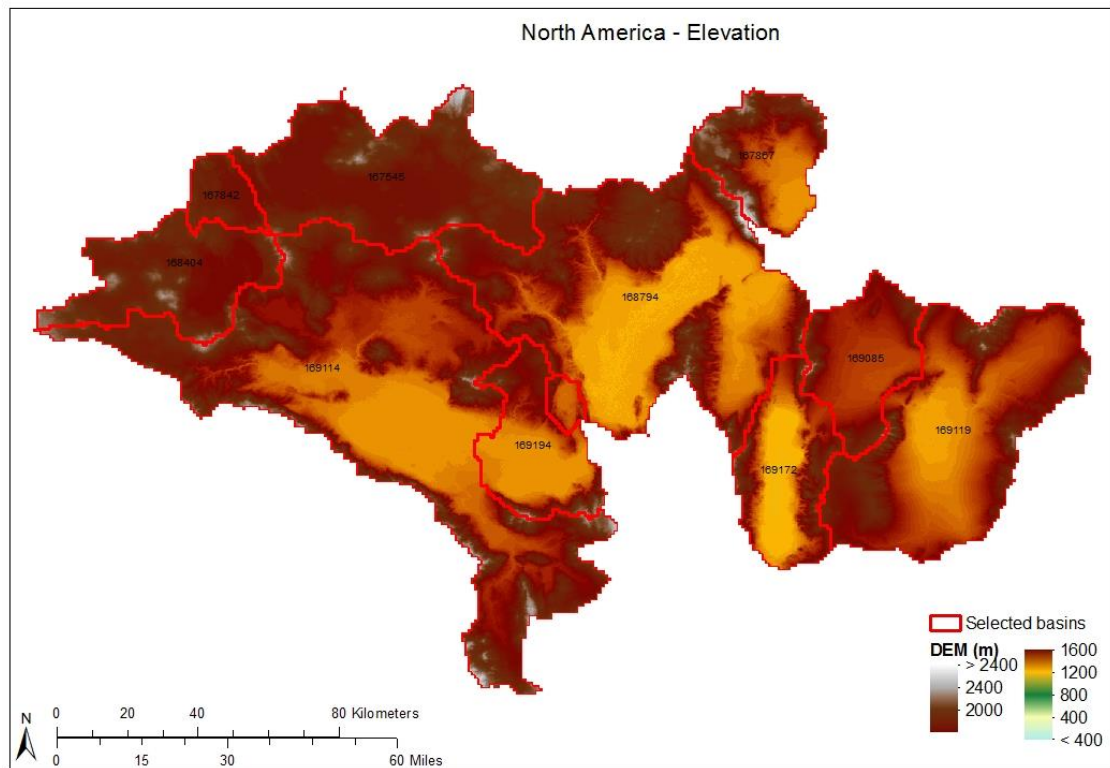
Layer	Product Name	Source	Web link	Accessed
MODIS - BA	Burned Area Monthly L3 Global 500m	NASA	https://modis.gsfc.nasa.gov/data/dataproducts/mod45.php http://modis-fire.umd.edu/pages/BurnedArea.php	19/04/2017
MODIS - AF	MODIS Active Fire Product	NASA	https://earthdata.nasa.gov/earth-observation-data/near-real-time/firms/active-fire-data	19/04/2017
DEM	SRTM 90m Digital Elevation Data	NASA	http://www.cgiar-csi.org/data/srtm-90m-digital-elevation-database-v4-1	19/04/2017
HydroSHEDS	Drainage directions Flow accumulation (number of cells) Drainage basins (watershed boundaries)	USGS	https://hydrosheds.cr.usgs.gov/hydro.php	19/04/2017
Land Cover	300 m annual global land cover time series from 1992 to 2015	ESA	https://www.esa-landcover-cci.org/	19/04/2017
Fuelbeds	Global Fuel Data set using the Fuel Characteristic Classification System	Pettinari	https://doi.pangaea.de/10.1594/PANGAEA.849808.	19/04/2017
Biomass	BIOMASAR	Santoro	www.biomasar.org.	19/04/2017
Biovolume	GEOCARBON	Thurner	https://www.bgc-jena.mpg.de/geodb/projects/Home.php	19/04/2017
Temperature	Global Meteorological Forcing Dataset for Land Surface Modeling	Princeton University	https://rda.ucar.edu/datasets/ds314.0/	19/04/2017
Precipitation				

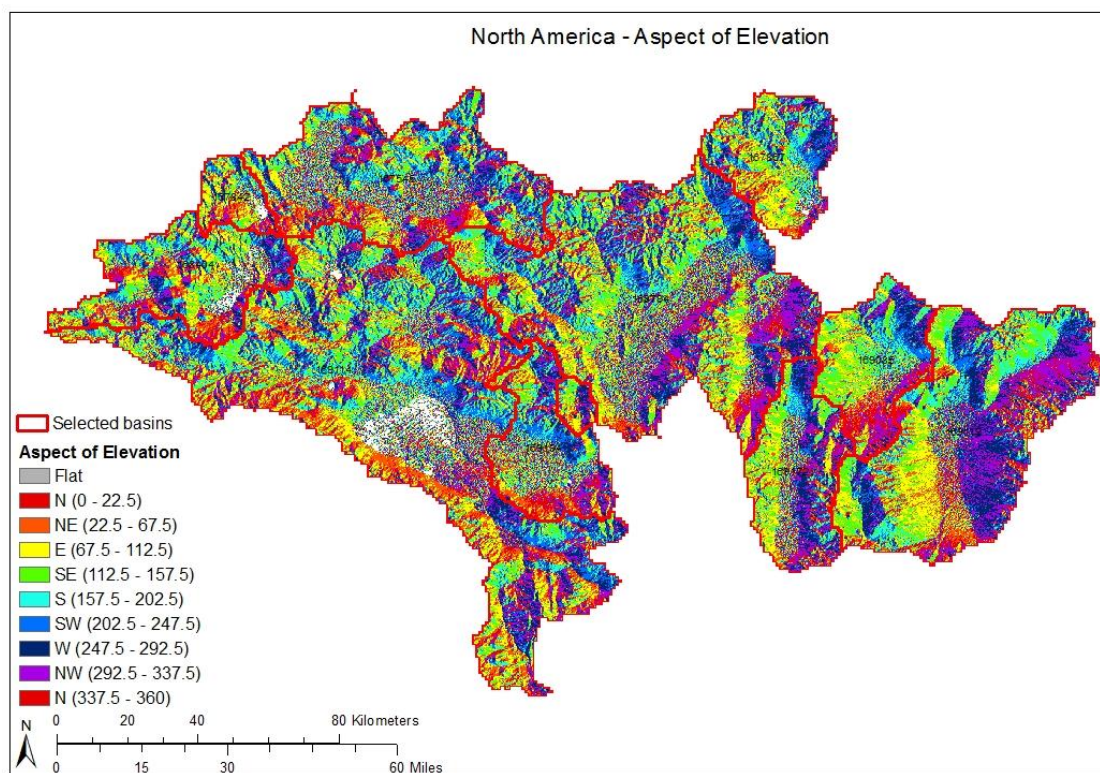
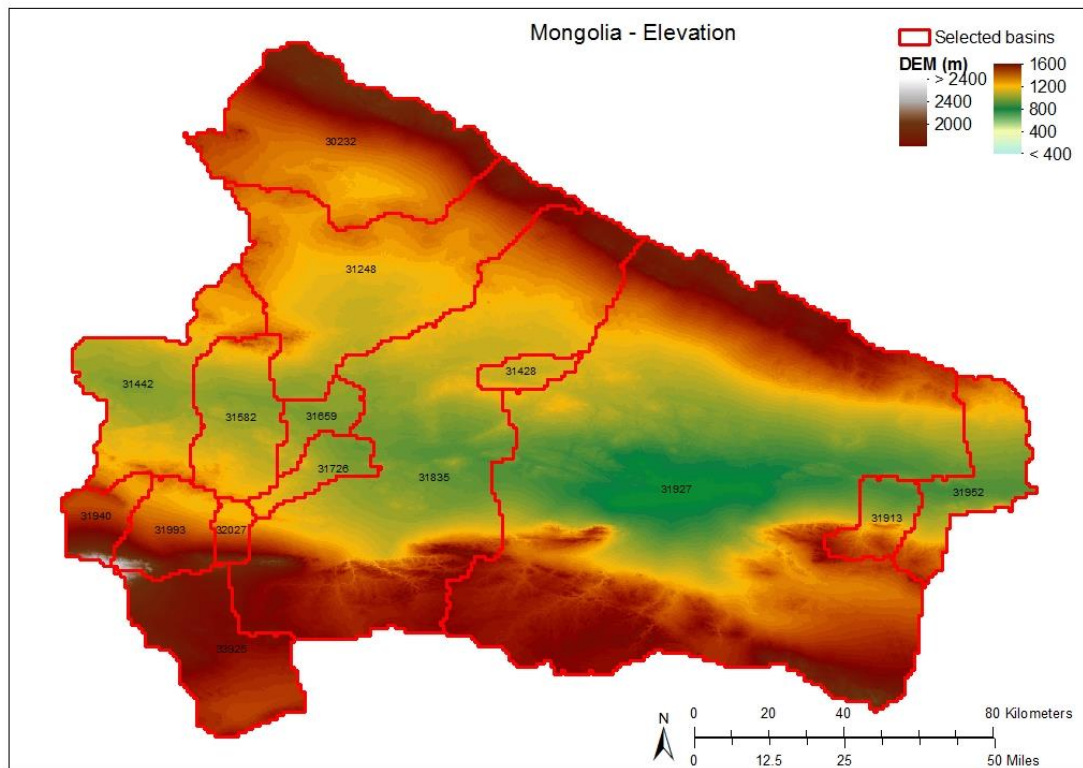
Appendix II – Study Areas

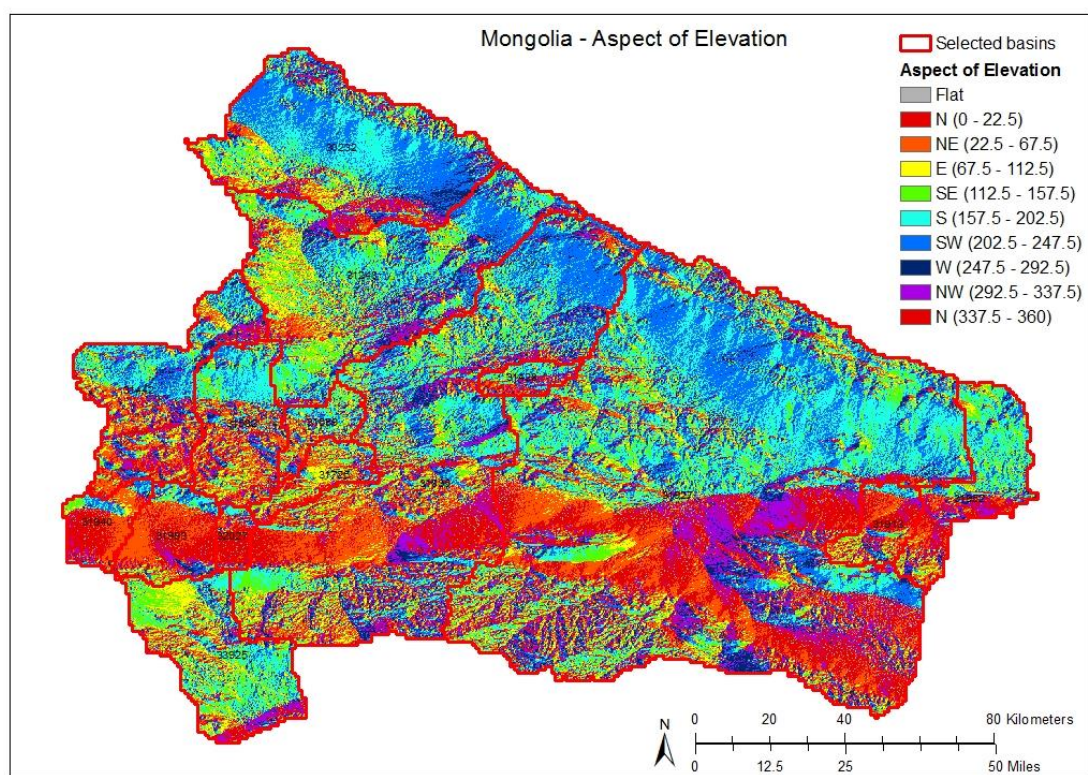
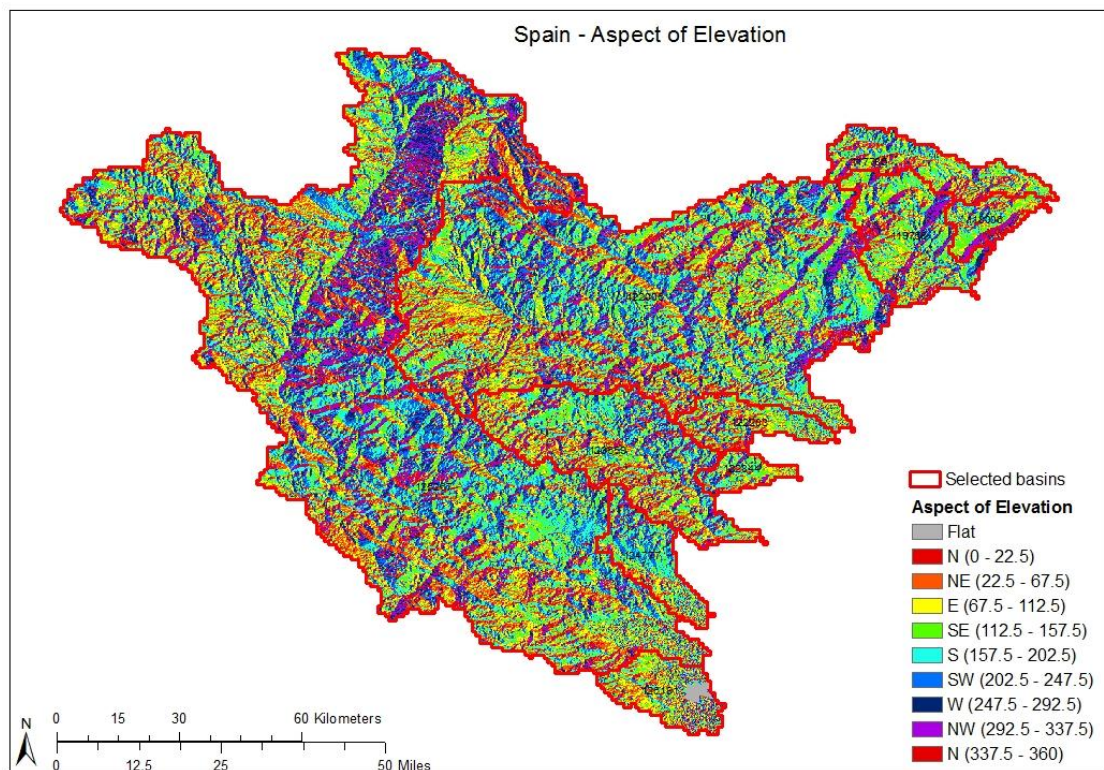


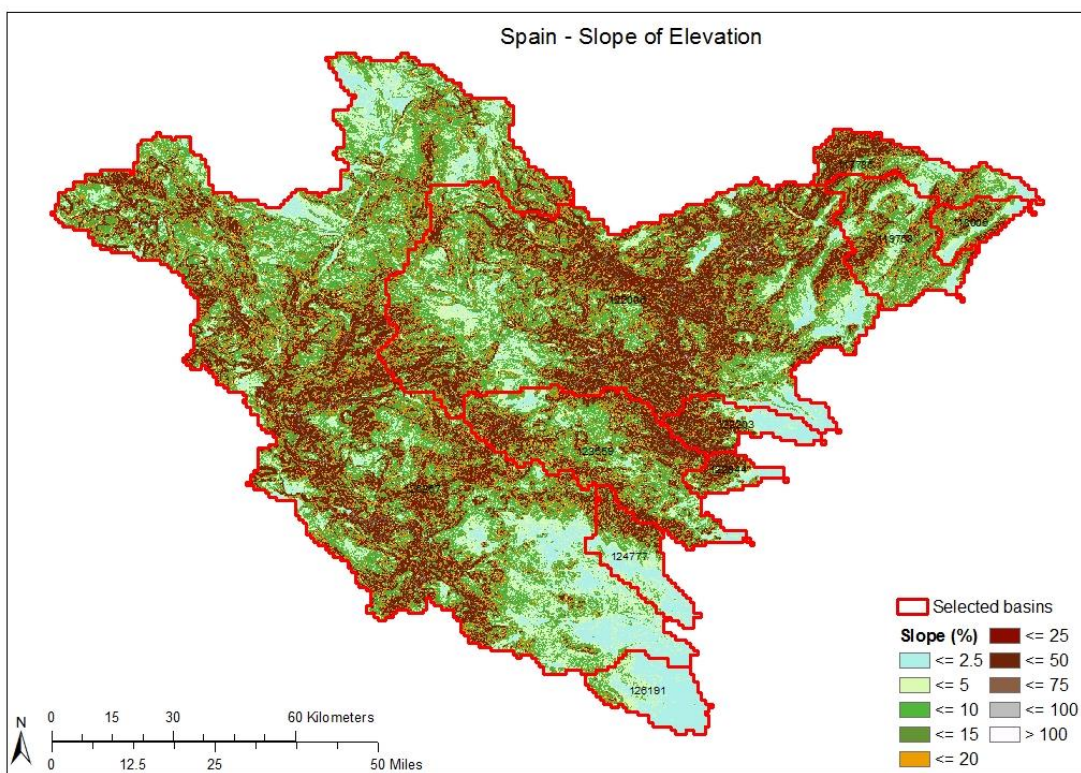
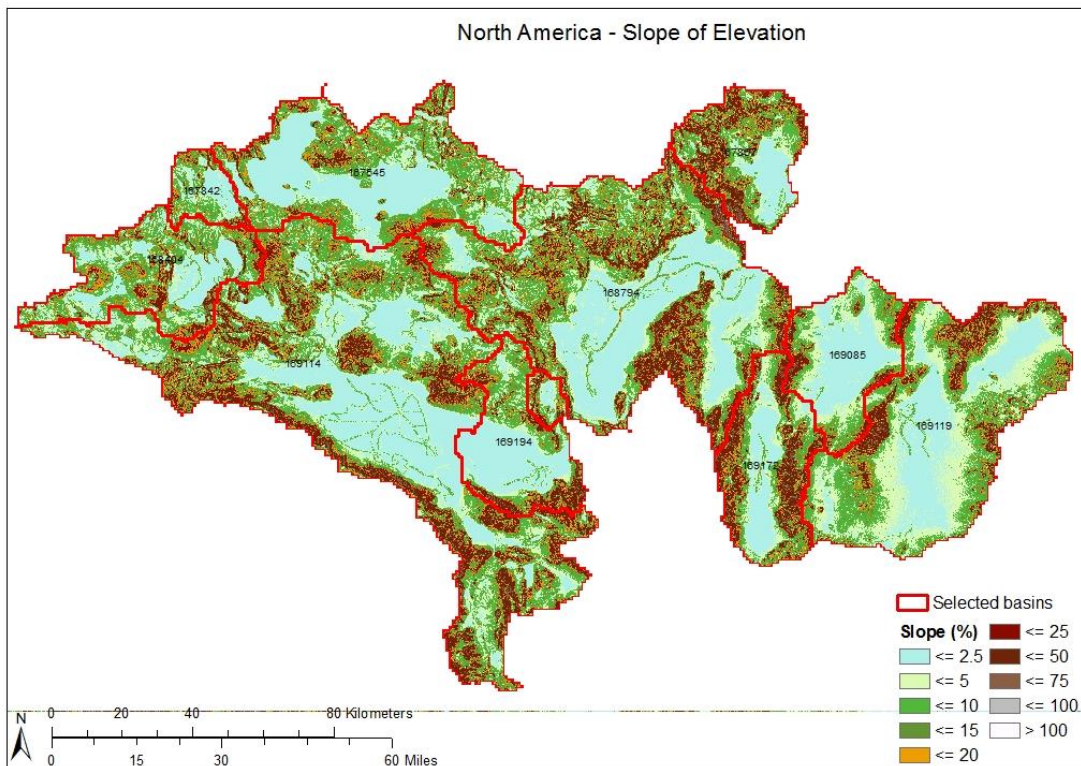


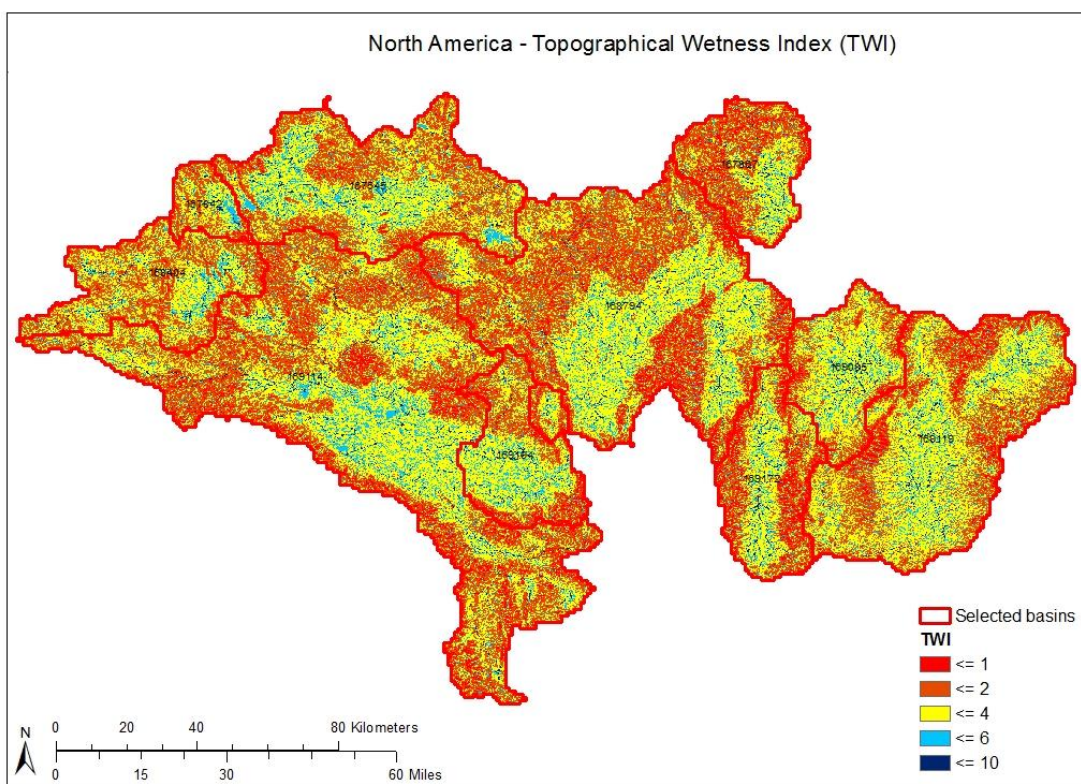
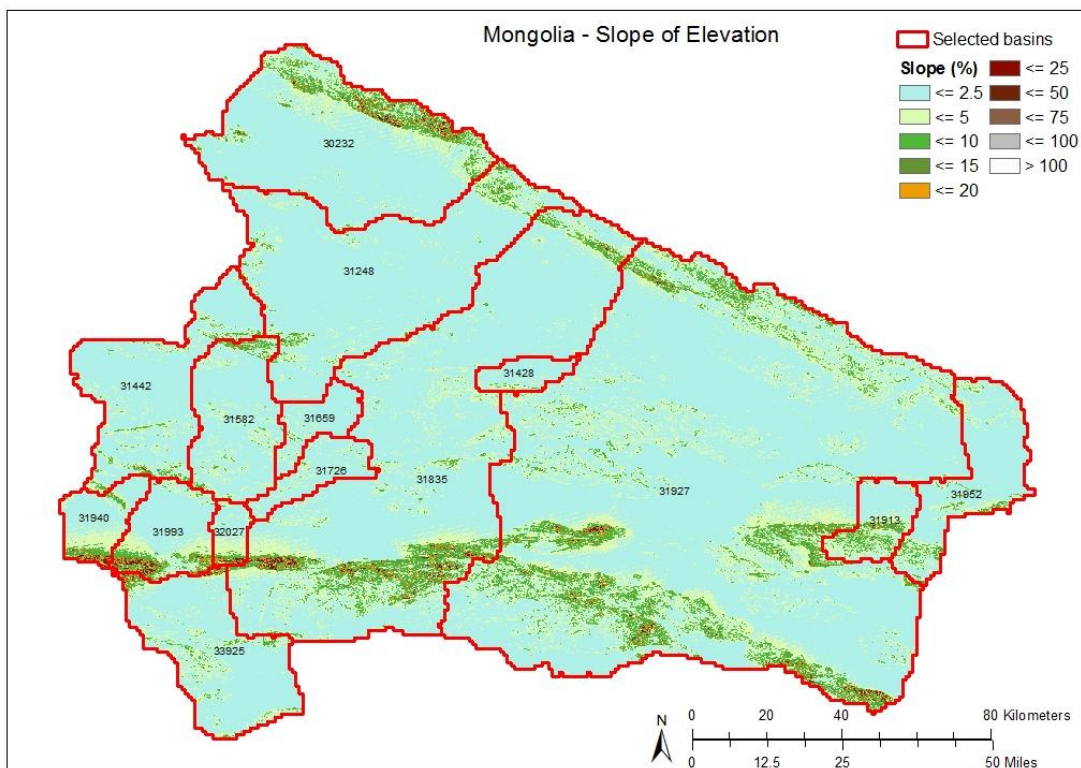
Appendix III – Topographical Indicators

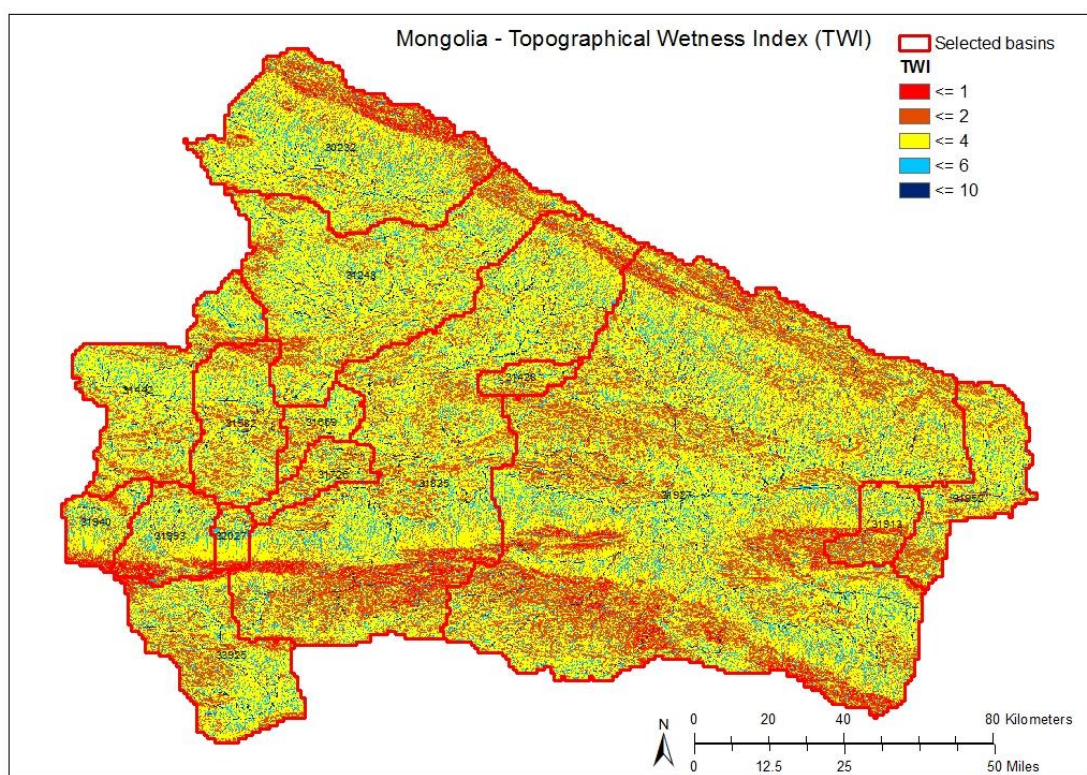
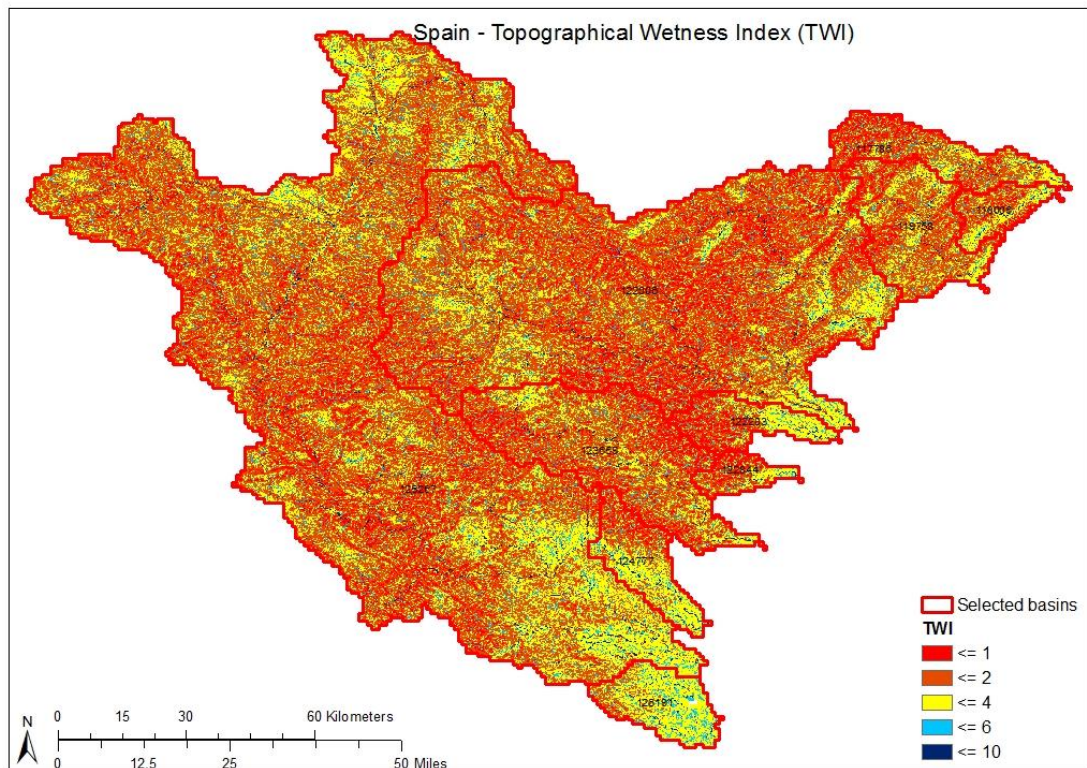


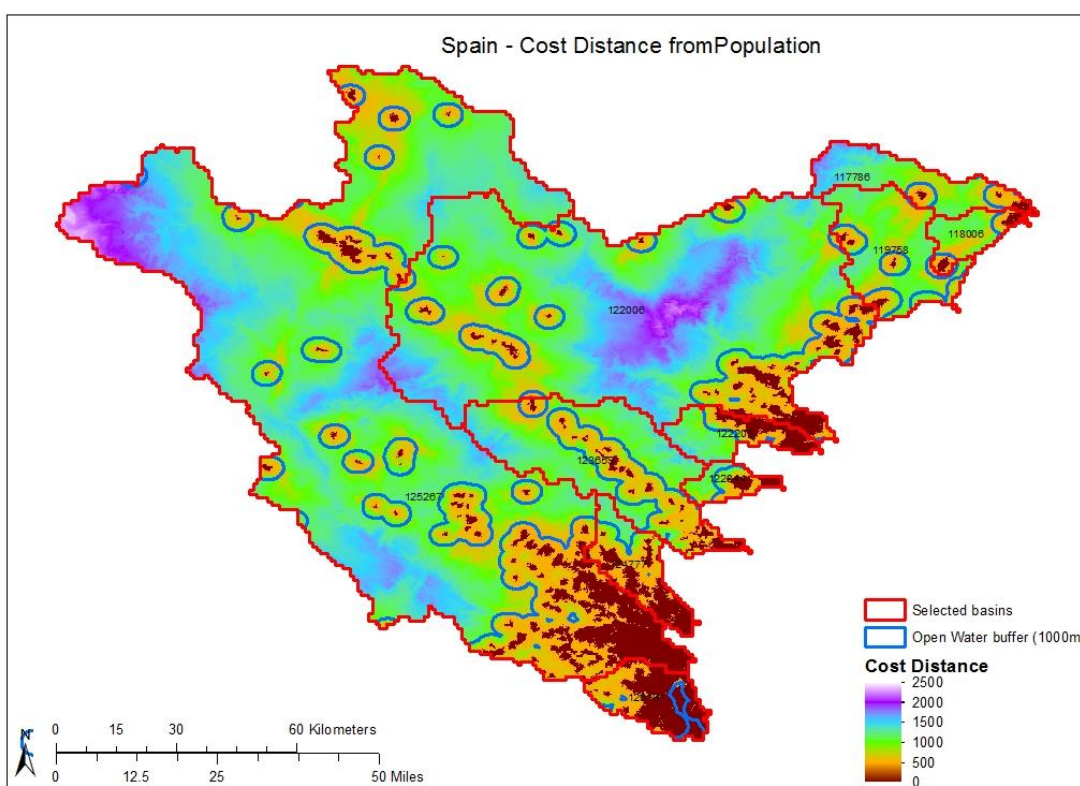
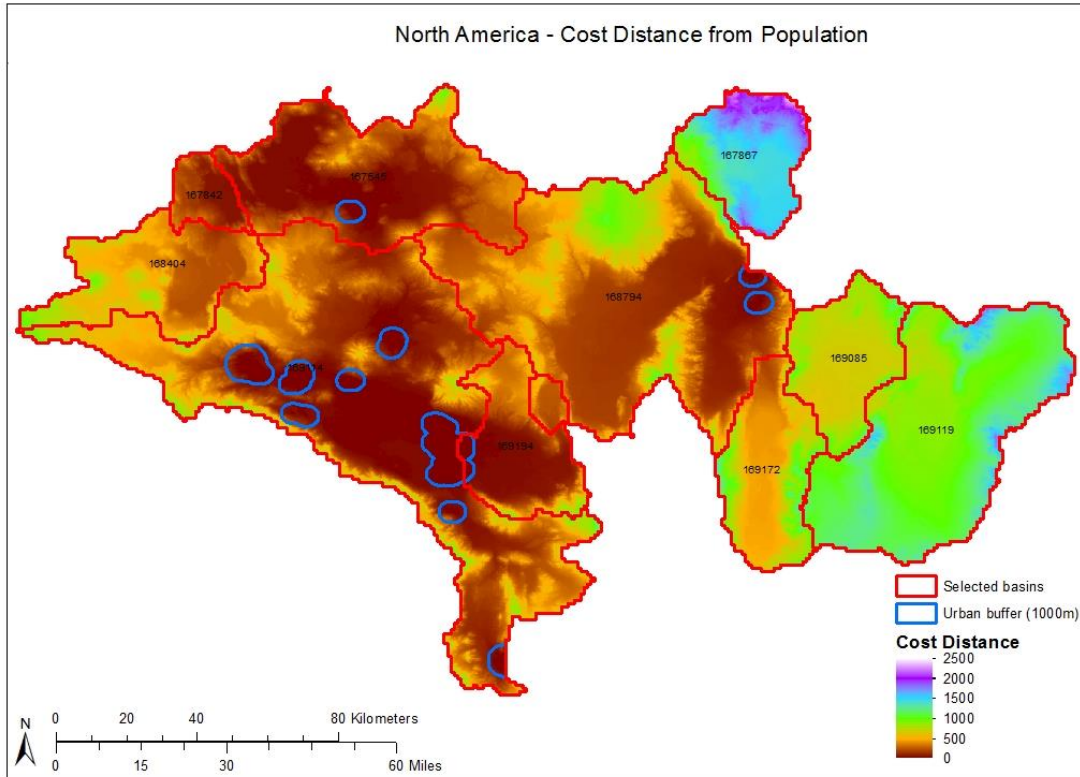


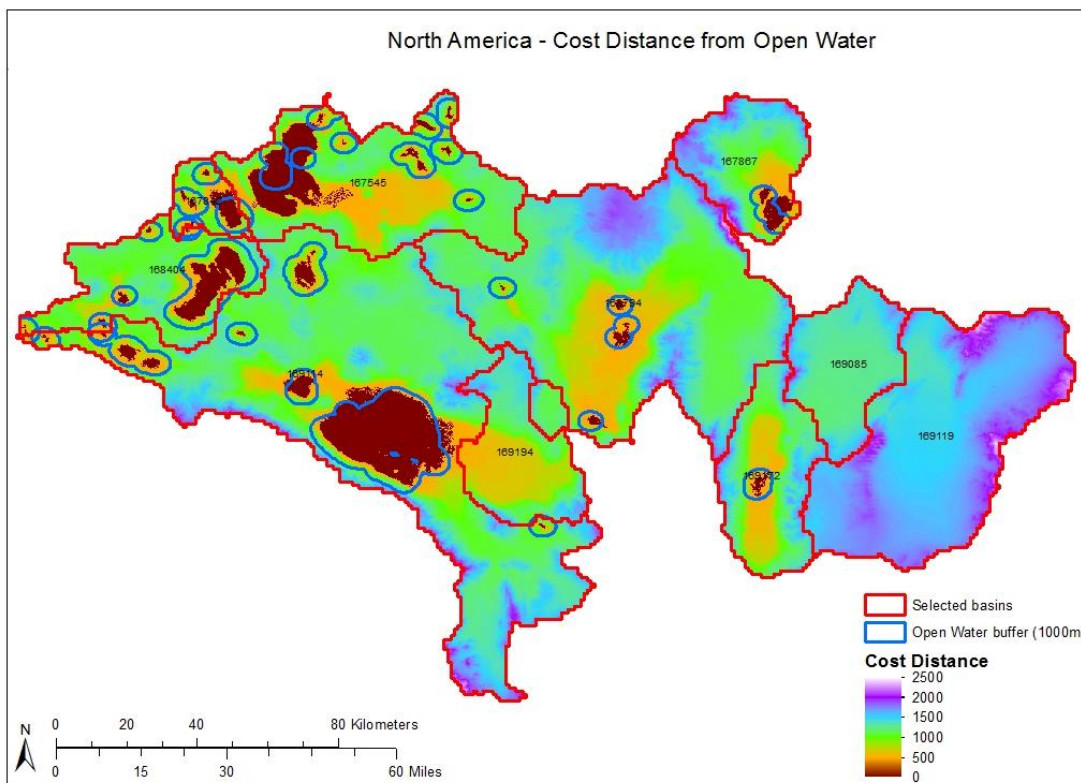
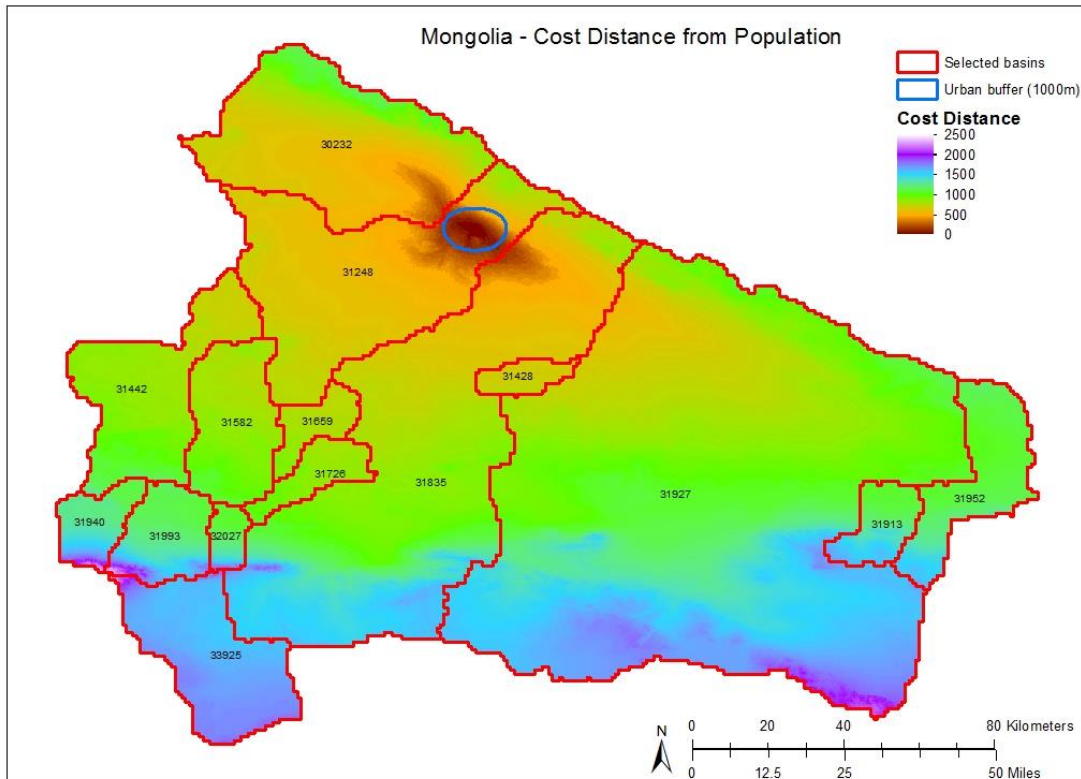


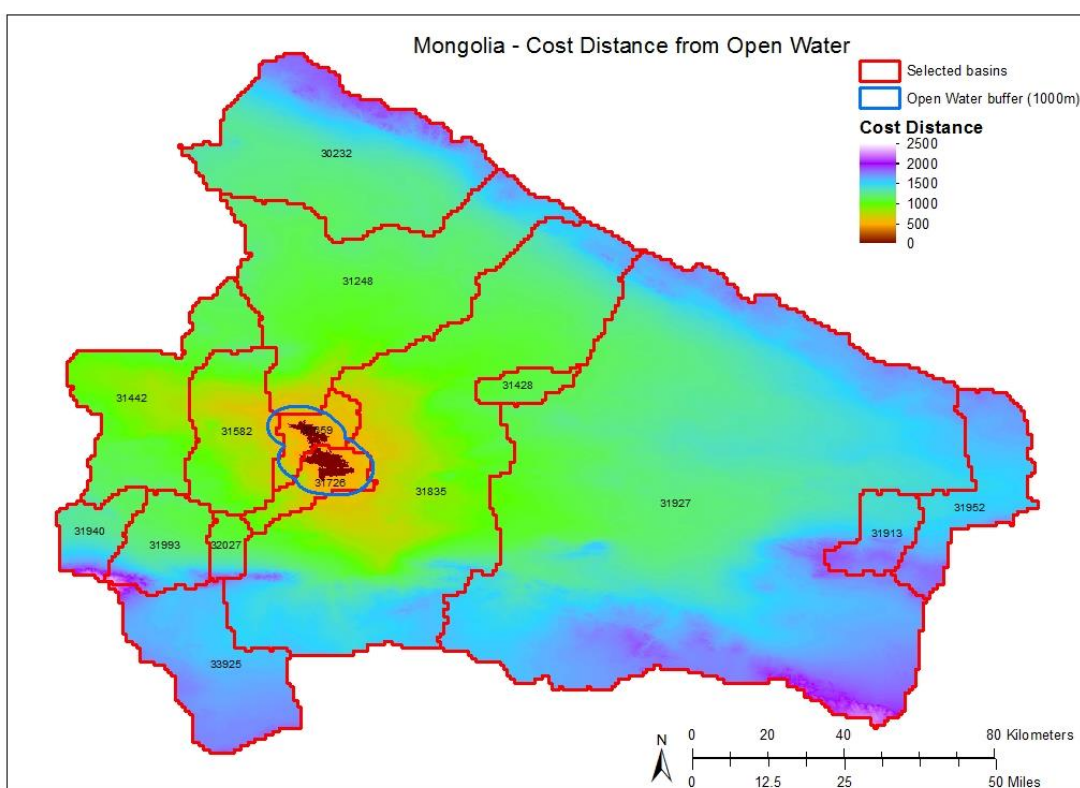
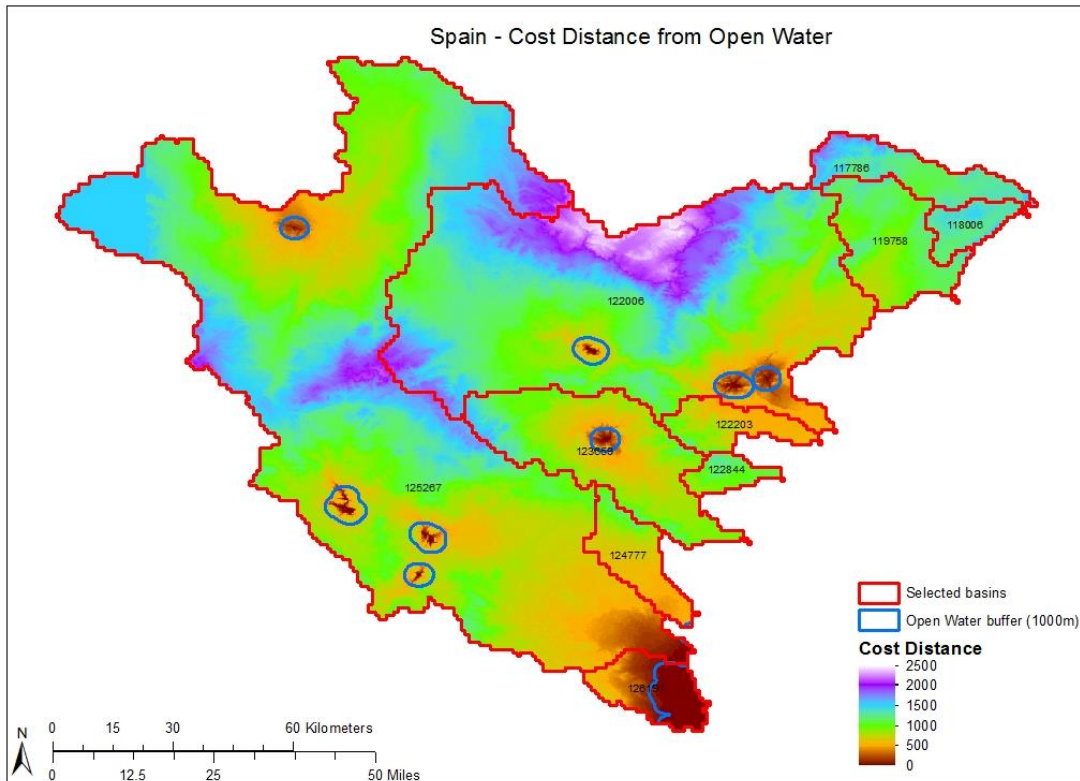




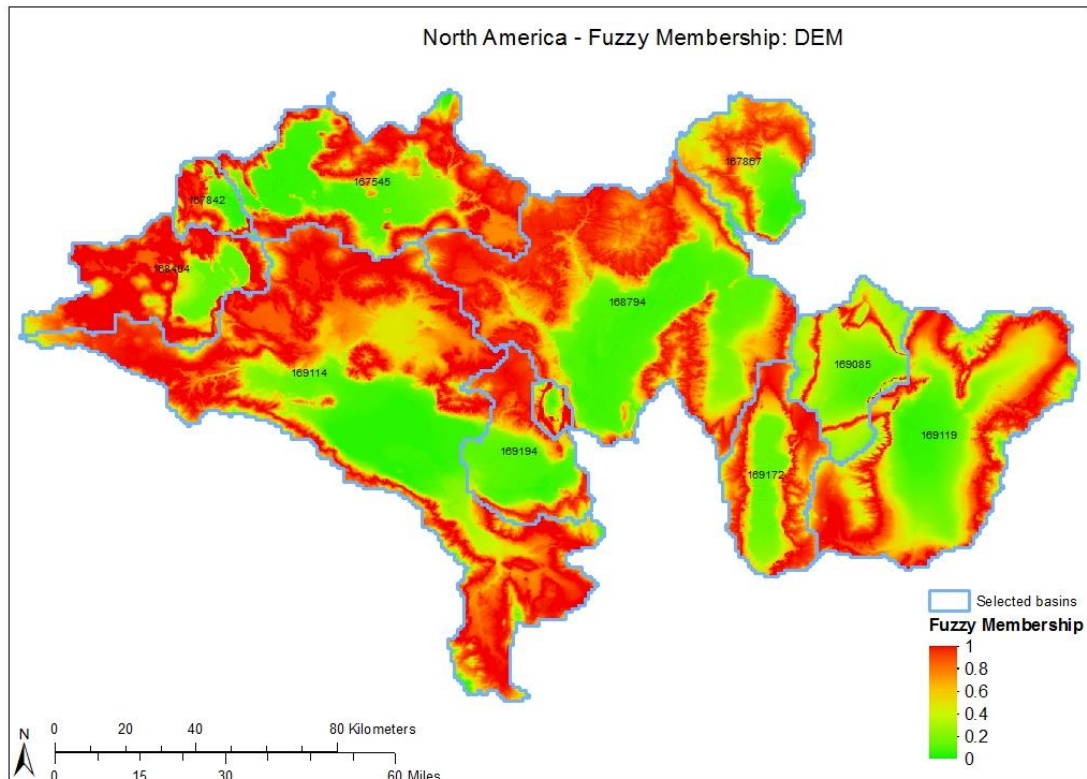


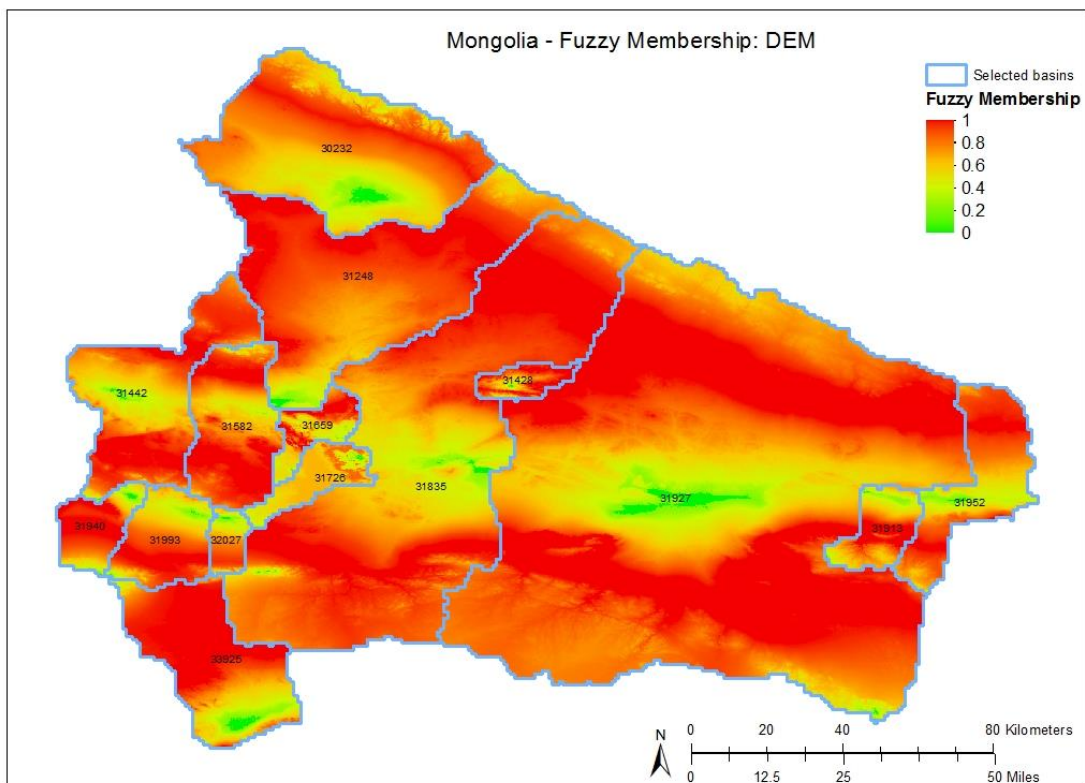
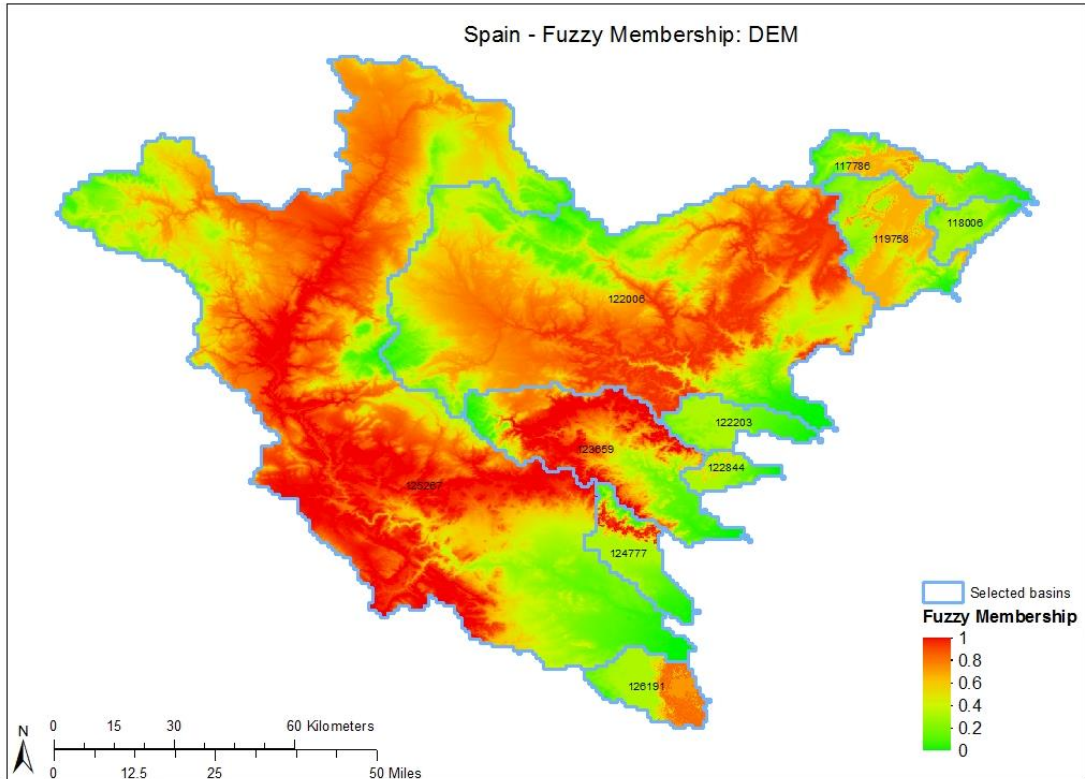


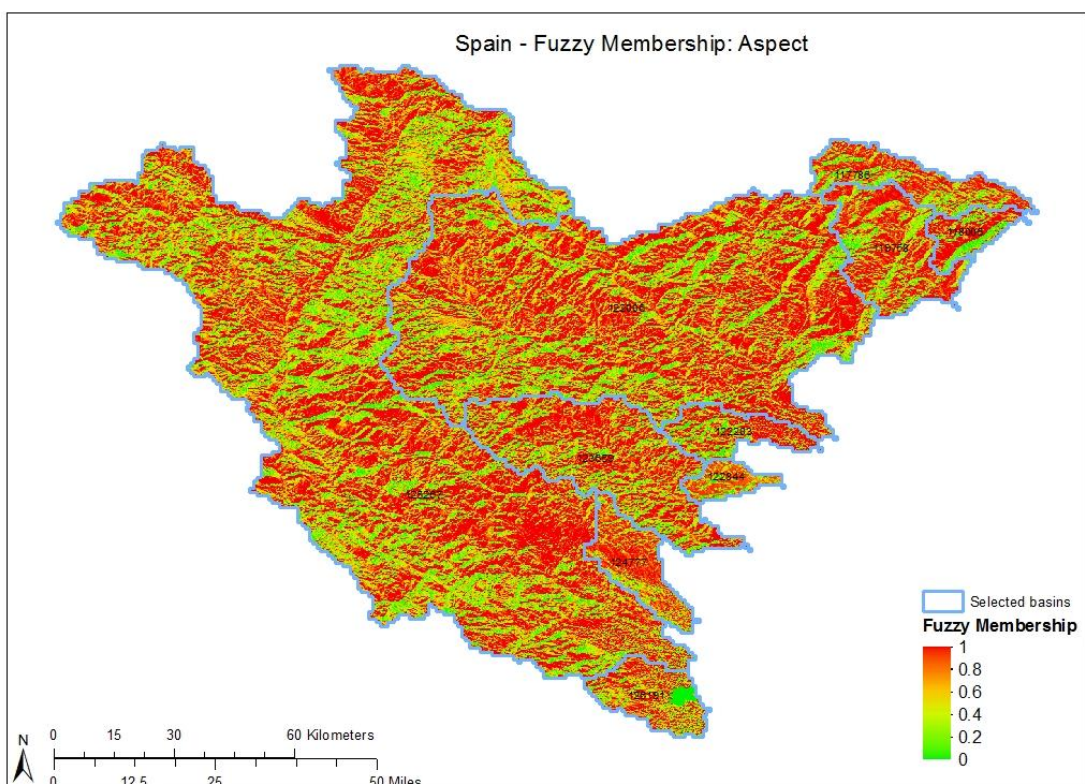
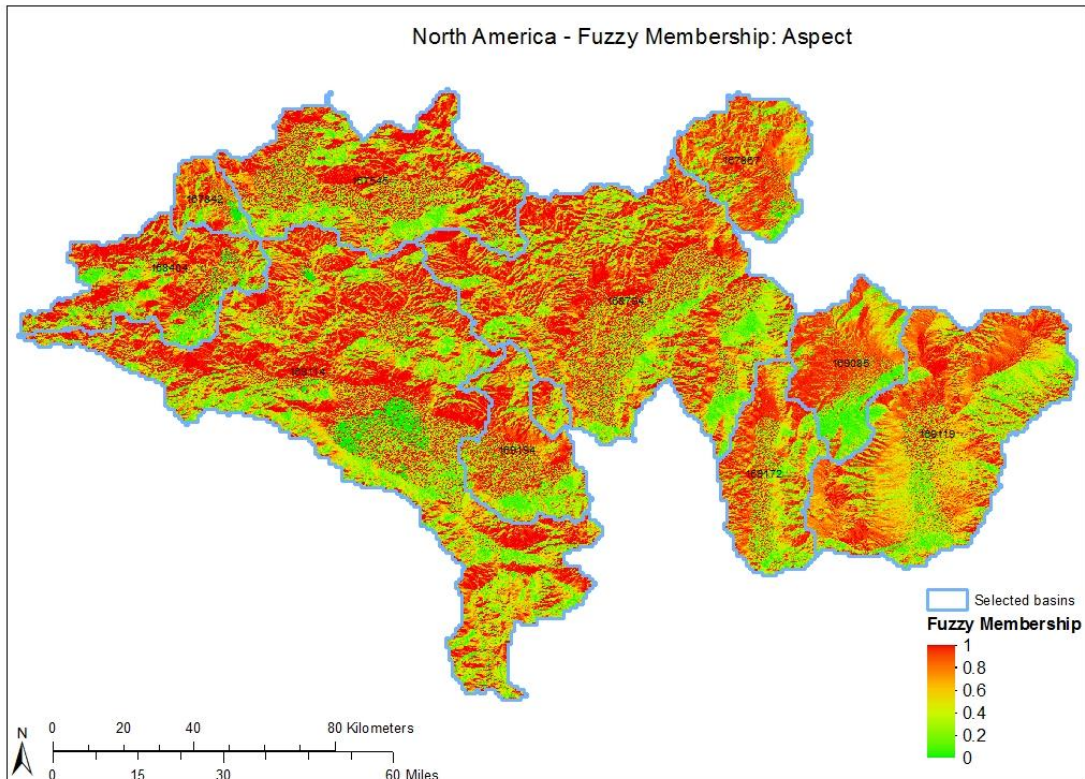


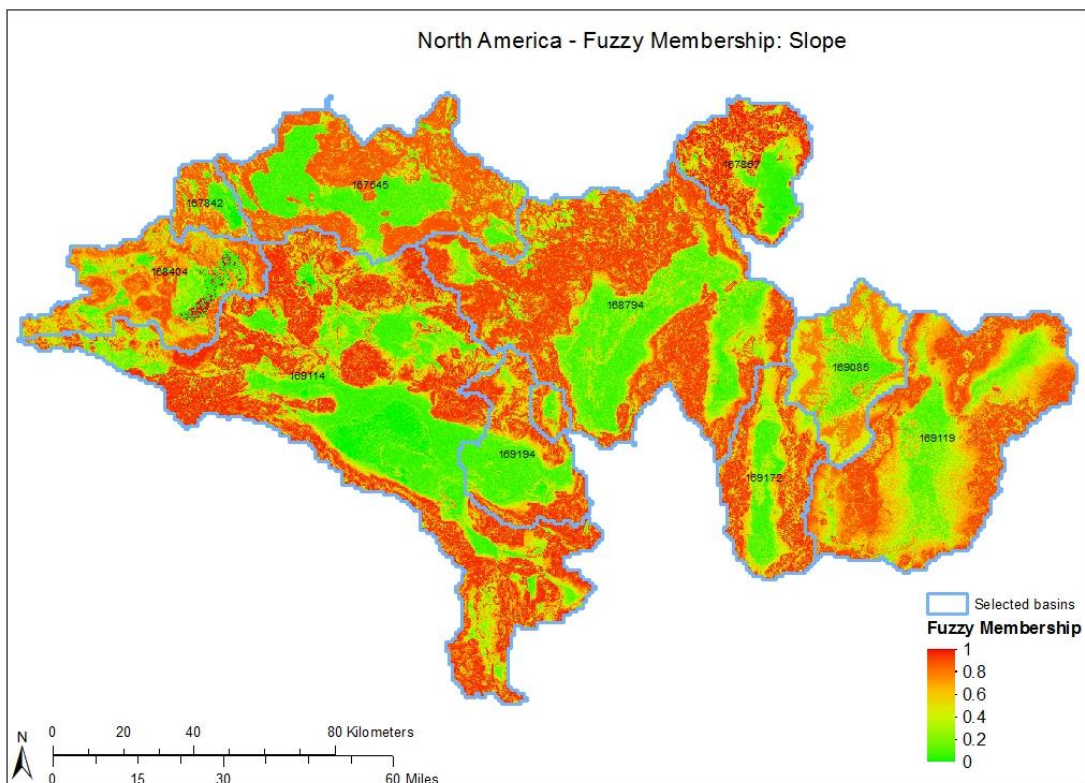
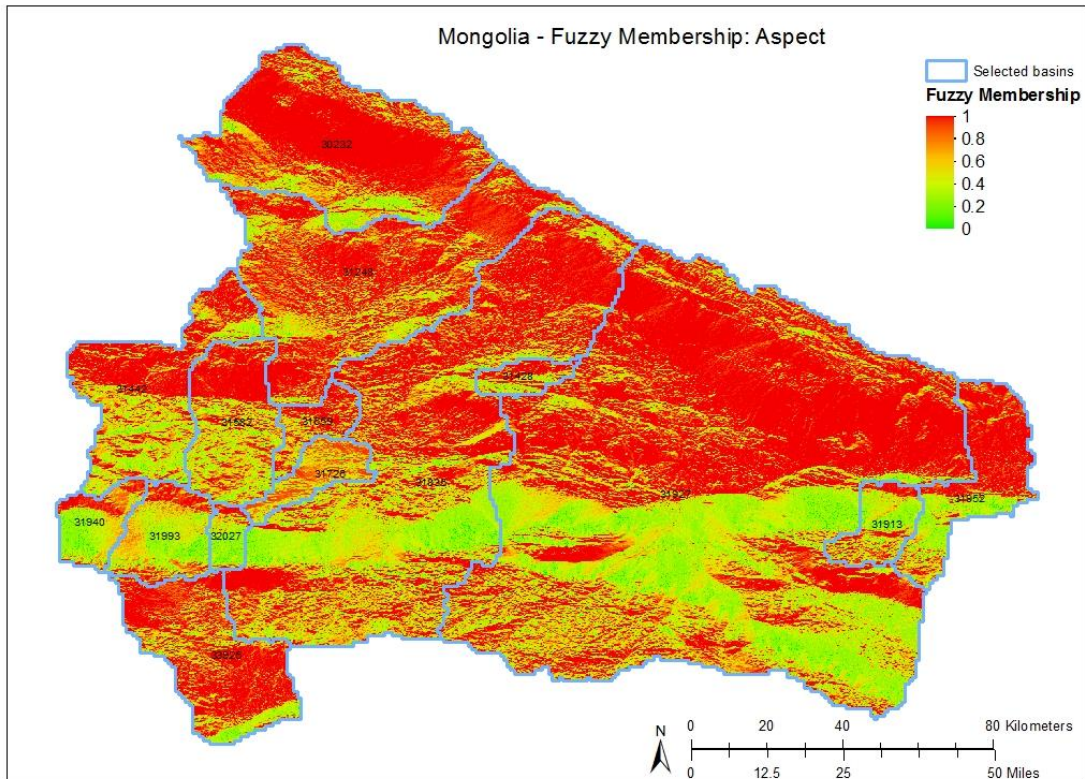


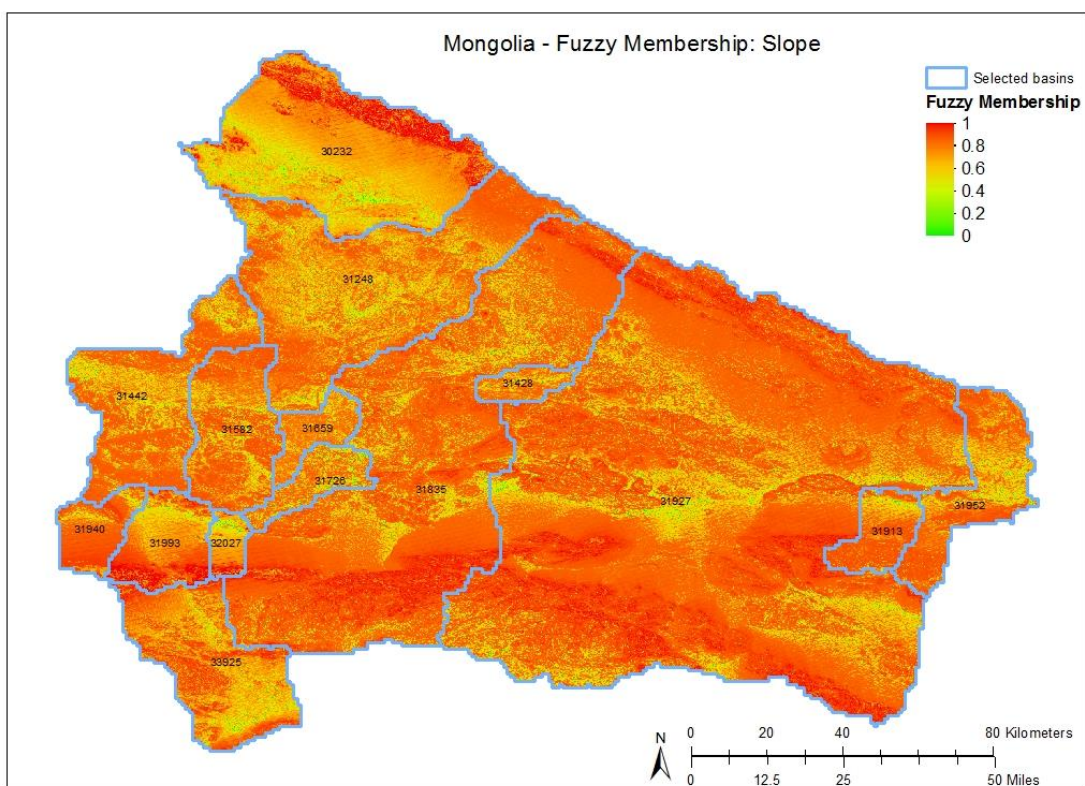
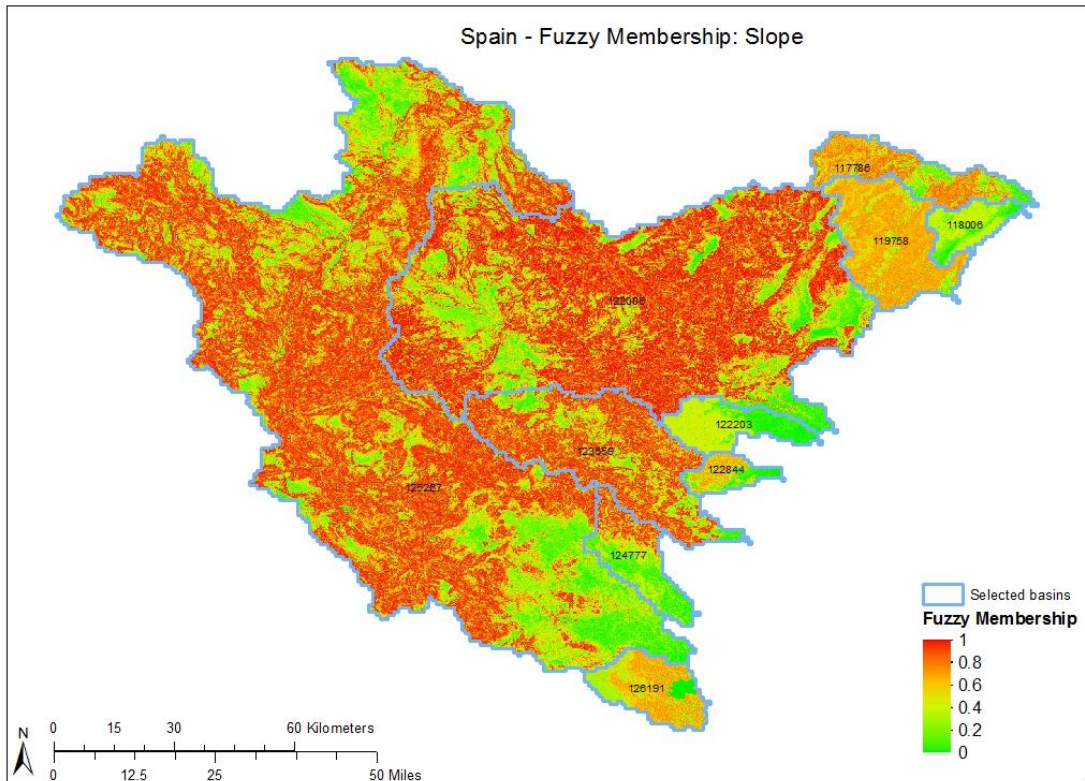
Appendix IV – Topographical Fuzzy Membership

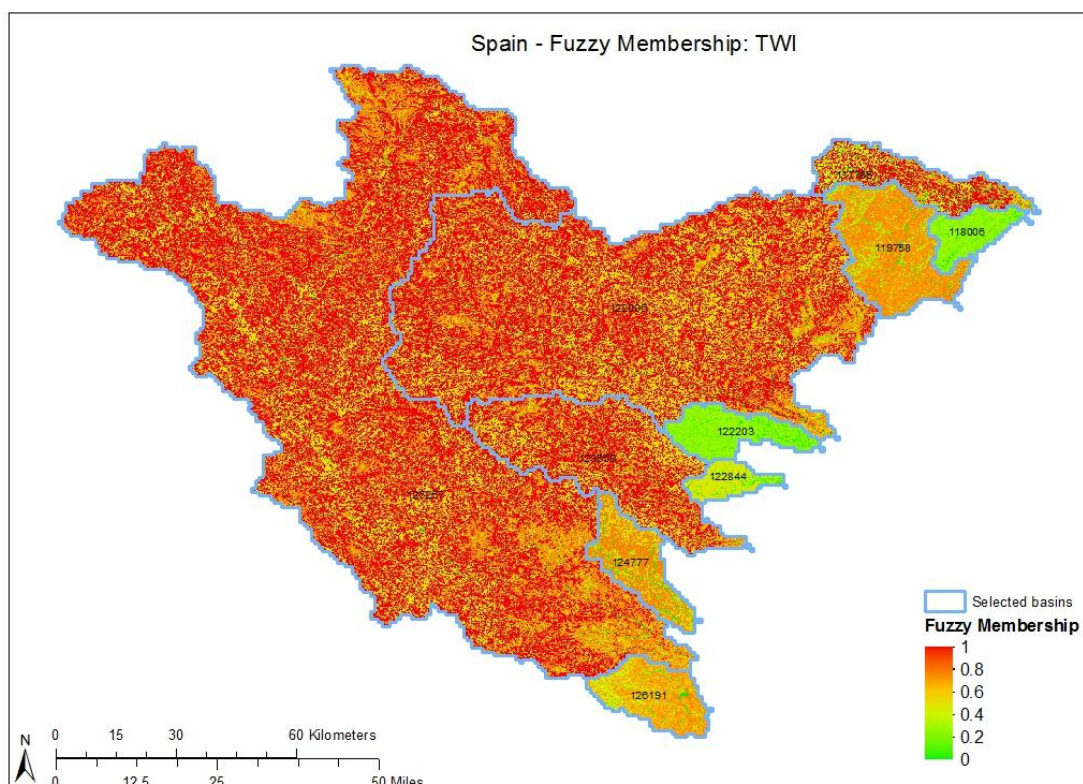
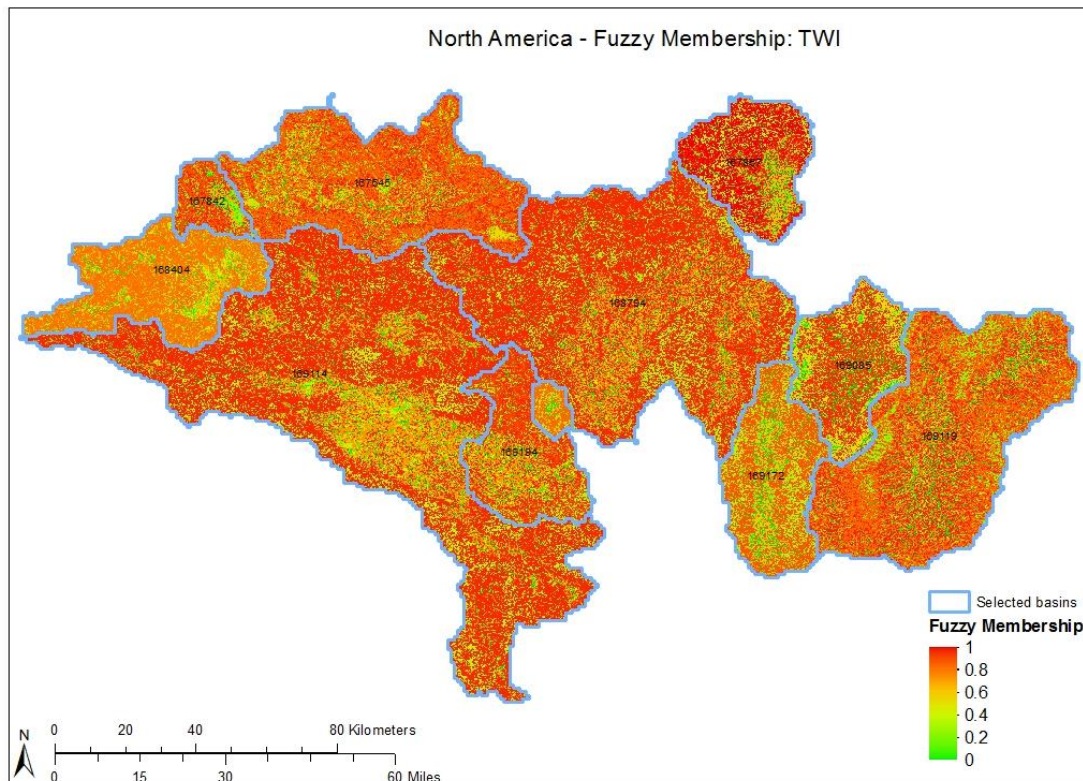


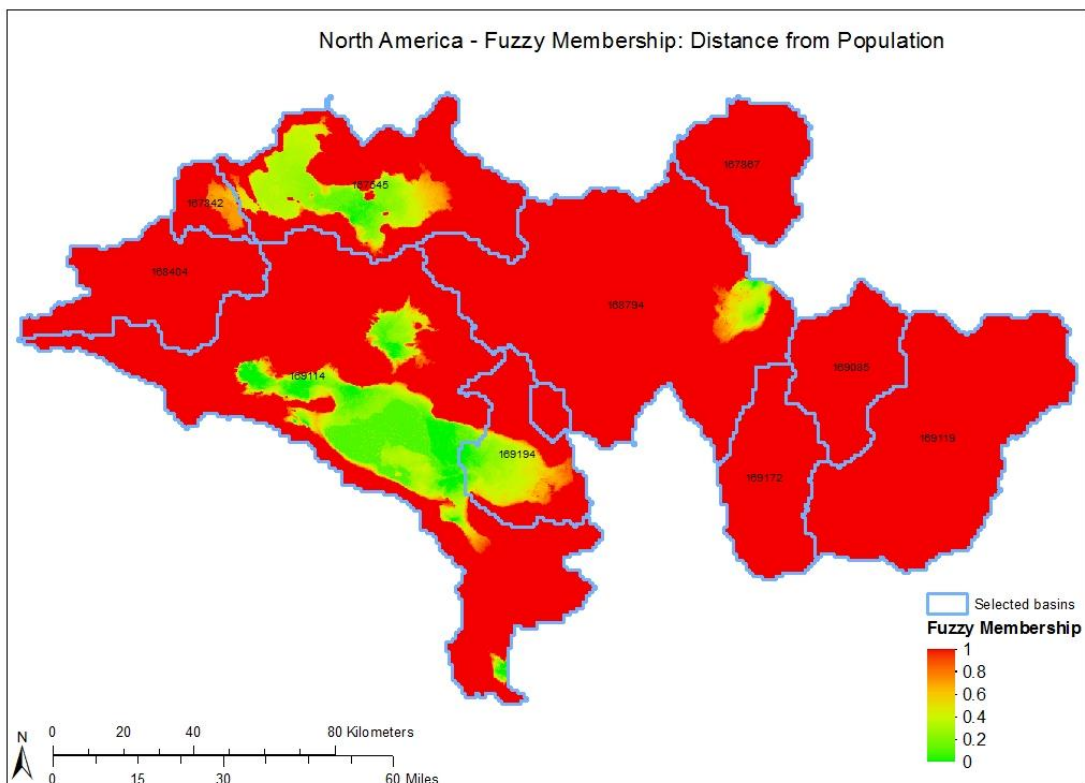
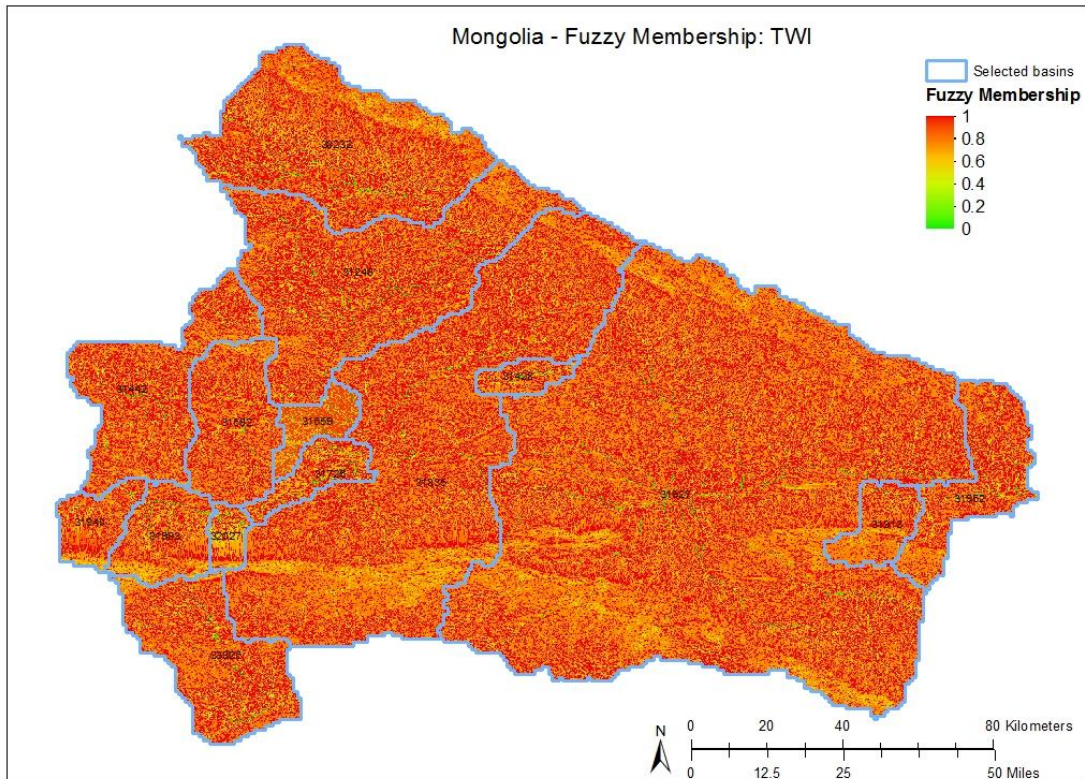


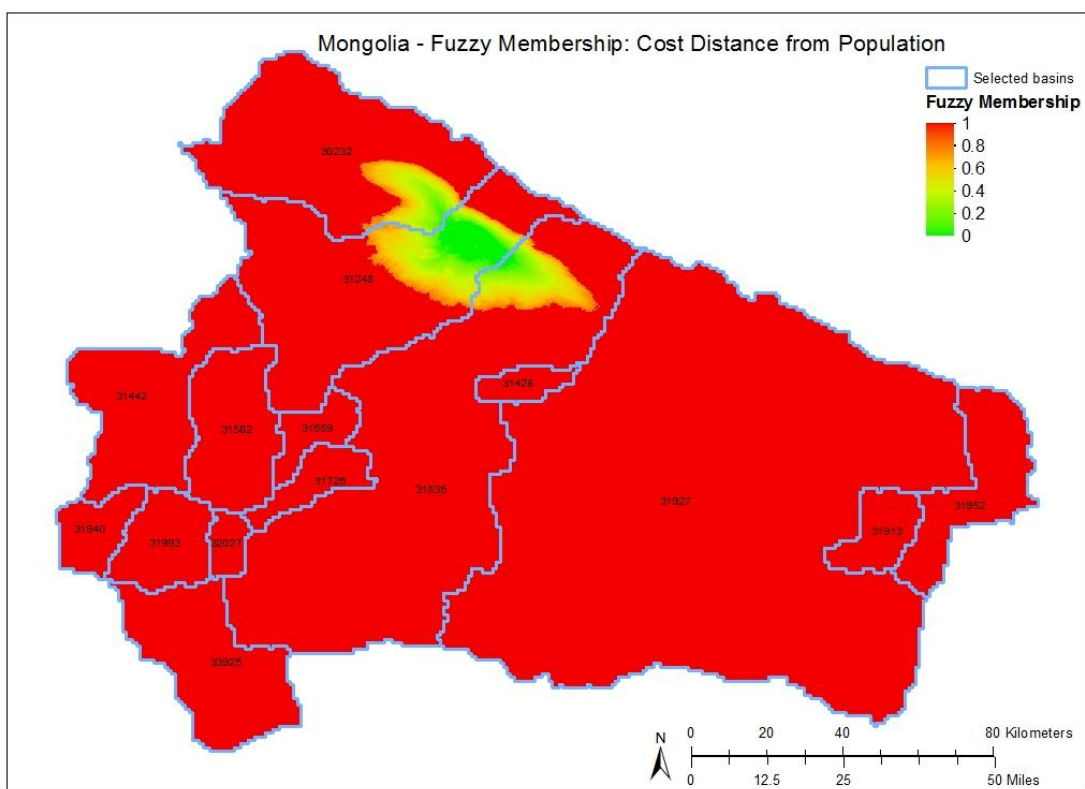
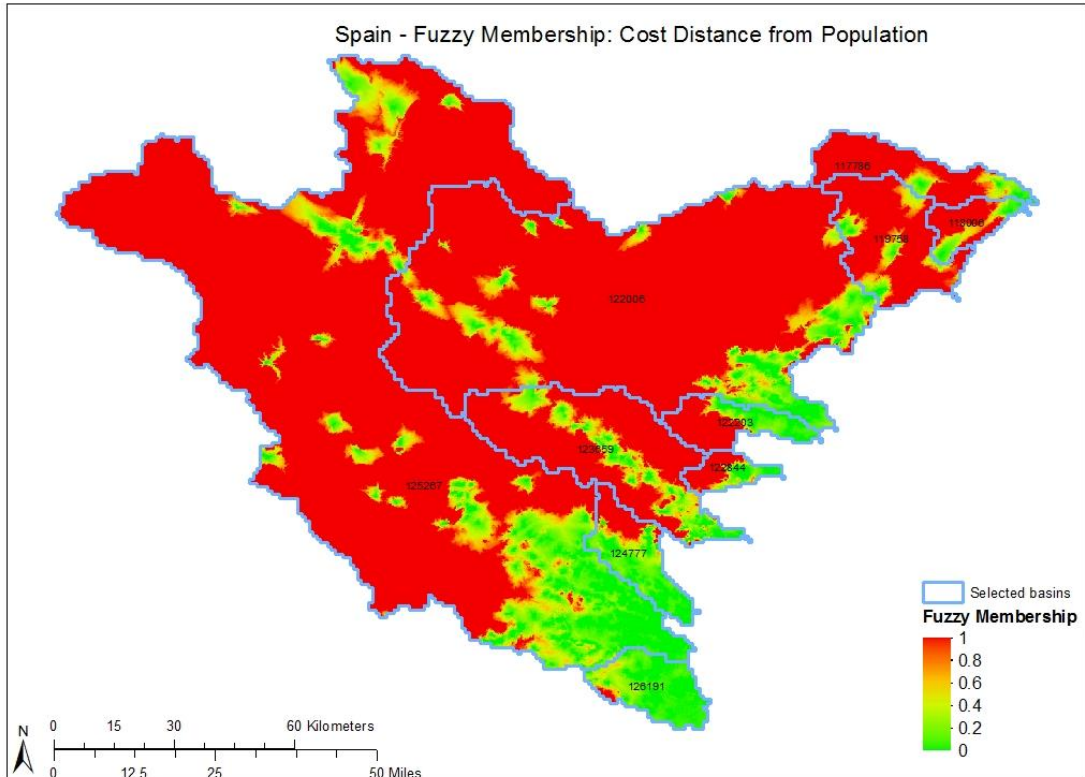


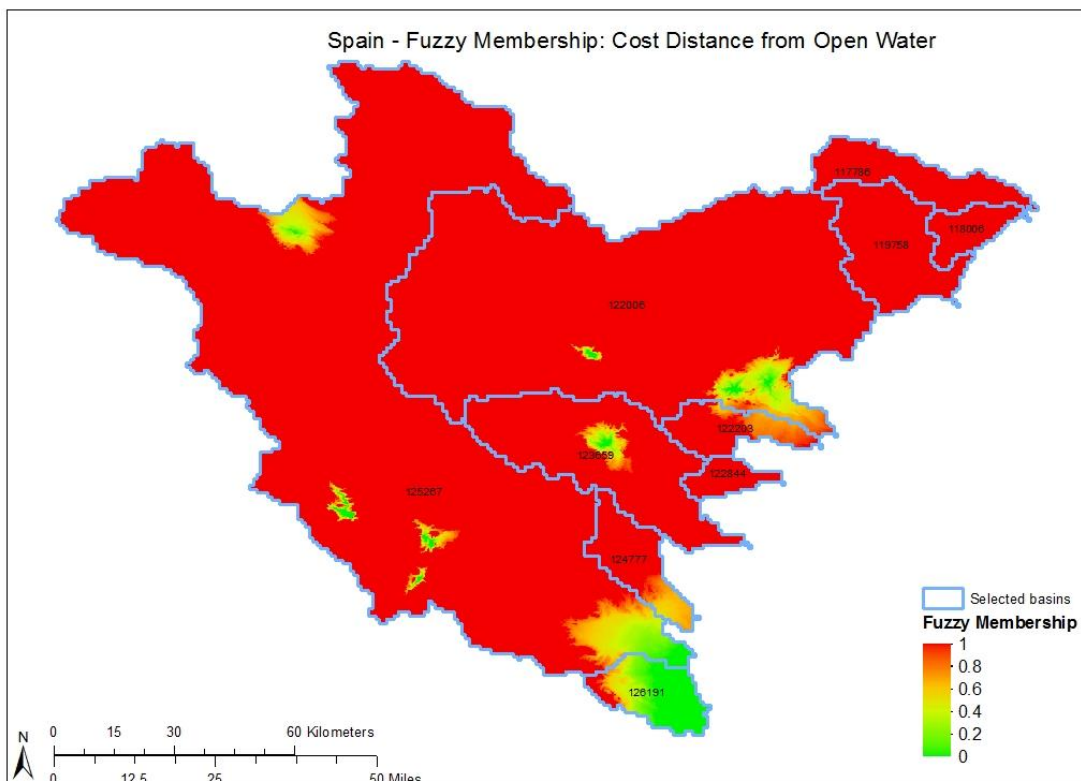
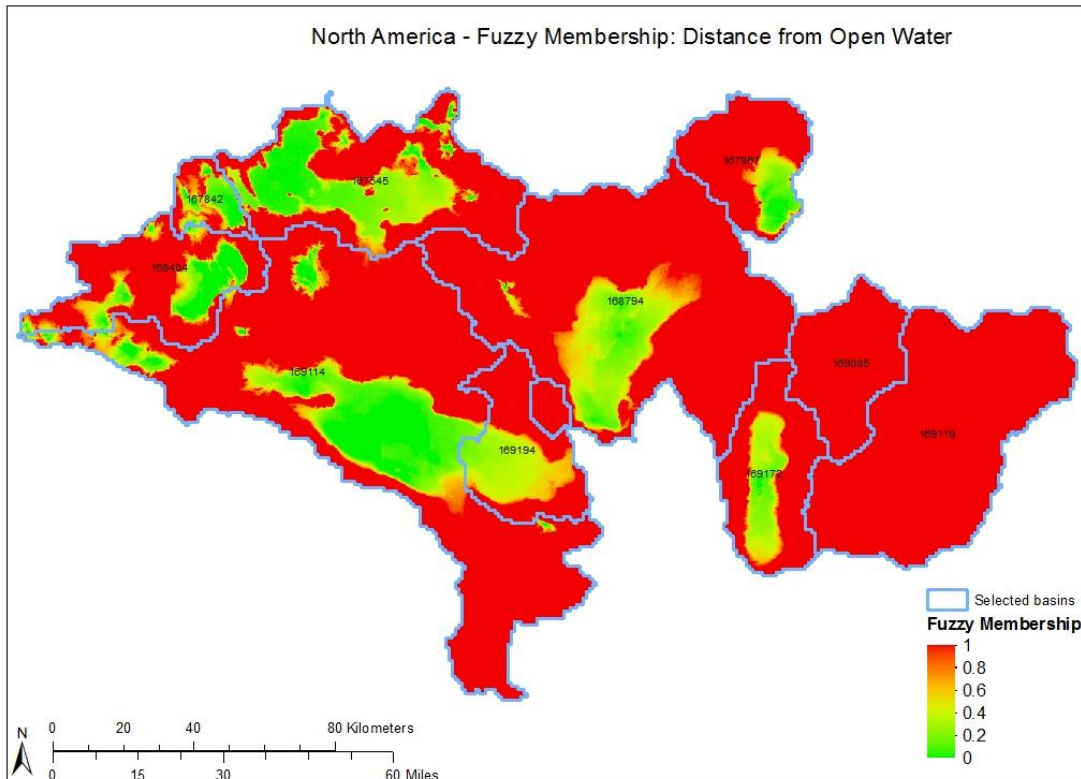


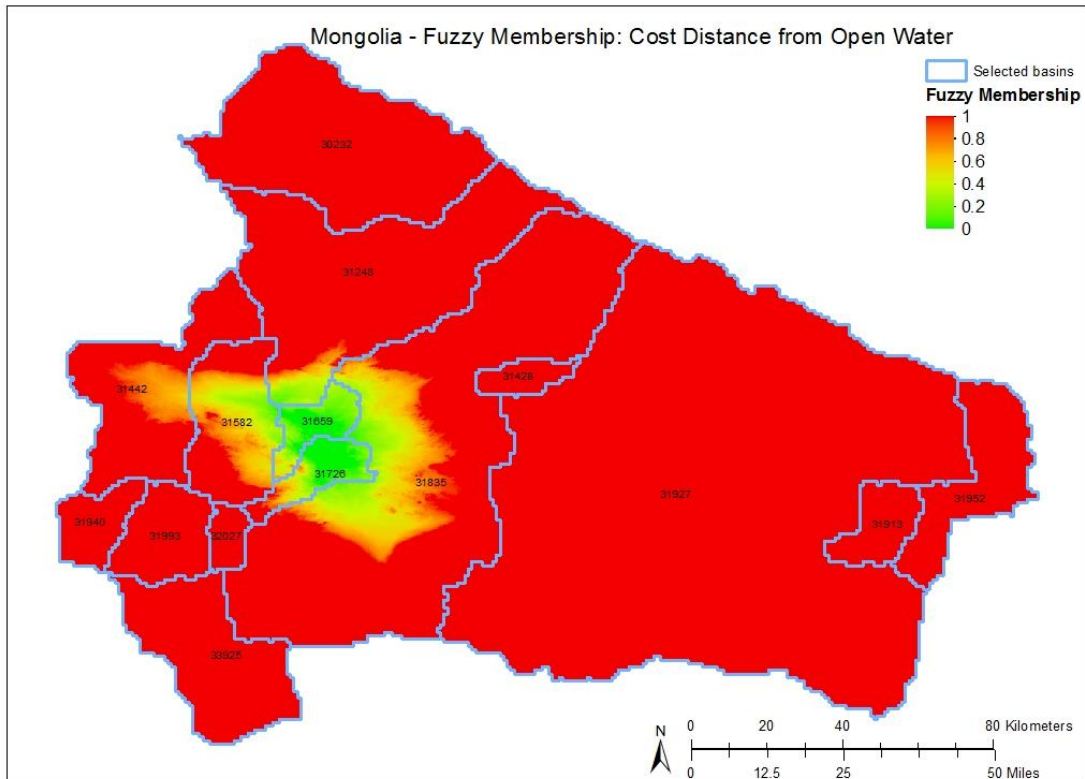




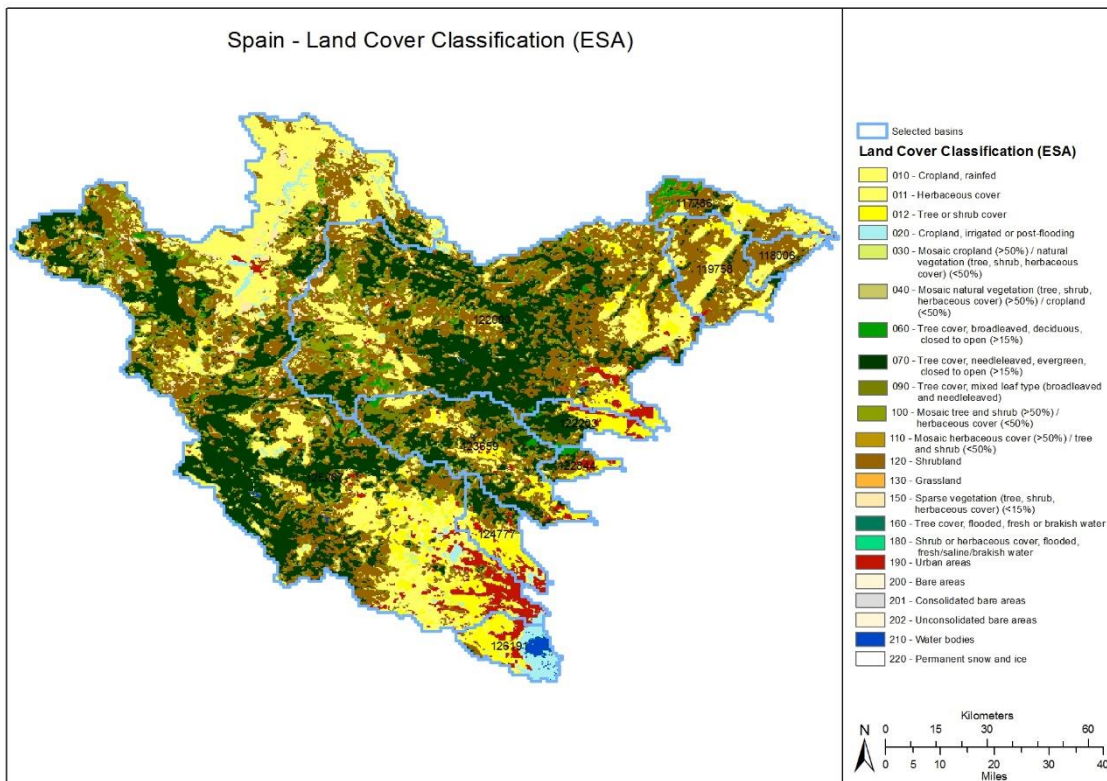
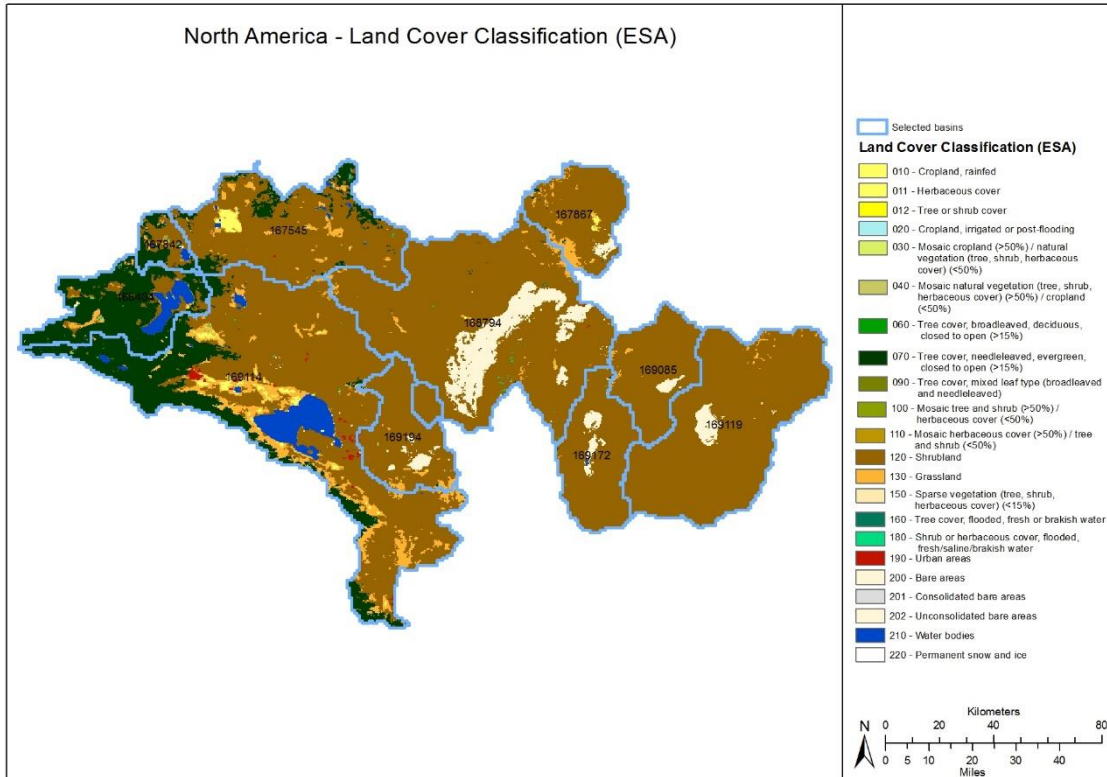


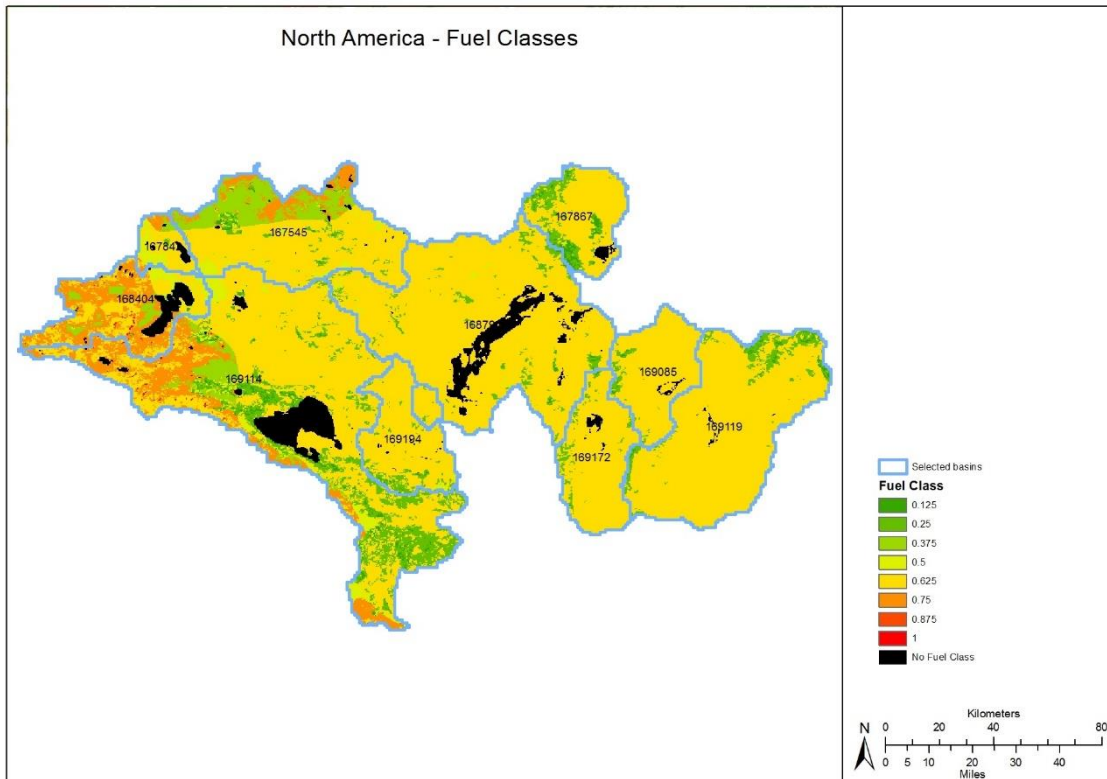
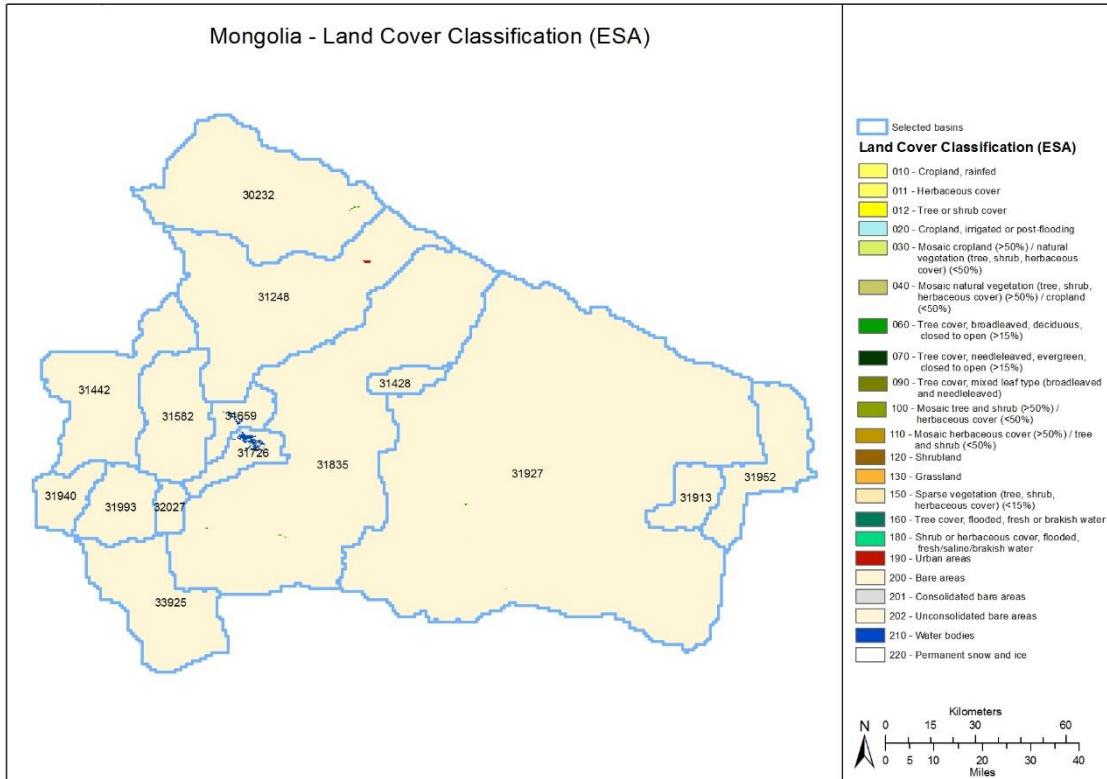


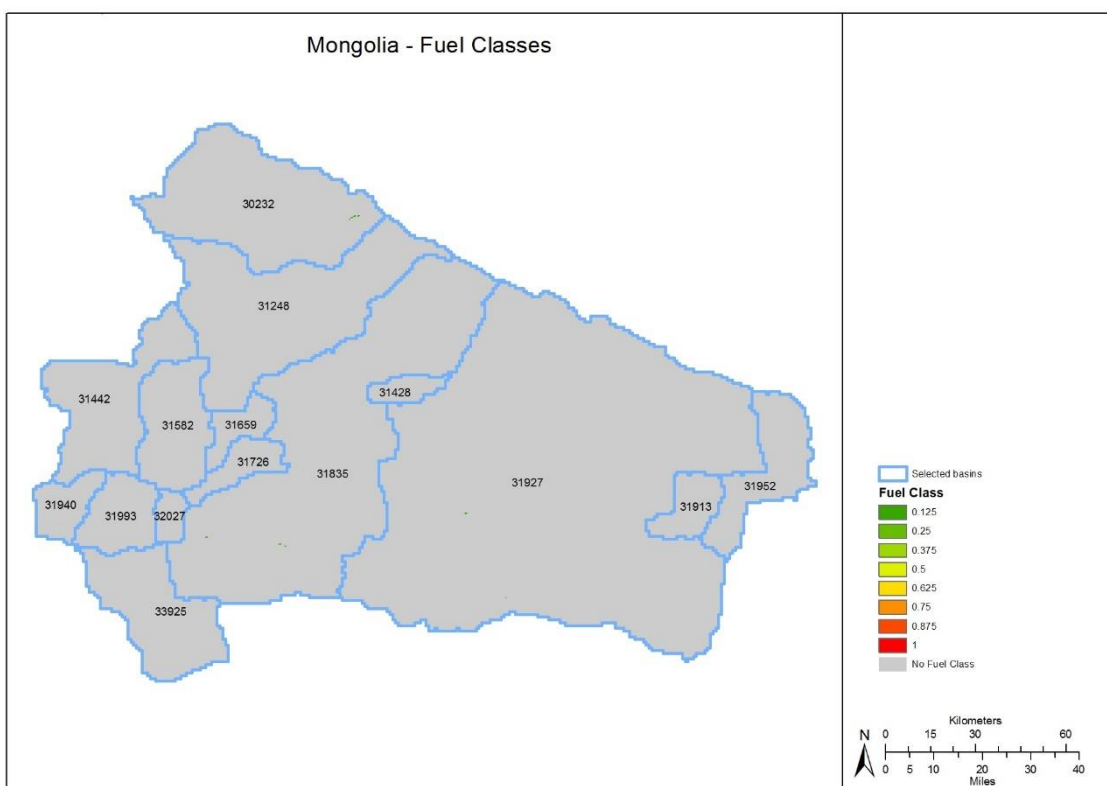
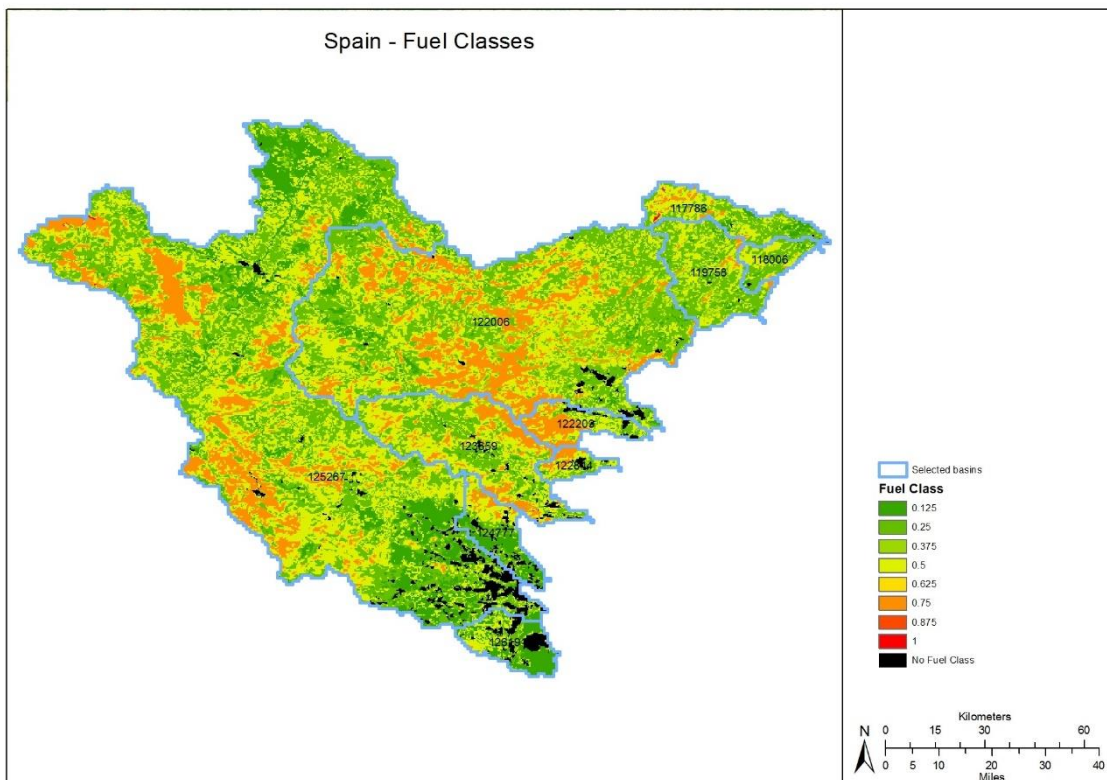




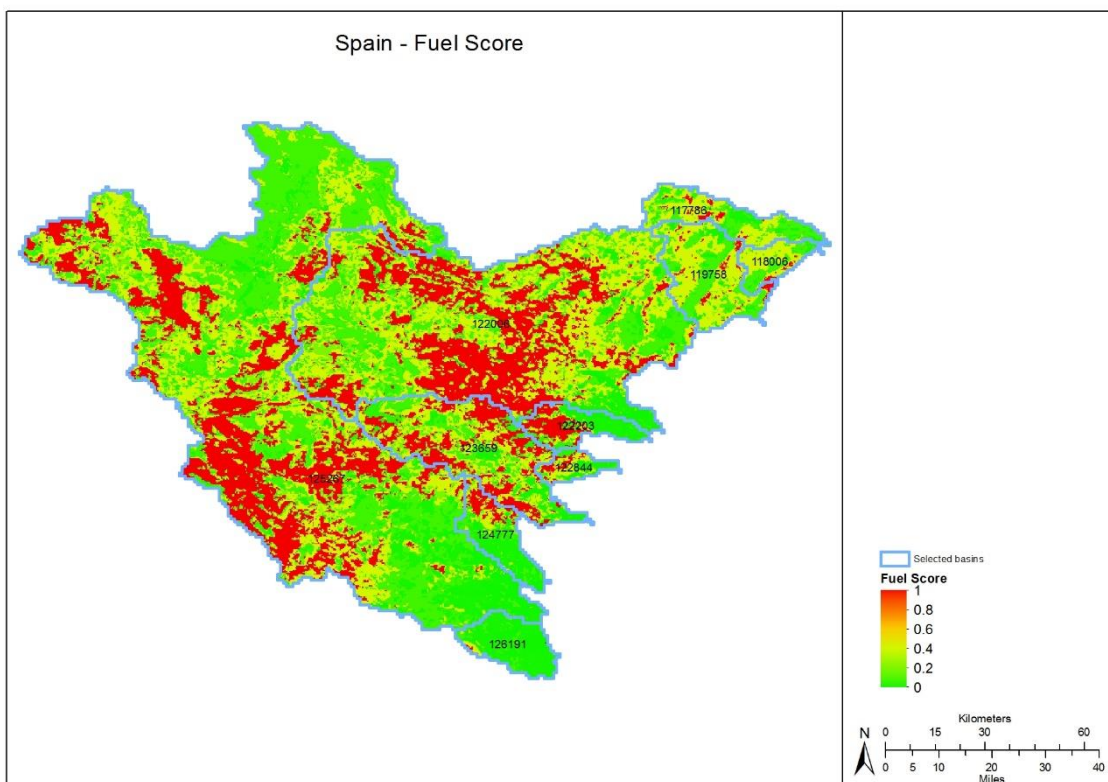
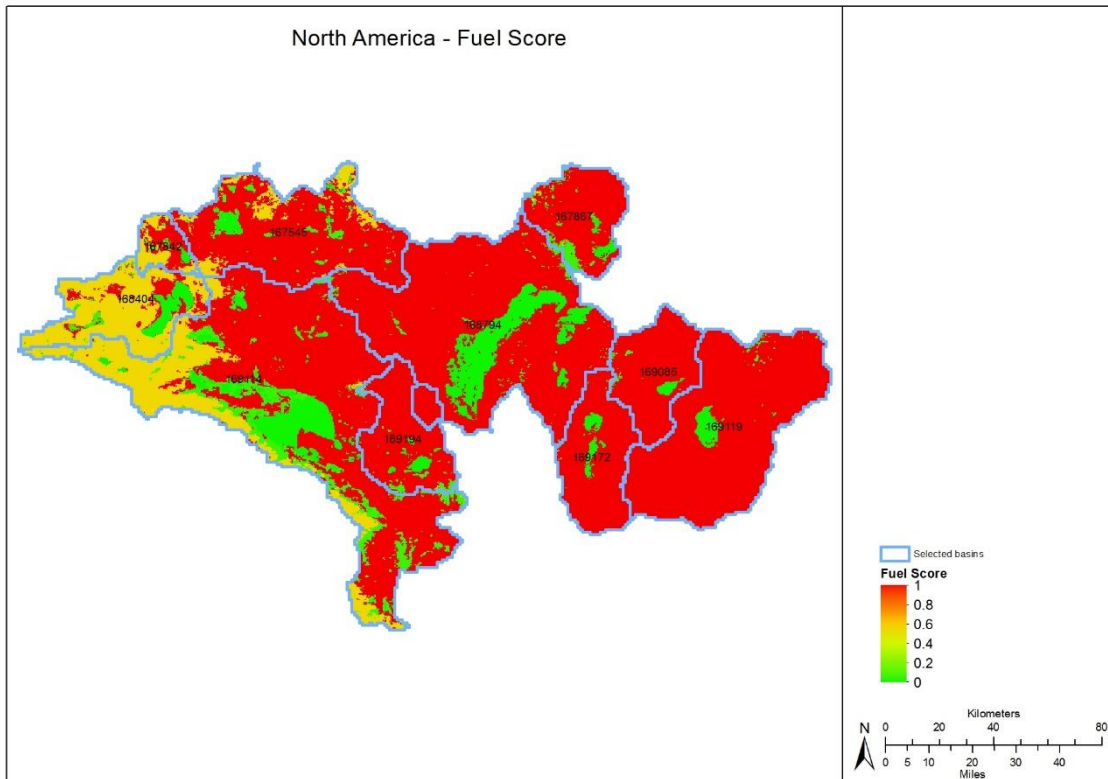
Appendix V – Fuel indicators



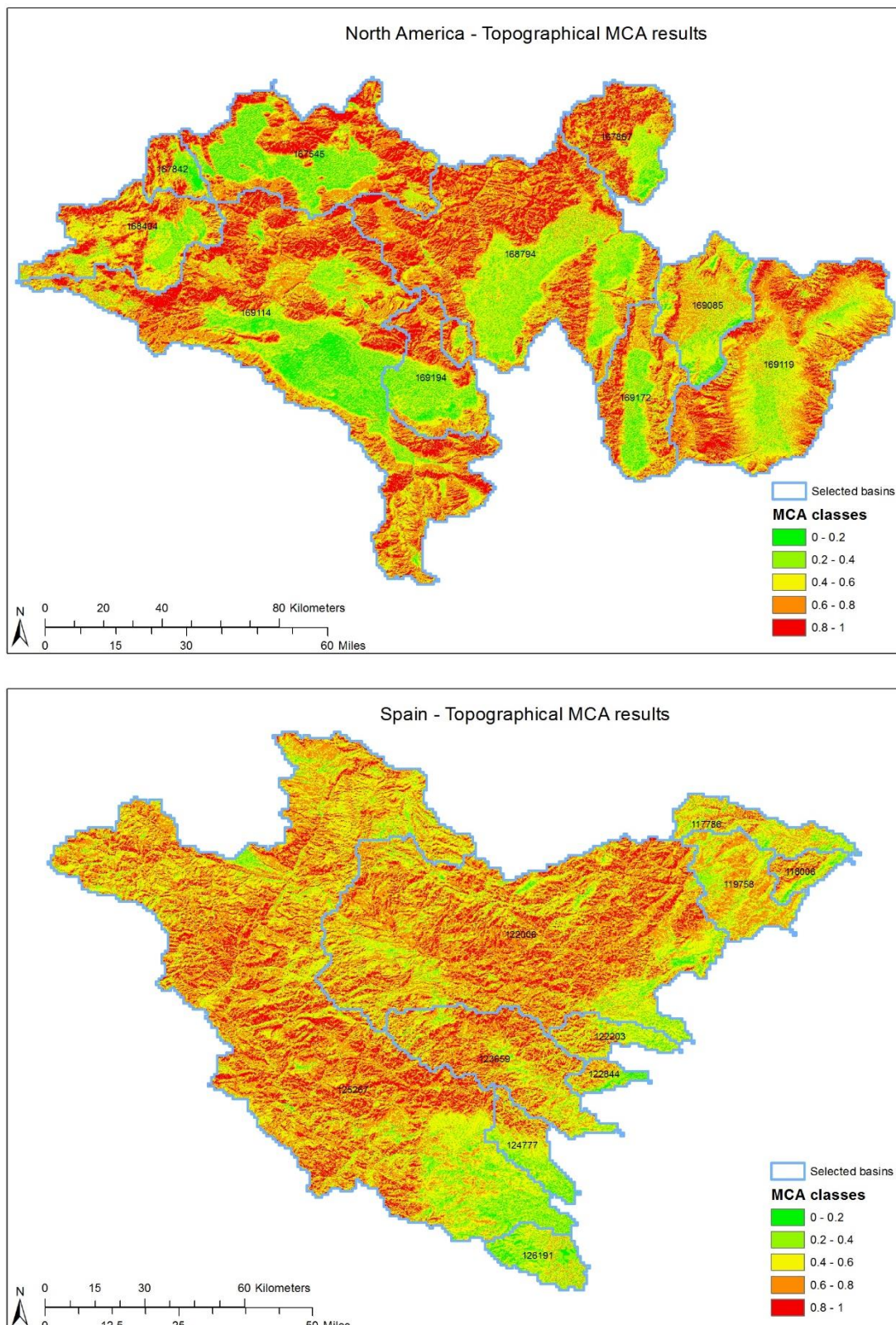


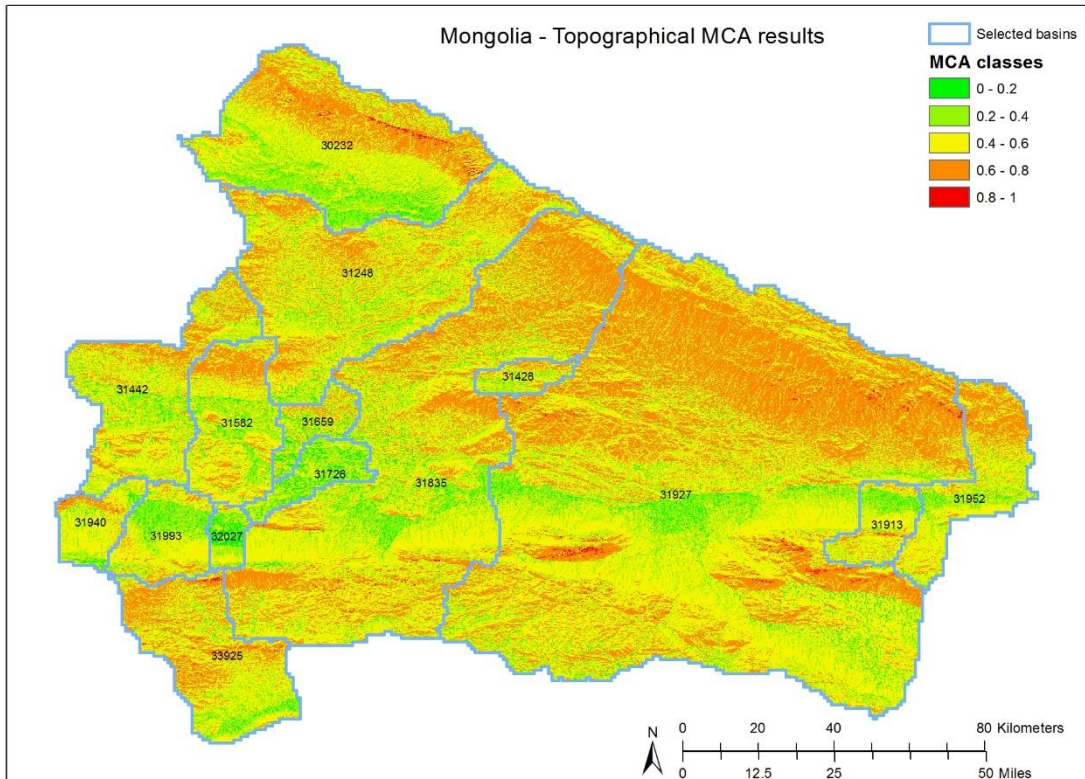


Appendix VI – Fuel Fuzzy Membership (Score)

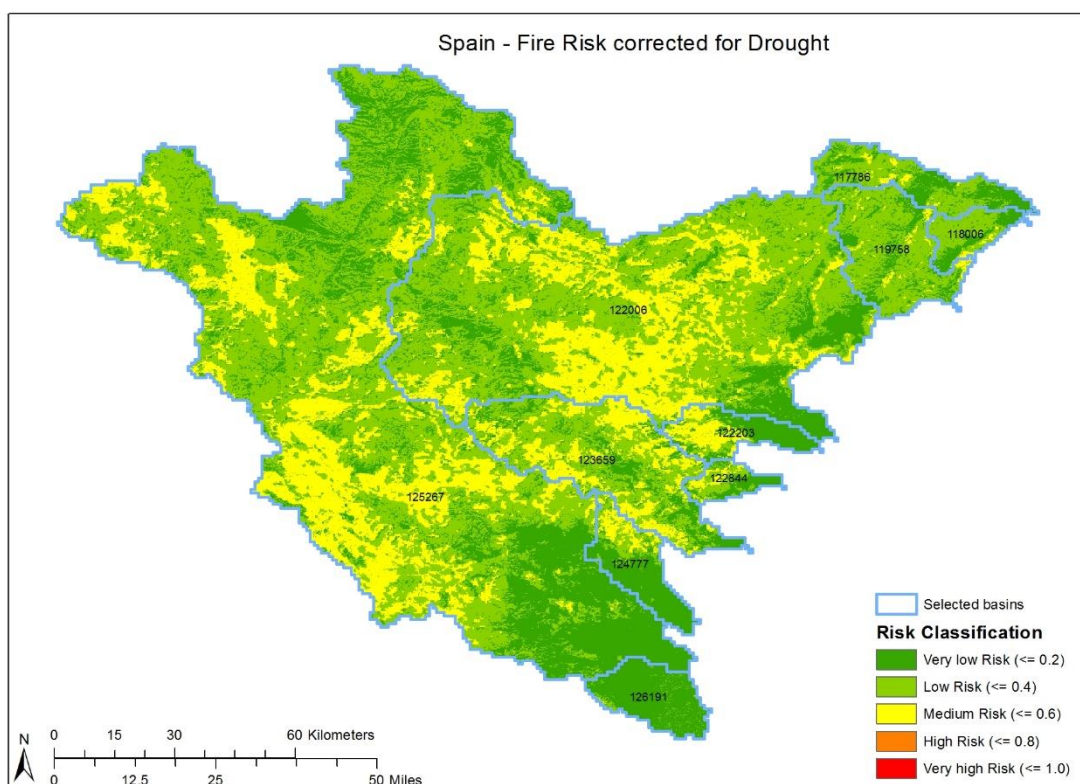
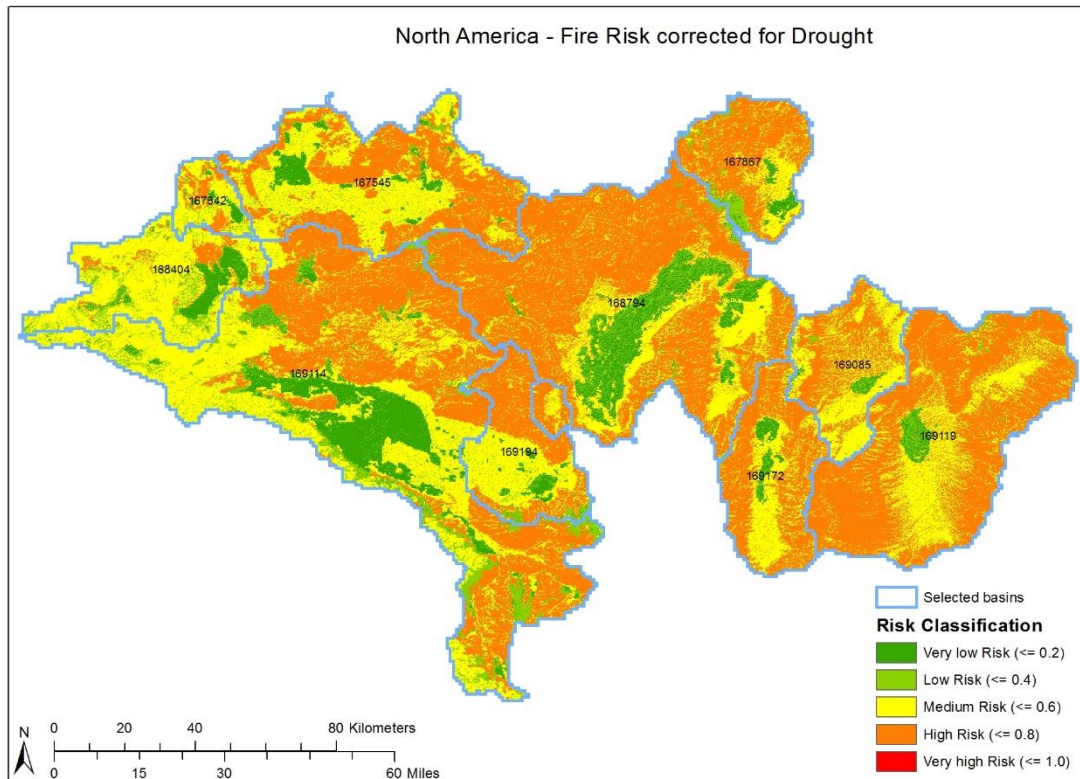


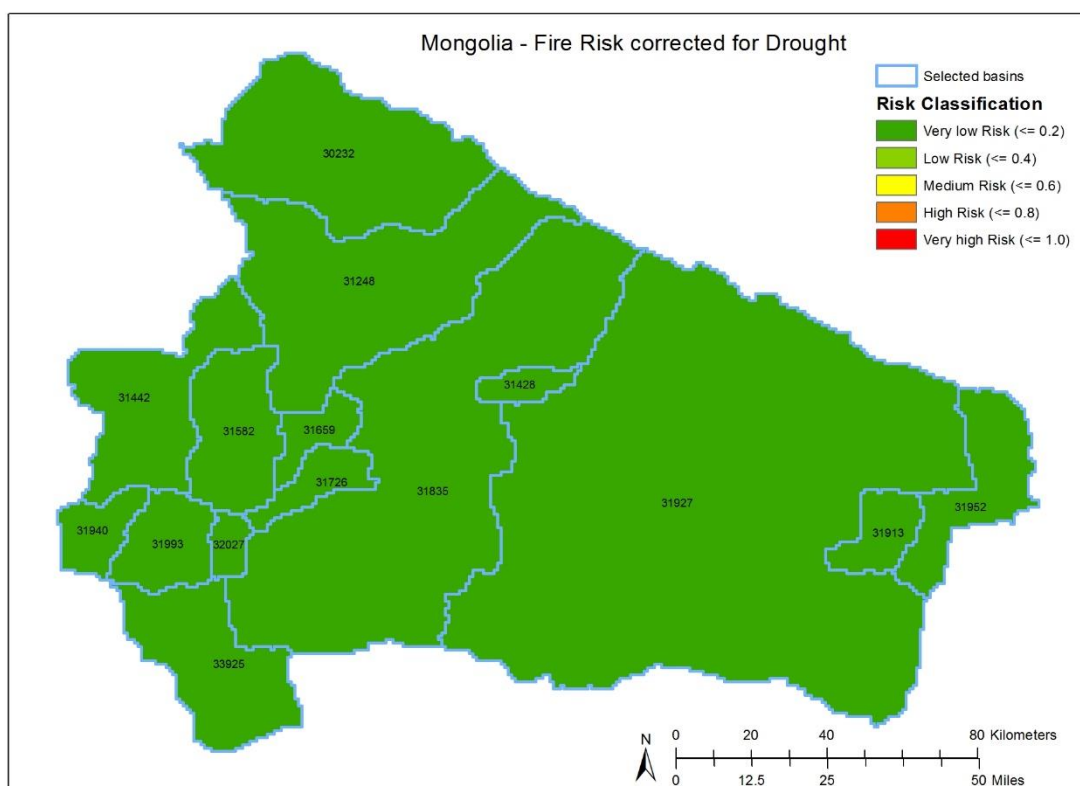
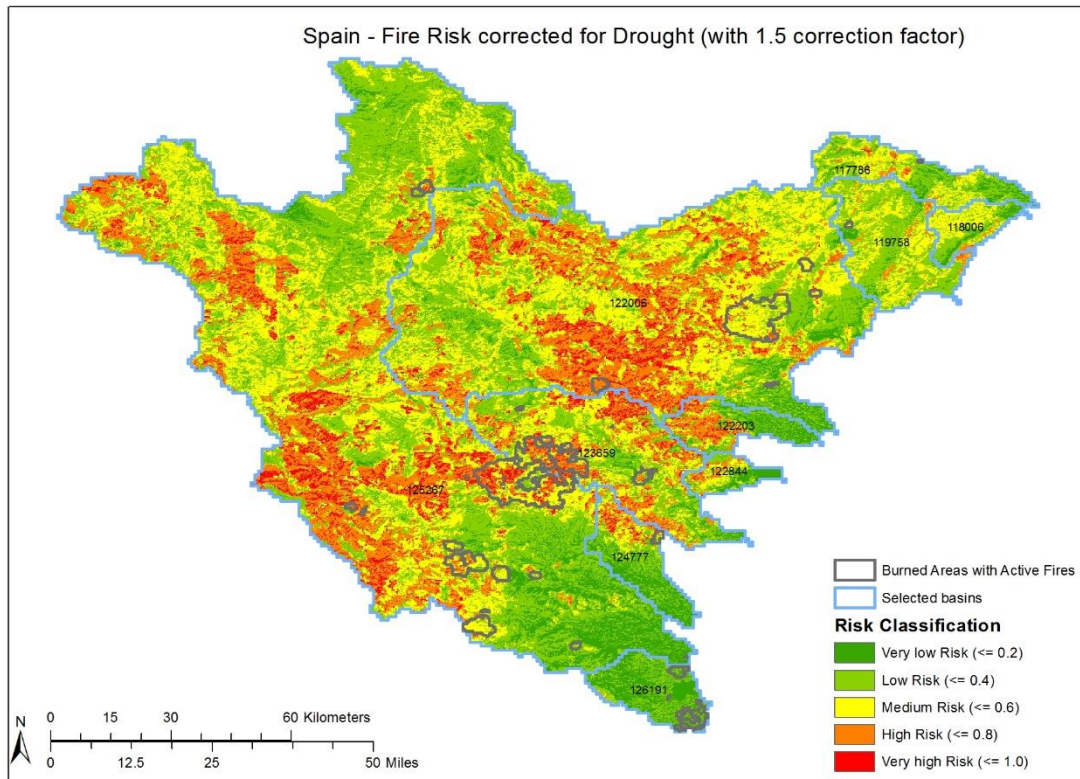
Appendix VII -Topographical MCA Results





Appendix VIII – Fire Risk corrected for Drought





GLOBAL PREDICTIVE WILDFIRE MODEL